2011

The Role of Structural Health Monitoring in Bridge Assessment and Management

Yingjun Zou
Lehigh University

The Role of Structural Health Monitoring in Bridge Assessment and Management

by

Yingjun Zou

A Thesis

Presented to the Graduate and Research Committee

of Lehigh University

in Candidacy for the Degree of

Master of Science

in

Structural Engineering

Lehigh University

May 2011

This thesis is accepted and approved in partial fulfillment of the requirements for the Master of Science.

_____

Date

_____

Dr. Dan M. Frangopol **Thesis Advisor**

_____

Dr. Stephen P. Pessiki **Chairperson of Department**

ACKNOWLEDGEMENTS

First of all, I would like to gratefully express my appreciation to my research advisor, Professor Dan M. Frangopol, for his continuous assistance and guidance. As my advisor, Prof. Frangopol has provided me the research direction and freedom to develop and explore my thesis topic.

I would also like to thank Professor Ben T. Yen and Mr. Ian C. Hodgson who have provided the data, other materials and assistance on the research of Commodore Barry Bridge. My colleagues Kwon Kihyon, Kim Sunyong and Tian Hao who provided help during my research.

Lastly and most importantly, I offer my appreciation and love to my parents who are always supporting and encouraging me.

TABLE OF CONTENTS

CHAPTER 7 CONCLUSIONS

LIST OF TABLES

LIST OF FIGURES

CHAPTER 3

CHAPTER 4

ABSTRACT

The past several decades have witnessed civil infrastructure design and assessment shift from deterministic methodology to probabilistic methodology. Structural Health Monitoring develops so rapidly that it is likely to become a predominant emerging technology to challenge and improve traditional way of design, assessment and management of civil infrastructure.

The objective of this study is to explore the approaches combining the monitoring technology with the reliability method to assess and predict the structural performance under uncertainty. Concepts and different approaches have been applied on two steel trusses and two existing bridges to reach the objective.

The time-dependent component reliability is investigated in the first two truss models to determine the most critical member. It is assumed that components with different material properties will deteriorate with various rates. Time-variant reliability is computed at discrete times. Reliability index, as one of the performance indicators including the uncertainties in resistance and loads, is used to estimate the component performance during its lifespan. Performance thresholds are established as the warning which provides the reference for scheduling monitoring inspection and making maintenance decisions. Due to the high cost of using monitoring technology, the search of an optimal balance between economic budget and safe performance is in great demand.

In the study of Commodore Barry Bridge, field monitoring data is used to find probability density functions of equivalent stress range to assess and predict the bridge's fatigue reliability. Three distribution types are compared by using goodness-of-fit test and

the optimum one is selected to determine the parameters for reliability computation. The lifetime performance of six critical bridge members and their effects on the whole structure are investigated.

The concept of the statistics of extremes is applied in the I-39 Northbound Wisconsin River Bridge to improve the performance prediction and assessment based on monitoring data. Two methods to account for the epistemic uncertainty based on 80 days of monitoring data are used in the reliability analysis.

CHAPTER 1
INTRODUCTION

1.1 Background

Civil infrastructure subjected to time-dependent loading and strength deterioration processes will experience changes due to internal and external factors. Some of these changes would make serious impact on the serviceability and the ultimate capacity of structures. The uncertainties associated with structural descriptive parameters and deterioration processes cannot be ignored. Structural Health Monitoring (SHM) technologies, which are popularly used and extensively researched, are anticipated to be cost-effective. The SHM data should be utilized in the reliability-based design and assessment. There are great potentials to adopt these technologies into structural engineering and reliability with special emphasis on life-cycle cost and performance prediction. (Frangopol et al. 2008b)

It is necessary to find out how the components make impact on the system for determining the monitoring priority. The strength properties of the components and the system model types are the two main factors for the researchers to make decisions on which component should receive monitoring priority. In consideration of environmental effect, deterioration process should be added into the analysis to decide when monitoring is appropriate.

The next step after determining what and when to monitor at the structural level is to integrate the monitoring information into the structural design and assessment. The

framework of bridge monitoring system consists of global monitoring and local monitoring. Global monitoring can be used in the analysis of acoustic emissions, deformations and displacements, frequency variations, model shape changes, dynamic flexibility and physical integrity; while local monitoring is applicable in research on cracking, corrosion, physical integrity and structural capacity. This study will focus on cracking with emphasis on fatigue in the existing bridges.

1.2 Research Objectives

The purpose of the study is to find out the most critical member in the system and integrate field test monitoring information into the probabilistic approach of structural assessment and performance prediction.

For truss structures, the effect of component failure on the system depends on many factors, such as material properties, deterioration rate, structural configuration and live loads. The behavior of perfectly brittle and ductile trusses will be investigated to find out how components will respond due to different ductilities and make impact on the system under various deterioration rates. As a result, the determination on monitoring scheduling can be made based on the time-dependent reliability study.

There are eight components of the Commodore Barry Bridge having the potential for crack growth. The fatigue reliability of the components is assessed using the PDFs of equivalent stress range based on the monitoring data provided by the ATLSS Research Center at Lehigh University. The deterioration of the bridge is analyzed by using annual accumulated number of stress cycles which is a time-dependent quantity. Due to loading uncertainties, the appropriate PDF for the stress range bin histogram based on monitoring

data is selected to provide parameters in determining fatigue life. The performance indicator to judge the lifetime behavior of the critical members is the system reliability index, which predicts how the system performs during the lifetime.

The monitoring data can also be integrated into the reliability assessment and performance prediction by introducing the concepts of the statistics of extremes. The I-39 Northbound Wisconsin River Bridge is studied by using this approach to formulate the PDF distributions of extreme value distributions (EVDs) in a selected timeframe based on daily maximum stress data obtained from field test monitoring. The effect of the epistemic uncertainty on the calculated reliability index is investigated by comparing two methodologies.

1.3 Organization of the Study

This thesis contains seven chapters including this introductory chapter. The following is a brief summary of the chapters.

Chapter 1 is introduction.

Chapter 2 introduces some background information. The concepts of reliability on the component and system levels are both reviewed. The time-variant reliability is emphasized.

Chapter 3 introduces the role of monitoring in bridge assessment. Some examples are given to explain the decision making on the timeline and location to monitor.

Chapter 4 analyzes two trusses with time-variant reliability of the components. The effects of the different positions of live loads, variations of the live loads and deterioration rates over time are investigated.

Chapter 5 presents an approach of analyzing available data to find the appropriate PDFs for the corresponding loading. The PDFs are formulated for three different distribution types based on developed stress-range bin histograms from the collected field monitoring data. Then the most suitable distribution type is determined by Goodness-of-fit test. The following fatigue reliability analysis is performed by using the reliability software RELSYS.

Chapter 6 presents a method of using the maximum observed stress value in a specified timeframe in a 93 days monitoring period. Type I EVDs are utilized to transform the PDF of EVDs during the monitoring period to the one at a series of discrete time points spanning the rest of its lifetime. Then the reliability for each girder and that of the whole bridge can be computed. Different cases for the lifetime system reliability are handled.

Chapter 7 provides the conclusions drawn from previous chapters and recommendations for further studies.

CHAPTER 2

TIME-INDEPENDENT & TIME-DEPENDENT RELIABILITY

2.1. Introduction

Civil engineers are always making effort to improve their designs to satisfy the budget and also assure the structural performance. The structural performance is one of the principal responsibilities for engineers to take. It is usual that complete information cannot be provided during the planning and design processes. Moreover, uncertainties existed along the process of design and assessment. Consider a beam example; its safety depends on both resistance and maximum load effect. The structural material properties, like strength, are not constant during its design life. The actual maximum applied load is also impossible to be predicted exactly. Therefore, probabilistic concepts and methods have to be used in a reliability-based approach.

2.2. Component reliability

The reliability of a component is usually related to the probability of occurrence of safe event, which can be defined by performance function of component as follows

$$g_{comp,i} = R_{comp,i} - S_{comp,i} \tag{2.1}$$

where $g_{comp,i}$ stands for component performance function under the limit state i, $R_{comp,i}$ stands for the resistance of component with limit state i, $S_{comp,i}$ means load effect associated with limit state i. When the load effect is larger than the resistance, the failure event occurs. Due to uncertainties associated with the component resistance and load effect, both resistance and load effect are treated as random variables. The probability of

failure of the component is predicted as

$$P_f = \phi(-\beta) \tag{2.2}$$

where ϕ is the cumulative Gaussian probability distribution function, β is the reliability index which usually is a quantitative measure of the safety, being expressed as

$$\beta = \frac{\mu_R - \mu_s}{\sqrt{\sigma_R^2 + \sigma_S^2}} \tag{2.3}$$

where both R and S are normally distributed, μ_R and μ_s are corresponding mean values, and σ_R and σ_S are the standard deviations for R and S, respectively.

If the resistance, R, and load effect, S, are lognormally distributed, the reliability index β is approximated as:

$$\beta = \frac{\ln(\frac{\mu_R}{\mu_s})}{\sqrt{V_R^2 + V_S^2}} \tag{2.4}$$

where $V_R = \sigma_R/\mu_R$ is the coefficient of variation (COV) of resistance, and $V_S = \sigma_S/\mu_S$ is the COV of component load effect.

2.3. System reliability

The reliability of a structural system is defined as the survival probability of a system, which is also a complementary part of probability of system failure, $P_{f(sys)} = 1 - P_{s(sys)}$. The violation of any limit state function result in the probability of failure of a system. One failure mode consists of a limit state function. The probability of failure of the system with n failure modes is expressed as:

$$P_{f(sys)} = P[any\ g_i < 0], i = 1,2, \dots, n \tag{2.5}$$

where g_i is the *i*th failure mode.

An exact calculation of $P_{f(sys)}$ can only be carried out by performing an integration of the joint probability density function $f_{X_1,X_2,\dots,X_k}(x_1,\dots,x_k)$ of the random variables $X=\{X_1,X_2,\dots,X_k\}$ involved in the problem over the failure region defined by the aforementioned performance functions (Ang and Tang 1984).

$$P_{f(sys)}=\int_{(E_1\cup\dots\cup E_n)}\int f_{X_1,X_2,\dots,X_k}(x_1,\dots,x_k)dx_1\dots dx_k \tag{2.6}$$

where E_i is the event of occurrence of *i*th failure mode. The failure of a system is a combination of all failure modes.

The First-order (FORM) or second-order (SORM) moment method is usually used to calculate the reliability of individual limit states. The lower and upper bounds for system probability of failure can be obtained as first-order bounds (Cornell 1967), or second-order bounds (Ditlevsen 1979). Another method to obtain the probability of failure of the system is by using Monte Carlo simulation. This simulation requires large number of samples and numerous repetitions to estimate system reliability.

2.4. Time-variant component and system reliability

The assumption that both loads and resistances are time-independent can simplify the calculation process. However, in reality, the probability density functions of resistances and load effects are experiencing changes during the structural life. The effects of corrosion, erosion and degradation make great impact on resistances of structural components. The live loads applied on the structure may also change over time. Ghosn et al. (2010) conclude that the connection between system safety and component safety depends on the system's topology, system model types (series, parallel, series-parallel),

member ductility and the statistical correlation between the strengths of the members. Combined these factors with the time effects, the components experiencing deterioration process may fail during the structural life. The failure of some components may result in the failure of system models or force redistribution in the system. Therefore, identification of the system model types and their members is essential for further time-variant reliability study.

CHAPTER 3

THE ROLE OF MONITORING IN BRIDGE ASSESSMENT

3.1 Introduction

According to NBI (National Bridge Inventory, www.fhwa.dot.gov/bridge/britab.cfm) data obtained from the U.S. Federal Highway Administration, it is found that the construction of bridges is developing rapidly since 1950s. Figure 3.1 shows the numbers of total bridges and deficient bridges constructed by year. From the figure, it is shown that the construction of bridges develops rapidly during 1960s-1970s. Figure 3.2 shows that many old bridges are now in need of maintenance, and that percentage of deficient bridges is growing.

Both figures indicate that there is an emerging need of maintenance, repair and replacement for deficient bridges. The research in establishing a practical and economic maintenance strategy by searching methods and applying technologies to assess deficient structures is in great demand.

3.2 Structural Health Monitoring Strategies

Structural health monitoring (SHM) is an area with growing concern and extending potential of exploring innovative approaches. The United States government makes an expense of more than $200 billion every year on maintenance and repair for facilities, plant and equipment (Balageas, 2006). As a process of implementing inspection and maintenance strategy on structures, SHM includes the observation and collection of data on a system during a period of time from an array of sensors, the extraction of related

data of damage-sensitive features from these measurements, and the statistical analysis of these data to determine the current state of structural health (Frangopol and Messervey, 2009).

For numerical structural analysis, structural responses such as displacement and strain at certain locations can be measured continuously or in intervals. The data obtained from monitoring can be applied to update reliability profiles of structure components and systems. However, the cost of SHM is expensive. Thus, making good use of monitoring data to enhance the reliability analysis to set up appropriate maintenance strategies within the budget is necessary and crucial.

3.3 Decision making about the timeline and location to monitor

Consideration of the uncertainty associated with critical loading and structural parameters is one of the most critical issues in assessing the condition of existing civil infrastructure (Catbas et al. 2008). Uncertainties are classified in two main categories: aleatory and epistemic. Aleatory uncertainty characterizes the inherent randomness in the behavior of the system under study. Epistemic uncertainty characterizes the lack of knowledge in monitoring (Frangopol & Messervey, 2009). The existence of these two types of uncertainties will probably result in the occurrences of many events, such as some component failure, monitoring data reading error. In order to prevent and minimize the economic loss due to these events, field monitoring data is used to update structural profiles and decisions have to be made on when and where to monitor based on updated monitoring information.

3.4 Time-dependent structural performance

It is common sense that structural reliability is decreasing during time. Therefore, the performance function changes over time.

$$g_i(t) = (R_s(t))_i - \big(Q(t)\big)_i \tag{3.1}$$

where $g_i(t)$ is performance function of failure mode i at the time of t. $R_s(t))_i$ and $(Q(t))_i$ are the corresponding values of component resistance and load effect, respectively. The data obtained from monitoring can be used to update the performance function. Before obtaining the data, one important thing is to determine where to focus on the monitoring priority. For example, Figures 3.3 and 3.4 show a three-component series and parallel system, respectively. In Figure 3.3, components 1, 2 and 3 are in a series with probability of failure 0.002, 0.006 and 0.004, respectively. For series system, any member failure will result in the failure of system. So the member with the highest probability of failure should receive the monitoring priority. In Figure 3.4, components 1, 2 and 3 are in parallel. For the parallel system, the failure of all members results in system failure. That is to say, the strongest member with the lowest probability of failure, which is the most critical member, should receive monitoring priority.

Various deterioration rates can be another factor affecting the monitoring priority. Figures 3.5 and 3.6 show series system and parallel system which are both comprised of three bars with variation in geometry and material properties. There is a concentrated load P applied on the three bars. It is assumed that the horizontal bar linking the three bars in the parallel system in Figure 3.6 is perfectly rigid and constrained to remain horizontal. Bars 1, 2 and 3 have the initial cross section areas of 2 in^2, 4 in^2 and 3 in^2,

respectively. All of the bars have the same mean value of yield stress 10 ksi. The standard deviations of resistances for the three bars are 2 ksi. Deterioration rates applied on bars 1, 2 and 3 are 0.01 in^2/year, 0.04 in^2/year and 0.04 in^2/year, respectively. The mean of applied load P is 5 kips. All the random variables in this example are assumed normally distributed.

The effects of time and deterioration rates on component reliability are investigated. Figure 3.7 presents the performance of three bars connected as a series system in a lifetime of 50 years. A reliability index threshold $\beta_{min} = 3.0$ is established for further study on maintenance and monitoring inspection schedule. It is shown that reliability of component 2 with the largest deterioration rate decreases sharply from the most reliable member in the system to the least reliable one. The more economical way to monitor the three bars is to give monitoring priority to the weakest member having the highest probability of inducing system failure. Therefore, the monitoring priority is given to component 1 initially, then moves to component 3 and shifts to component 2 at last. However, different from series system, Figure 3.8 indicates a different critical monitoring path for parallel system. For system safety, it is supposed to find the strongest member whose failure will probably result in the system failure. Component 2 is selected to receive monitoring priority until point A, then the priority shifts to component 1. Both cases show that monitoring priority is changing due to different deterioration rates.

In general, thresholds of performance indicators are helpful in making inspection and maintenance decisions. Being able to provide data to formulate time-variant performance indicators, SHM is a potential important technology optimizing allocation of available

funds via assessing structures accurately and prioritizing repairs and maintenance (Frangopol and Messervey, 2009).

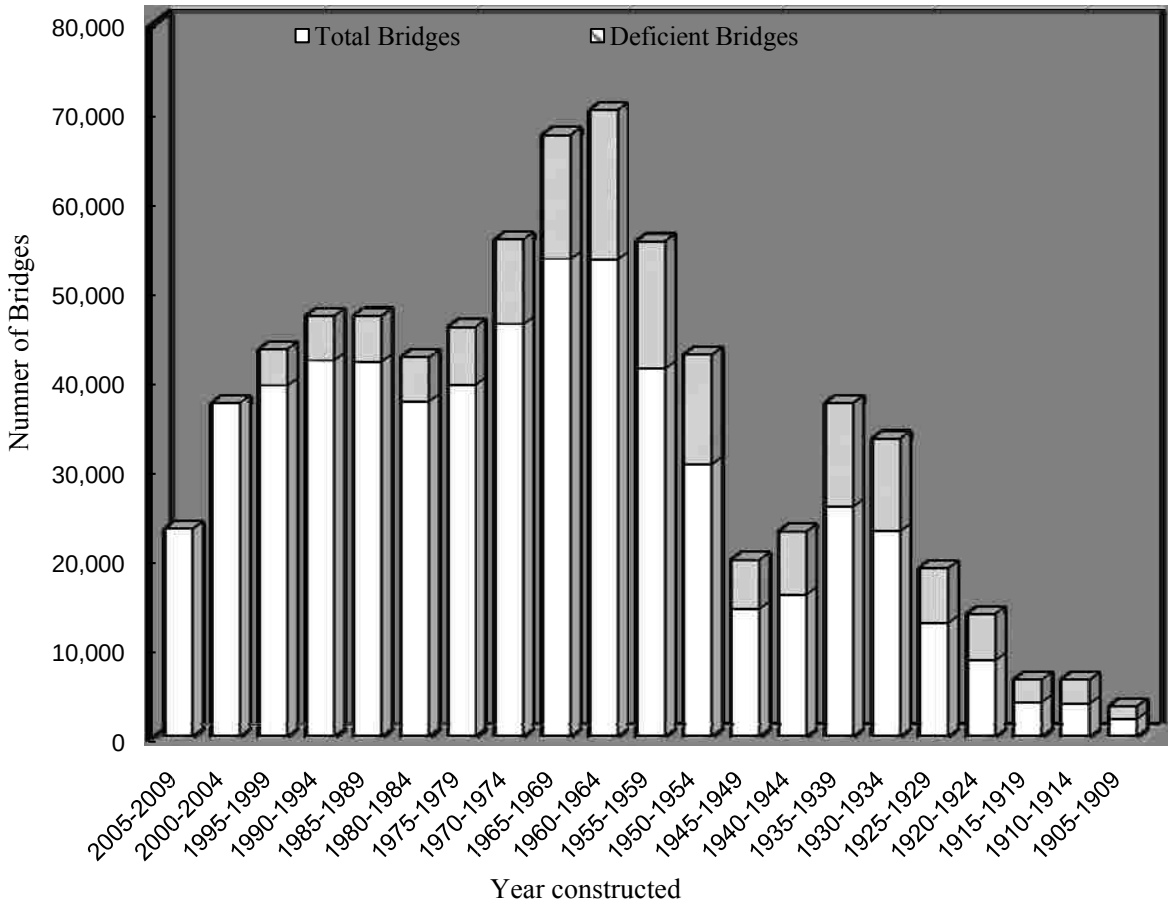

Figure 3.1 Numbers of total and deficient bridges in US classified by year constructed. (Adapted from National Bridge Inventory Statistics, http://www.fhwa.dot.gov/bridge/britab.cfm.)

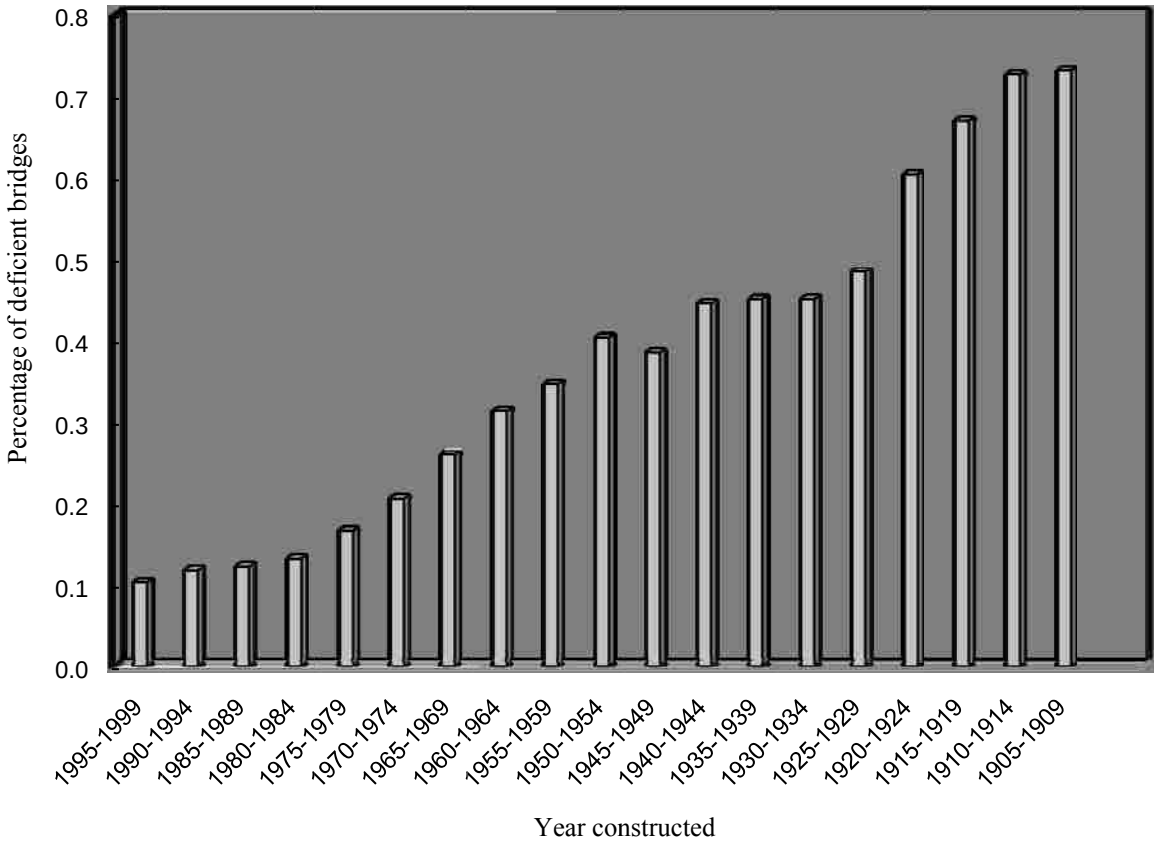

Figure 3.2 Percentage of deficient bridges over total numbers in US classified by year constructed. (Adapted from National Bridge Inventory Statistics, http://www.fhwa.dot.gov/bridge/britab.cfm.)

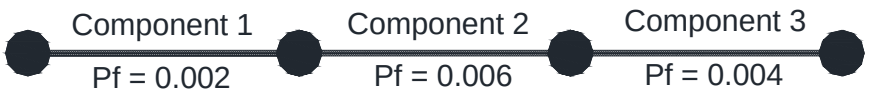

Figure 3.3 Three-component-series system with probabilities of failure of 0.002, 0.006 and 0.004 respectively

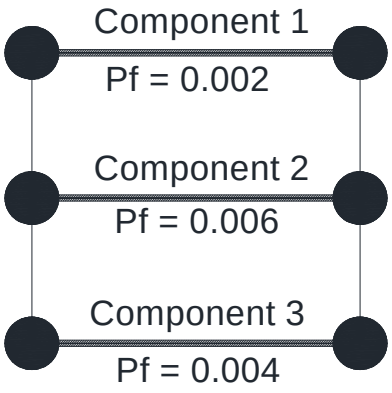

Figure 3.4 Three-component-parallel system with probabilities of failure of 0.002, 0.006 and 0.004 respectively

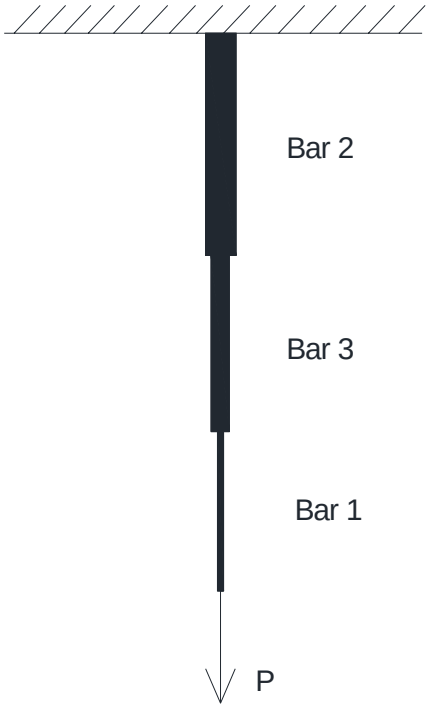

Figure 3.5 Three bar series system

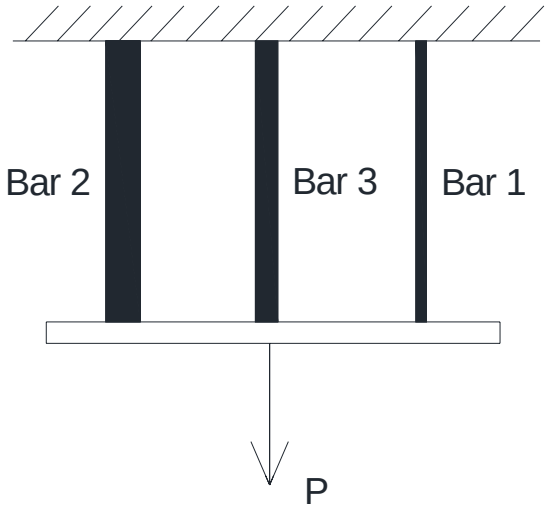

Figure 3.6 Three bar parallel system

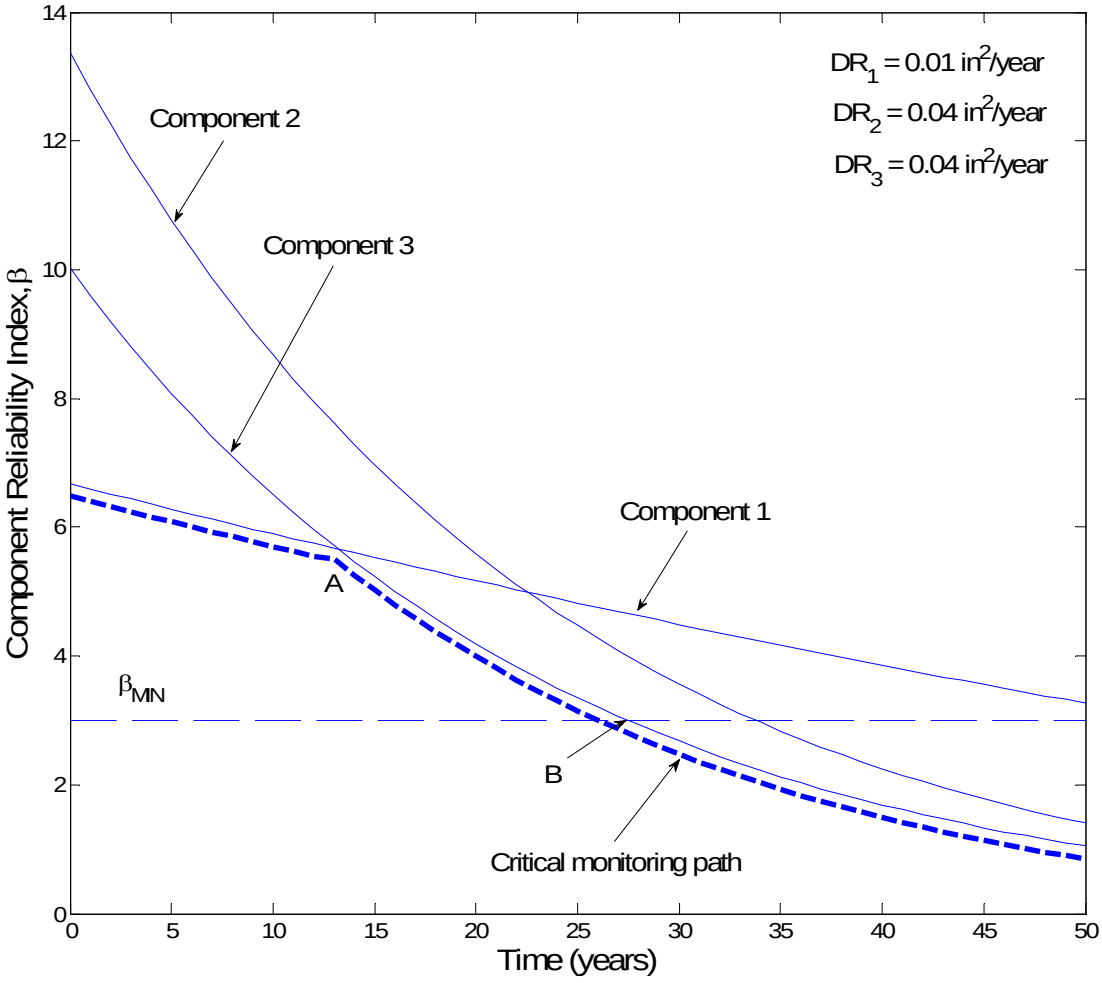

Figure 3.7 Time-variant component reliability of series system

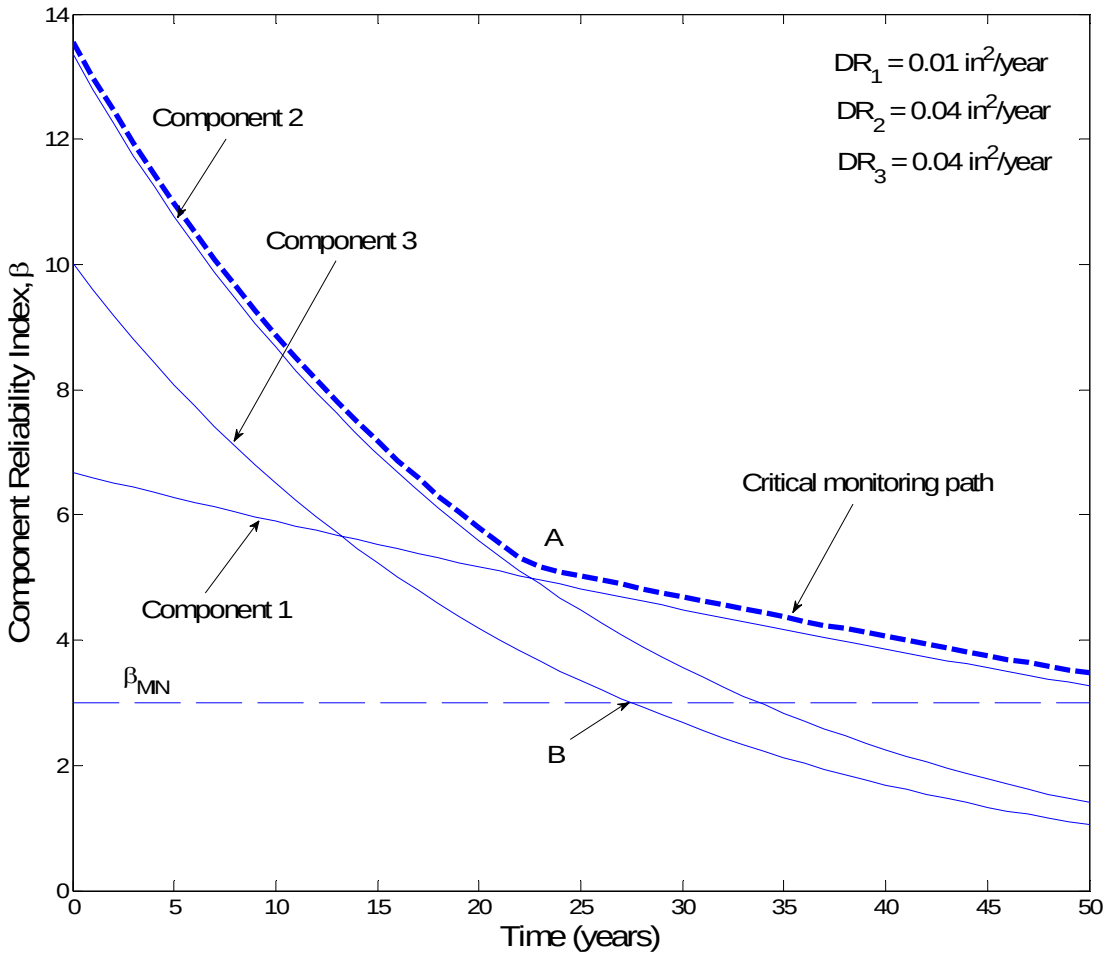

Figure 3.8 Time-variant component reliability of parallel system

CHAPTER 4

APPLICATIONS TO TRUSSES

4.1. Ten Bar Truss

The time effect on structural reliability will be studied in this chapter. Consider the ten-bar symmetric truss system shown in Figure 4.1. The truss is subjected to three load cases. Some bars are assumed to have different deterioration rates (DR) in each case. The strength of all the components is supposed in a normal distribution with initial mean and standard deviation of 36 ksi and 2.88 ksi, respectively. The coefficient of variation of the strength is 0.08. The applied load P is also supposed normally distributed with initial mean and standard deviation of 20 kips and 2 kips. Its coefficient of variation remains 0.1. The annual live load increase rate (LIR) is assumed to be a constant value of 0.01 kips /year. All the bars are assumed to have the same initial cross section areas 2 in^2 and modulus of elasticity E = 29000 ksi.

The purpose here is to compute the time-variant component reliability index of each bar for every load case and find the most critical member for different reliability index thresholds under the various deterioration rates.

Consider the effect of load and environment on component reliability. Predictive models for live load and resistance deterioration are introduced in detail below.

Live load predictive model:

(1) Vertical load P (case 1 & case 2):

The vertical load P is assumed to be normally distributed and has an initial mean

value $\mu_p(0) = 20\ kips$ with a constant annual increase rate (LIR) of 0.01kips/year. The mean of the time-variant load is given by:

$$\mu_P(t) = (1 + LIR) \times \mu_P(t-1) = (1 + LIR)^t \times \mu_P(0) \tag{4.1}$$

where $\mu_P(t), \mu_P(t-1)\ and\ \mu_P(0)$ is the mean value of vertical load P at time *t*, *t*-1 and 0, respectively.

The standard deviation of the vertical load P is also assumed to increase over time with a constant annual increase rate IR = 0.01 kips /year. Initial standard deviation of vertical load P is $\sigma_P(0) = 0.2$ kip. The standard deviation of the time-variant load is given by:

$$\sigma_P(t) = (1 + IR) \times \sigma_P(t-1) = (1 + IR)^t \times \sigma_P(0) \tag{4.2}$$

The coefficient of variation (COV) is useful because the standard deviation must always be understood in the context of the mean of the load. For the vertical load P, its COV is given by:

$$COV_P = \frac{\sigma_P(t)}{\mu_P(t)} = 0.1 \tag{4.3}$$

(2) Horizontal load H (case 2 & case 3):

Assume the horizontal load H is normally distributed and has an initial mean value $\mu_H(0) = 20$ kip with a constant annual increase rate (LIR) of 0.01 kips /year. The mean of the time-variant load is given by:

$$\mu_H(t) = (1 + LIR) \times \mu_H(t-1) = (1 + LIR)^t \times \mu_H(0) \tag{4.4}$$

The standard deviation of the horizontal load H is also assumed to increase over time with a constant annual increase rate IR=0.01 kips /year. Initial standard deviation of horizontal load H is $\sigma_H(0) = 0.2$ kip. The standard deviation of the time-variant load is given by:

$$\sigma_H(t) = (1 + IR) \times \sigma_H(t-1) = (1 + IR)^t \times \sigma_H(0) \tag{4.5}$$

For the horizontal load H, its COV is given by:

$$COV_H = \frac{\sigma_H(t)}{\mu_H(t)} = 0.1 \tag{4.6}$$

Time-variant mean, standard deviation and COV for the vertical load P are shown in Figure 4.2.

Resistance degradation predictive model:

(1) Cross section area of the component

The truss system is assumed to begin to deteriorate the day it is placed in service, which means deterioration begins when t = 0. A predictive model is needed to estimate how the resistance changes over time. The resistance deterioration model is usually derived theoretically, obtained from laboratory data or extrapolated from the behavior of similar structures under the same conditions (Estes and Frangopol 2005). The resistance deterioration model used in this example is deterministic. It is assumed that the resistance deterioration is due to the loss of cross section area over time. The remaining cross section area of component i at time t is given as:

$$A_i(t) = (1 - DR_i) \times A_i(t-1) = (1 - DR_i)^t \times A_i(0) \tag{4.7}$$

where DR is the deterioration rate of component i, $A_i(t), A_i(t-1)$ *and* $A_i(0)$ is the cross section area of the component i at time *t*, *t*-1 and 0, respectively.

(2) Mean of the resistance

The mean of the resistance of component at time t is described as follows:

$$\mu_{Ri}(t) = A_i(t) \times (\mu_{Fy})_i \tag{4.8}$$

where $(\mu_{Fy})_i$ is the mean of the random yield stress Fy of component. For ductile structure, the member will still carry loads when its strength reaches its yield stress. For brittle structure, the member will fail completely, and it stops carrying any load after failing.

(3) Standard deviation of the resistance

The standard deviation of the resistance is assumed to change over time with a constant rate of 0.01, due to existed uncertainties. The standard deviation of resistance of component i at time t is described as:

$$\sigma_{Ri}(t) = (1 + DR_i) \times \sigma_{Ri}(t-1) = (1 + DR_i)^t \times \sigma_{Ri}(0) \tag{4.9}$$

where $\sigma_{Ri}(t), \sigma_{Ri}(t-1)$ *and* $\sigma_{Ri}(0)$ stands for the standard deviation of the resistance of component i at time *t*, *t*-1 and 0, respectively.

The components are considered to deteriorate in different rates. Figure 4.5 shows eight deterioration rates ranging from 0.01 in^2/year to 0.08 in^2/year will be used during the truss design life of 50 years.

Three load cases are described below, the behavior of components under different reliability index thresholds are studied.

Load case 1:

In Figure 4.6, the truss is subjected to two concentrated loads P. Three situations are considered: 1. Only one bar is deteriorating; 2. Two bars are deteriorating with different deterioration rates; 3. Three bars are deteriorating with different deterioration rates. For all the situations considered, the other members remain intact. The forces in each member are shown in Table 4.1.

Figure 4.7 shows the time-variant component reliability for load case 1 when a deterioration rate of 2% is imposed on bar 4. Statistical independence is assumed among the resistances of all the bars. When a bar begins to deteriorate, the truss is not assumed symmetric due to the changes occurred on the stiffness of the bars.

It is seen from Figure 4.7 that bar 4 deteriorates so fast that its component reliability index decreases far beyond bars 1 and 9 which have the lowest initial reliability index β. The reliability index threshold is set as $\beta = 6.08$. With the establishment of the reliability threshold, it is found that the most critical member is bars 1 and 9 before year 12. After that, the critical member is bar 4. After bar 4 fails, the critical members become to be bars 1 and 9 again. It is interesting to find out that bars 5 and 6 become more reliable since their member forces decrease after first member fails.

Consider bars 3 and 4 which deteriorate with different rates 0.03 in^2/year and 0.04 in^2/year, respectively, and a constant live load increase rate of 0.01 kips/year. Figure 4.8 shows how damages on bars 3 and 4 make impact the variation of the reliability indices of the other bars when symmetric loads P are applied on ductile members. Two reliability index thresholds are set: $\beta_1 = 6.04$, where the reliability indices of member 4 and

members 1 and 9 are equal and $\beta_2 = 2.67$, where the reliability indices of bars 3 and 4 are equal at year 27.

Finally, the case of three bars with different deterioration rates is shown in Figure 4.9. Bars 4, 5 and 6 deteriorate with individual rates of 0.05 in^2/year, 0.07 in^2/year and 0.04 in^2/year, respectively. Before the component with lowest reliability index reaches the first threshold $\beta_1 = 6.5$, the critical members are 1 and 9. Then bar 4 becomes the most critical one until its failure. Bars 1 and 9 are critical members again until bar 6 deteriorates faster and its component reliability becomes the most critical after the second reliability index threshold $\beta_2 = 4.2$ is reached at year 41.

Load case 2:

Figure 4.10 shows the truss subjected to the horizontal load H. Three situations are considered: 1. Only one bar is deteriorating; 2. Two bars are deteriorating with different deterioration rates; 3. Three bars are deteriorating with different deterioration rates. For all the situations considered, the other members remain intact. The member forces are shown in Table 4.2.

Figure 4.11 indicates that bar 4 deteriorates with a rate of 0.02 in^2/year, live load increases with a constant annual rate of 0.01 kips/year. With only one horizontal load applied, the initial component reliability indices of most bars are higher than in the first case.

Figure 4.12 shows the second situation of load case 2: bars 3 and 4 deteriorate with rates 0.02 in^2/year and 0.03 in^2/year, respectively, live load increases with an annual rate

of 0.01 kips/year. The change of bar 3's reliability index over time is not as obvious as that of bar 4.

Figure 4.13 shows the third situation considered for load case 2: bars 4, 5 and 6 deteriorate with individual deterioration rates: 0.05 in^2/year, 0.07 in^2/year and 0.04 in^2/year, respectively, and live load increases with a rate of 0.01 kips/year. Obviously, bars 4 and 5 become much less reliable than other members due to their large deteriorating rates, and bar 5 becomes the critical member after the failure of bar 4.

Load case 3:

Figure 4.14 shows the truss subjected to load case 3: two symmetric concentrated vertical loads P plus one horizontal load H. The same three situations are considered: 1. Only one bar is deteriorating; 2. Two bars are deteriorating with different deterioration rates; 3. Three bars are deteriorating with different deterioration rates. For all the situations considered, the other members remain intact. The forces in each member are shown in Table 4.3.

Figure 4.15 shows the effect of bar 4 with a deterioration rate of 0.02 in^2/year on the variation of component reliability indices of all members. Compared with Figures 4.7 and 4.11, the third load case is much more critical regarding the reliability loss. The reliability index threshold is set as 4.18 in this case. Bars 1 and 9 are the critical members before the failure of member 4 and become the most critical after the failure of bar 4. The reliability index of bar 2 increases after the first member fails.

Comparing intact member forces in Tables 4.1, 4.2 and 4.3, it is found that member forces in Table 4.3 are the sum of forces in Tables 4.1 and 4.2. Figure 4.15 indicates that

component reliability indices are not simply the sum of reliability indices associated with cases 1 and 2.

The second situation considered for load case 3 is that two bars are deteriorating, DR3 (deterioration rate) = 0.03 in^2/year, DR4 = 0.02 in^2/year, and the load annual increase rate is 0.01 kips/year. At the beginning, bar 9 is the most critical member in the system, then the effect of deterioration on bar 4 makes its reliability decrease very fast until reaching the first threshold 4.20.

Figure 4.17 shows the effect of various deteriorating rates of bars 4, 5 and 6 on time-variant reliability indices: DR4 = 0.05 in^2/year, DR5 = 0.07 in^2/year and DR6 = 0.04 in^2/year. Member force in bar 6 changes from compression force to tension force after the failure of bar 4.

4.2. 11 Bar Truss

A second example is shown in order to demonstrate the effect of resistance deterioration and live loads on structural reliability. Consider the 11 bar truss in Figure 4.18, including loading, deterioration, geometry and strength characteristics. The cross section areas of bars 1 to 7 are 1 in^2 and bars 8 to 11 are 0.25 in^2. Yield stresses and live load are assumed random variables with a normal distribution. The mean of yield stresses for bars 1 to 7 are 20 ksi in tension and 10 ksi in compression, for bars 8 to 11 are 10 ksi in tension and 5 ksi in compression. The coefficient of variation (c.o.v) for all the resistances of components is 0.1. The applied loads increase constantly by 0.01 kips/year, its initial mean value is 1 kip with a constant c.o.v 0.1. Modulus of elasticity E = 29000 ksi. Two load cases applied on the truss are studied to investigate the effect of time and

deterioration on structural reliability, respectively. The situations of time-independent and time-dependent are both considered.

For the time-independent case, two unsymmetrical loads increase constantly from zero are applied. The truss members will be analyzed by brittle and ductile behaviors. Compute component reliability index for each bar when loads P increase constantly. Five categories of member damage states considered are shown in Table 4.6.

Figures 4.19 and 4.20 show component reliability index of each bar versus mean value of loads P applying on the intact truss. Two assumptions are made: First, the member is assumed to fail when its reliability index drops to zero. Second, all the components are considered as perfectly ductile or brittle. Ductile members will carry their mean load-carrying capacity after failure. Brittle members cannot carry any load after β reaches zero.

Figures 4.21 and 4.22 show the effect of "moderate damage" (DF = 0.50) applied on member 5, which causes variation of reliability indices on the other members for brittle and ductile failure of components.

Figures 4.23 and 4.24 show the case when "complete damage" (DF = 1.0) is applied on member 5 and member 10 of the truss for brittle components, respectively.

For the time-dependent case, Figure 4.25 presents that a horizontal load P which increases nonlinearly is applied on the truss, as indicated in Equation (4.4).

Case 1: in Figure 4.26, it is assumed that bar 9 deteriorates with a rate of 0.02 in^2/year and the load increases with the rate 0.01 kips/year. Before the failure of first member, the

reliability indices of bars 9 and 11 decrease faster than the other bars due to their smaller cross section areas and lower yield stresses of compression members.

Case 2: Figure 4.27 shows case 2 with two deteriorating bars: bars 8 and 9 deteriorate with rates of 0.03 in^2/year and 0.02 in^2/year, respectively. After the failure of members 9 and 11, the truss becomes deterministic structure. The member forces on bars 8 and 10 increase so rapidly that their reliability indices decrease to zero until the truss fails.

Case 3: it shows three bars deteriorating with deterioration rates of DR1 = 0.05 in^2/year, DR8 = 0.04 in^2/year and DR9 = 0.02 in^2/year. From Figure 4.28, bar 1, which has the greatest deteriorates rate, becomes the most critical member after the failure of bars 9 and 11 until its failure induces system failure. Bar 10's reliability index value fluctuates due to increasing applied load and member force redistribution.

4.3. Conclusions

This chapter proposes an approach to examine the effects of structural deterioration and load increase on the time-variant reliability of truss members and systems.

From the results obtained from different load cases applied on two deteriorating truss structures, the time-variant reliability of structural members may decrease, remain the same or even increase, depending on member forces, material properties, cross section areas, deterioration rates, component ductility and structural configuration.

Member forces may experience sudden changes due to force redistribution after failure of some component. Ductile members are more reliable than brittle members.

Reliability index can be used to evaluate structural lifetime performance by weakest-link systems. The component with the lowest value of reliability index should receive

monitoring priority. Conversely, in parallel fail-safe systems, the most reliable component should also receive monitoring priority.

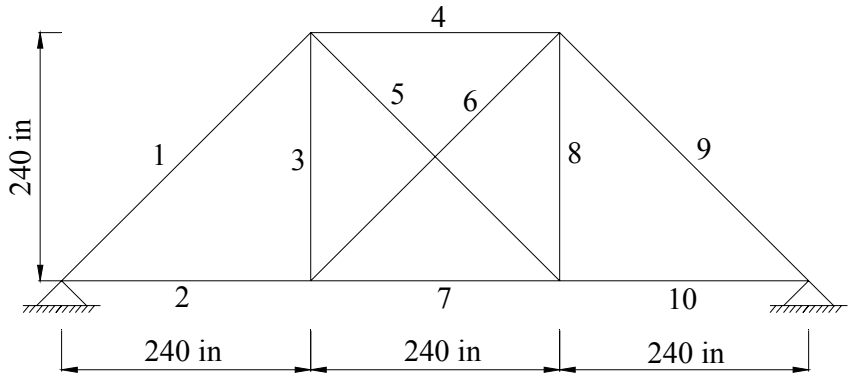

Figure 4.1 Ten-bar one-story truss example (From Frangopol and Curley, 1987)

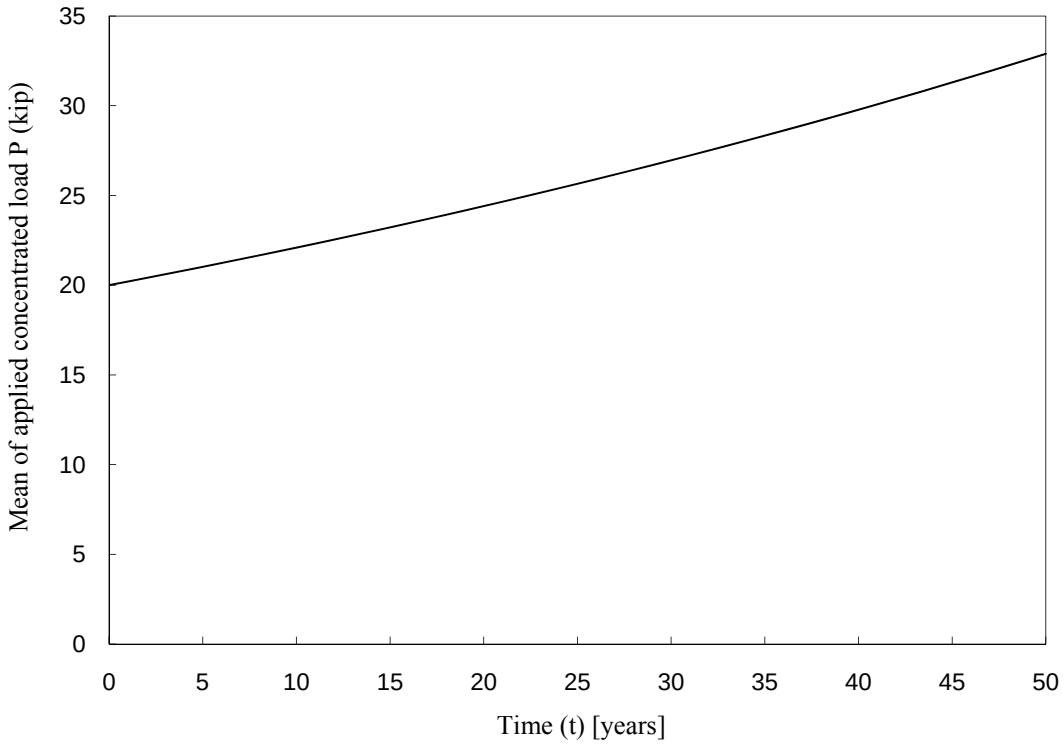

Figure 4.2 Time-variant mean of vertical load P

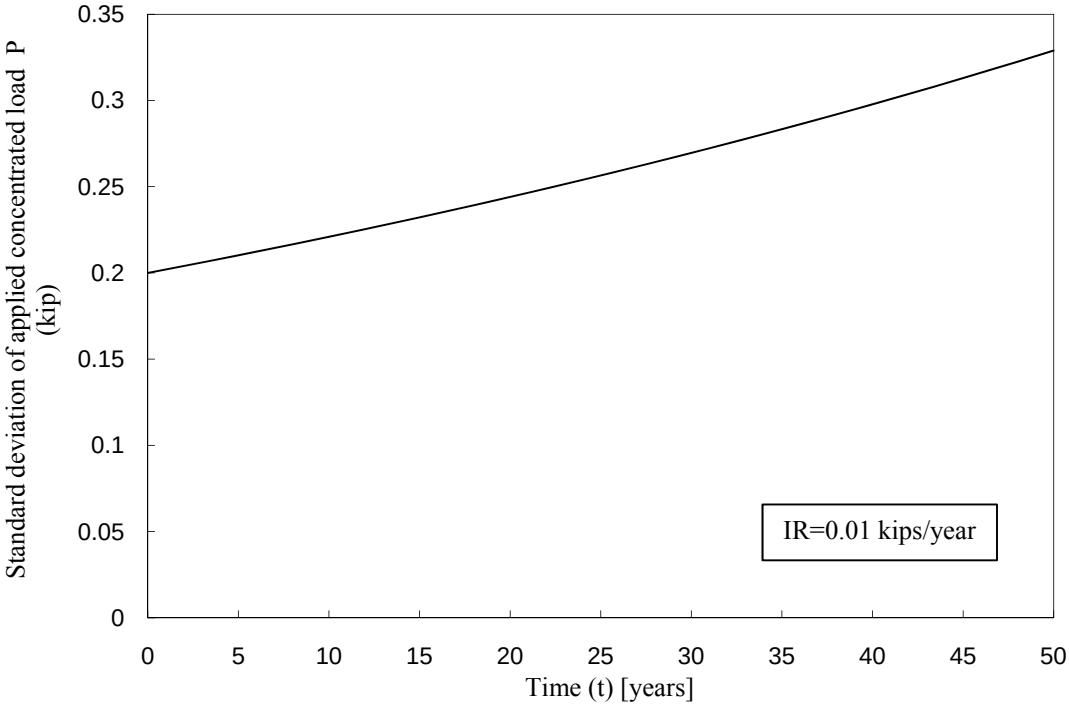

Figure 4.3 Time-variant standard deviation of vertical load P

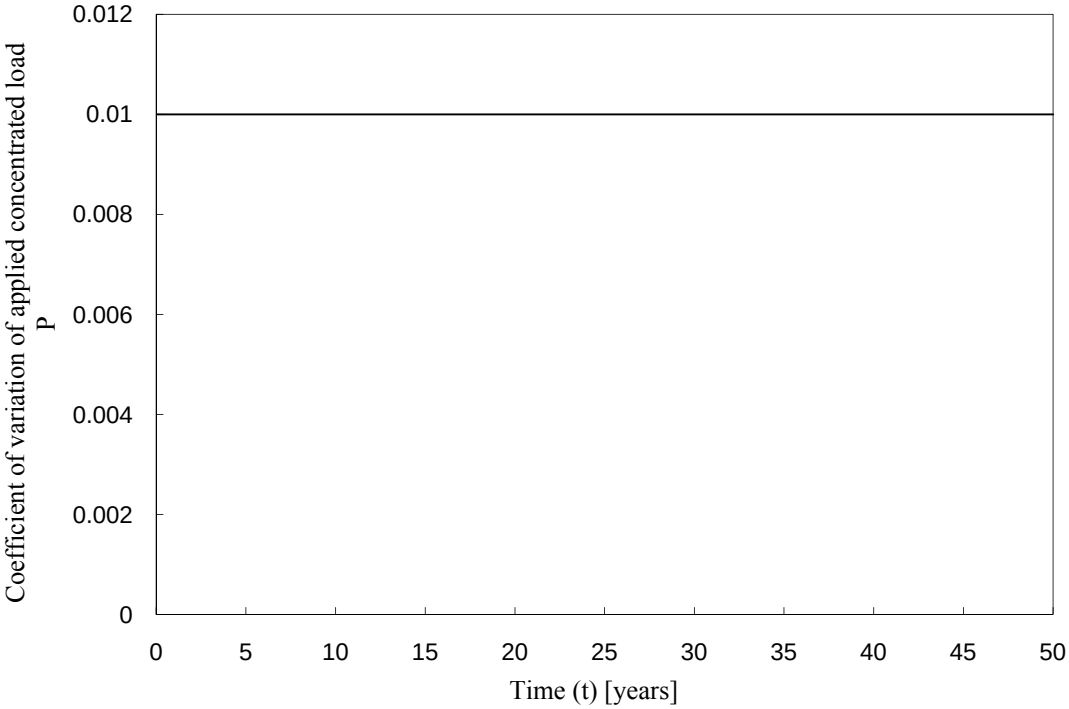

Figure 4.4 Time-variant coefficient of variation of vertical load P

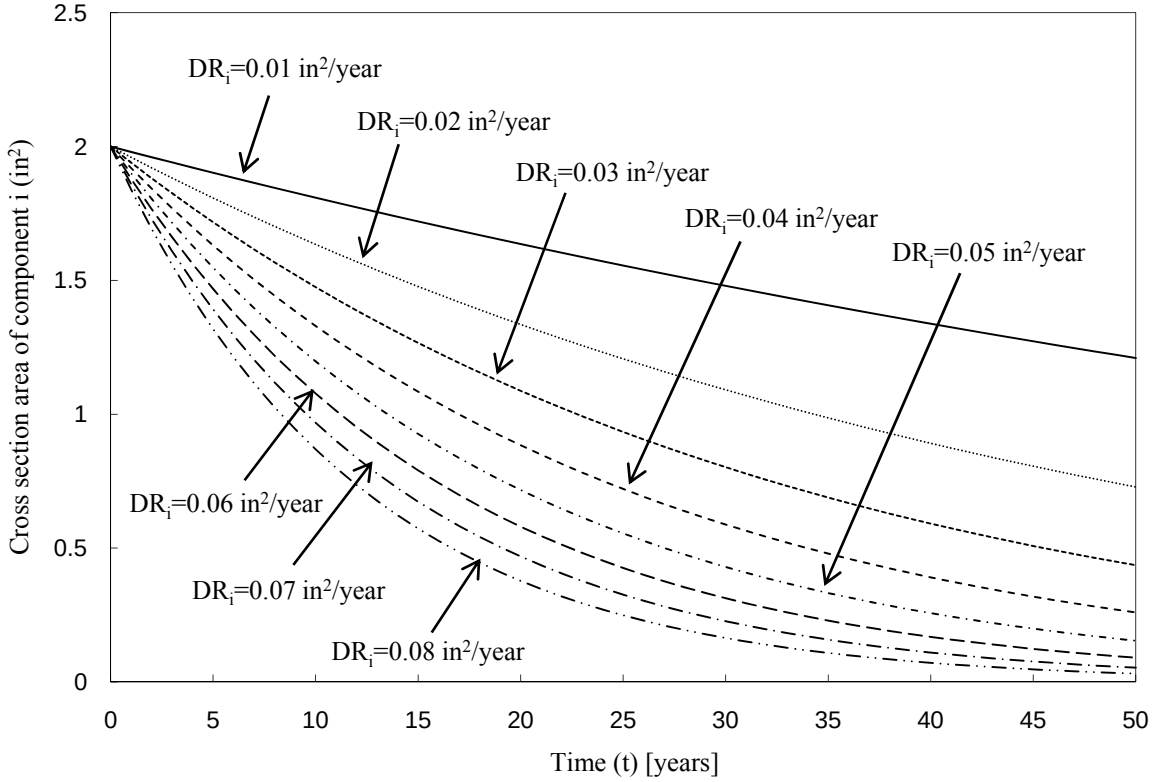

Figure 4.5 Time-variant cross section area of component *i*

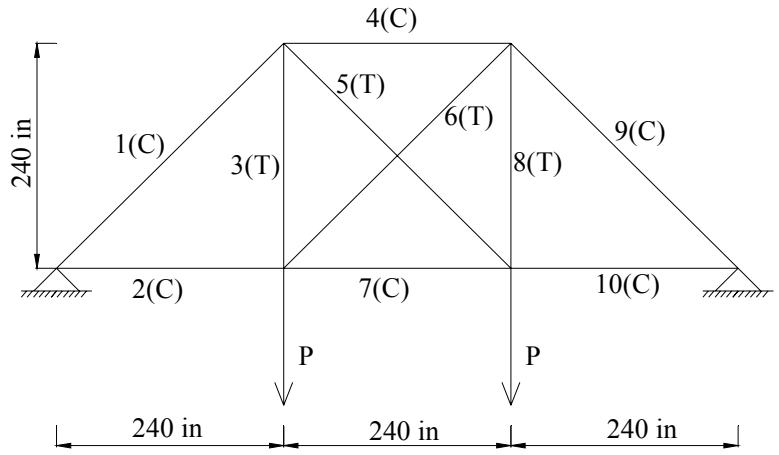

Figure 4.6 Load case 1: two symmetric concentrated loads

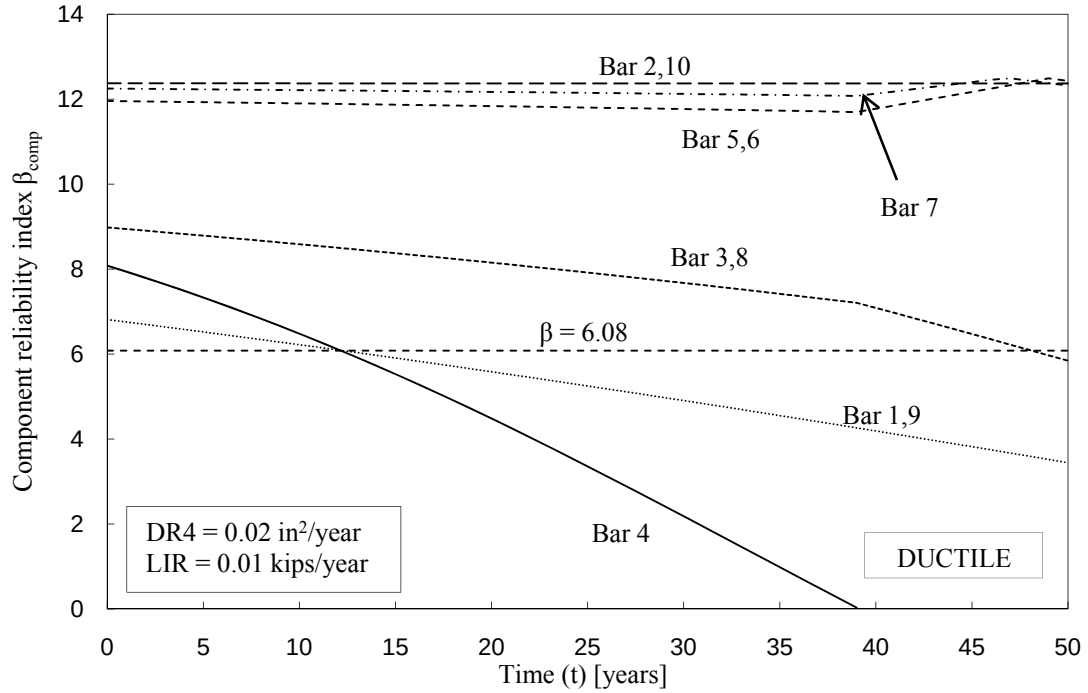

Figure 4.7 Effect of deterioration on bar 4 and load increase on the time-variant component reliability index β

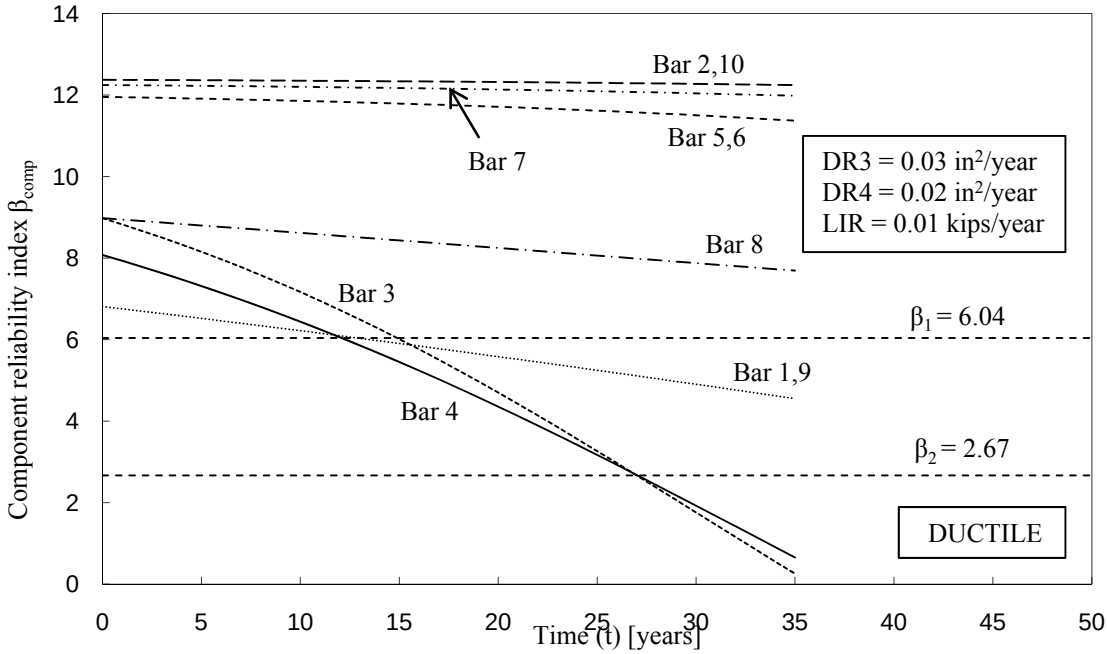

Figure 4.8 Effect of deterioration on bars 3 and 4 and load increase on the time-variant component reliability index β

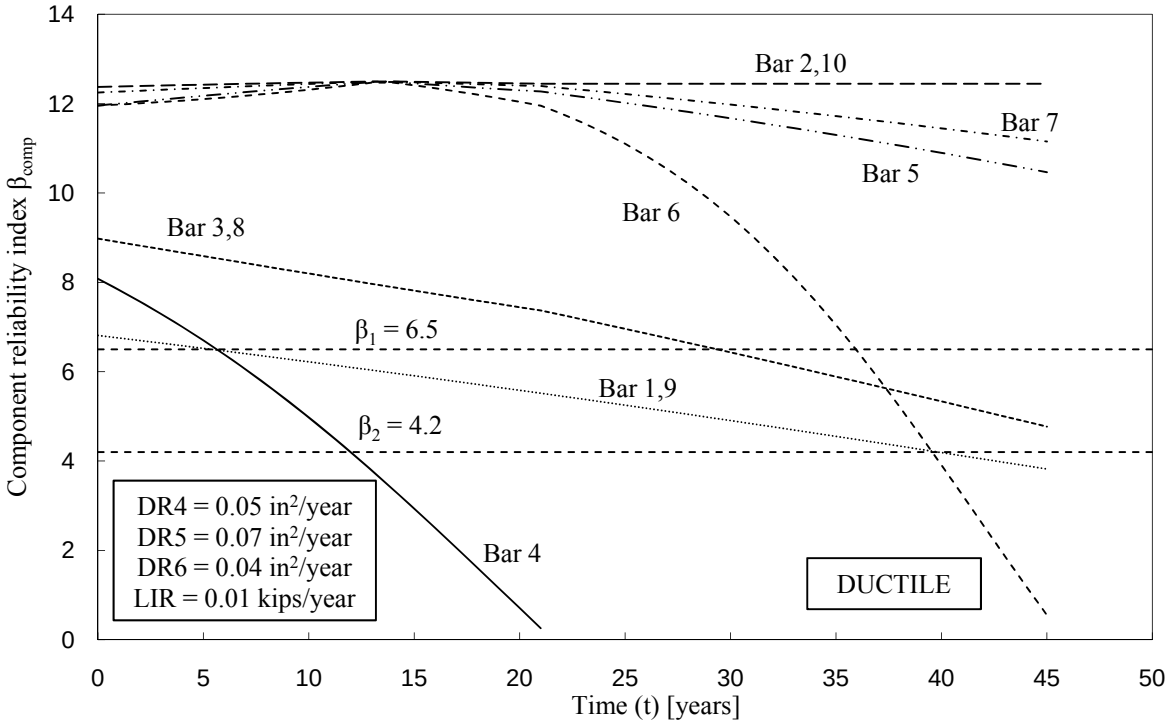

Figure 4.9 Effect of deterioration on bars 4, 5 and 6 and load increase on the time-variant component reliability index β

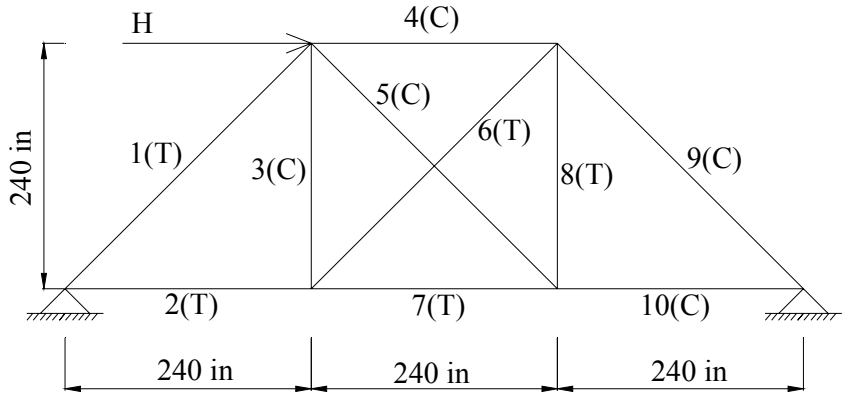

Figure 4.10 Load case 2: one horizontal load

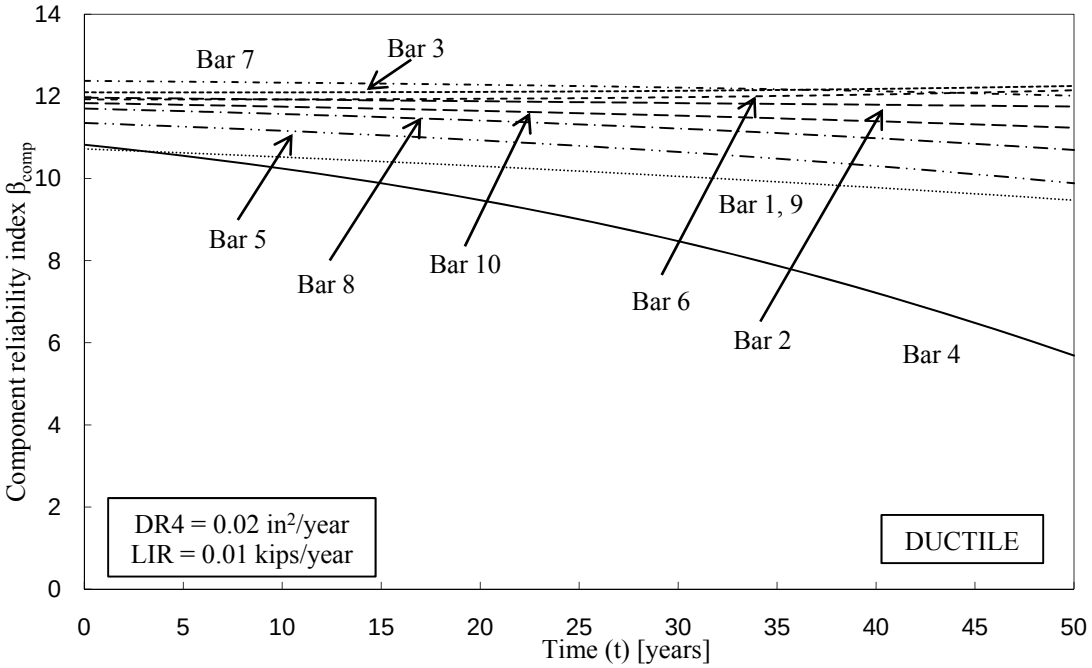

Figure 4.11 Effect of deterioration on bar 4 and load increase on the time-variant component reliability index β

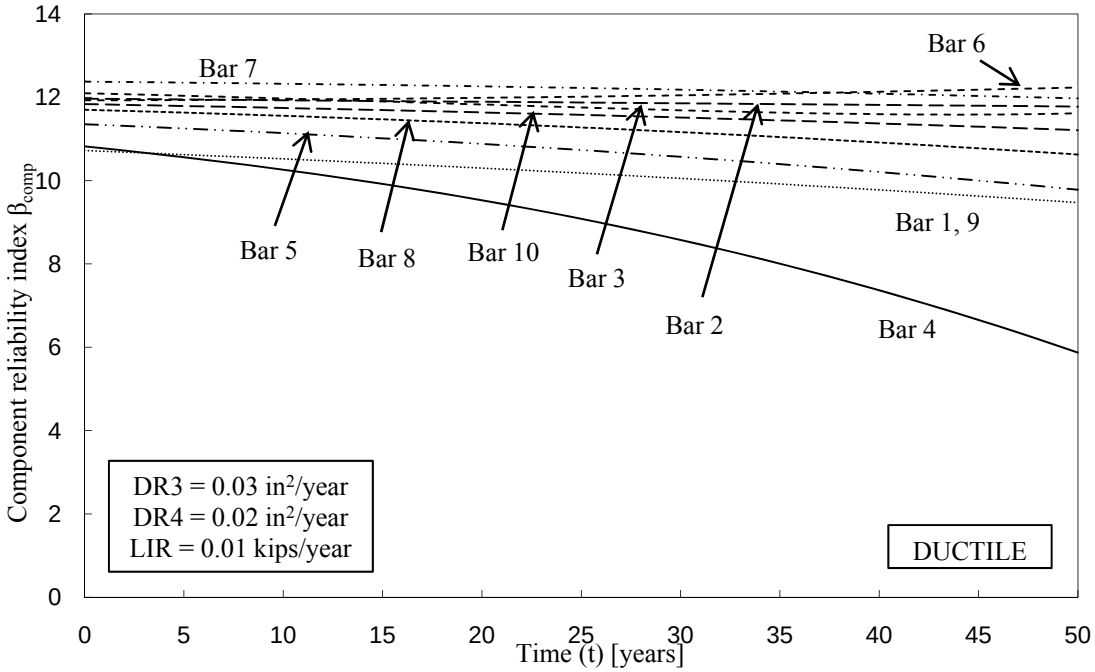

Figure 4.12 Effect of deterioration on bars 3 and 4 and load increase on the time-variant component reliability index β

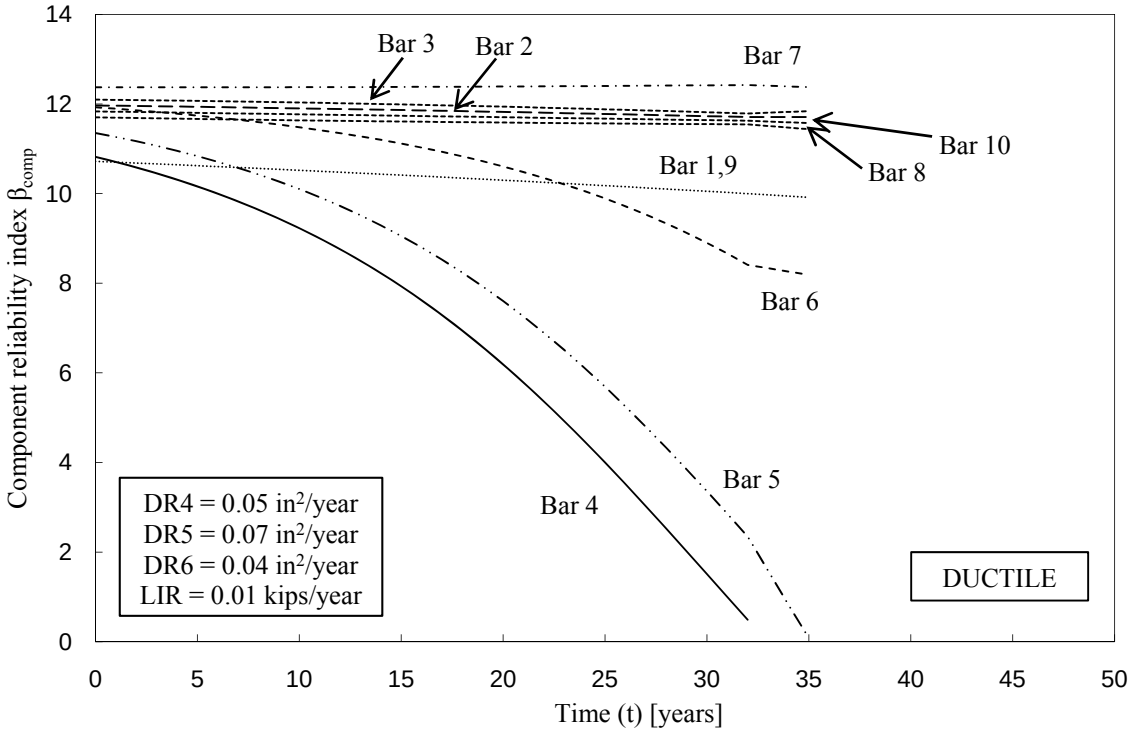

Figure 4.13 Effect of deterioration on bars 4, 5 and 6 and load increase on the time-variant component reliability index β

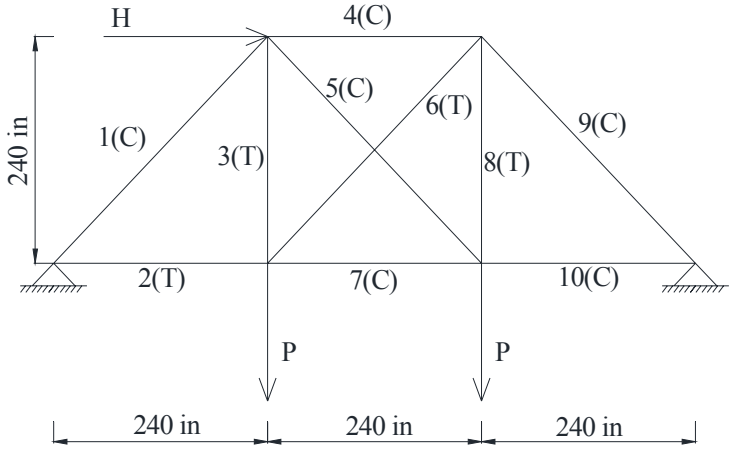

Figure 4.14 Load case 3: two symmetric concentrated loads plus one horizontal load

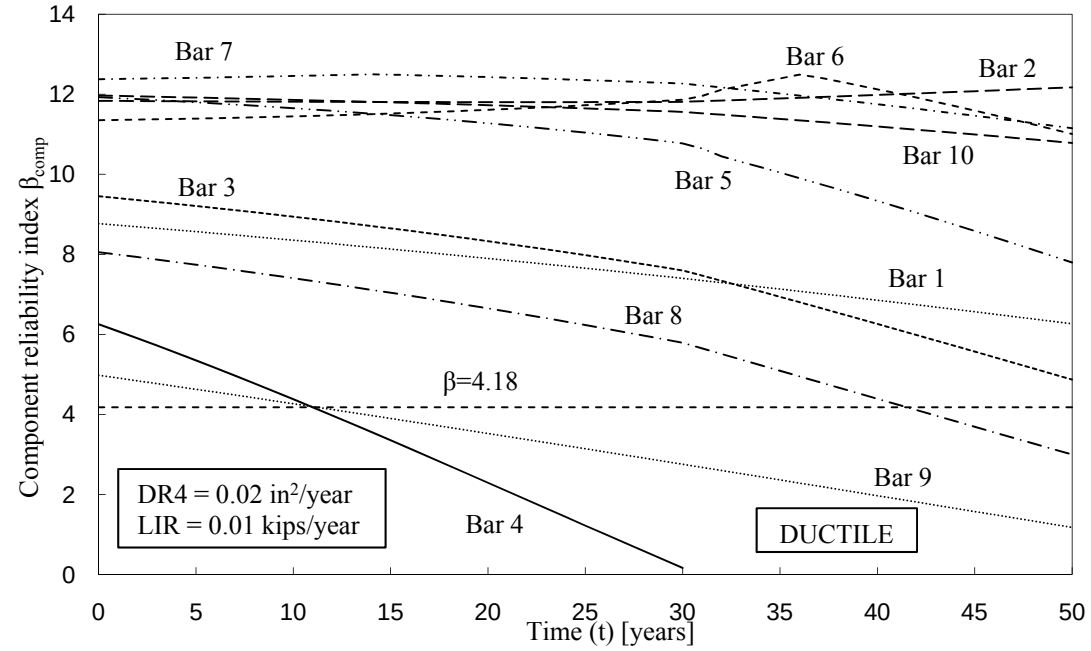

Figure 4.15 Effect of deterioration on bar 4 and load increase on the time-variant component reliability index β

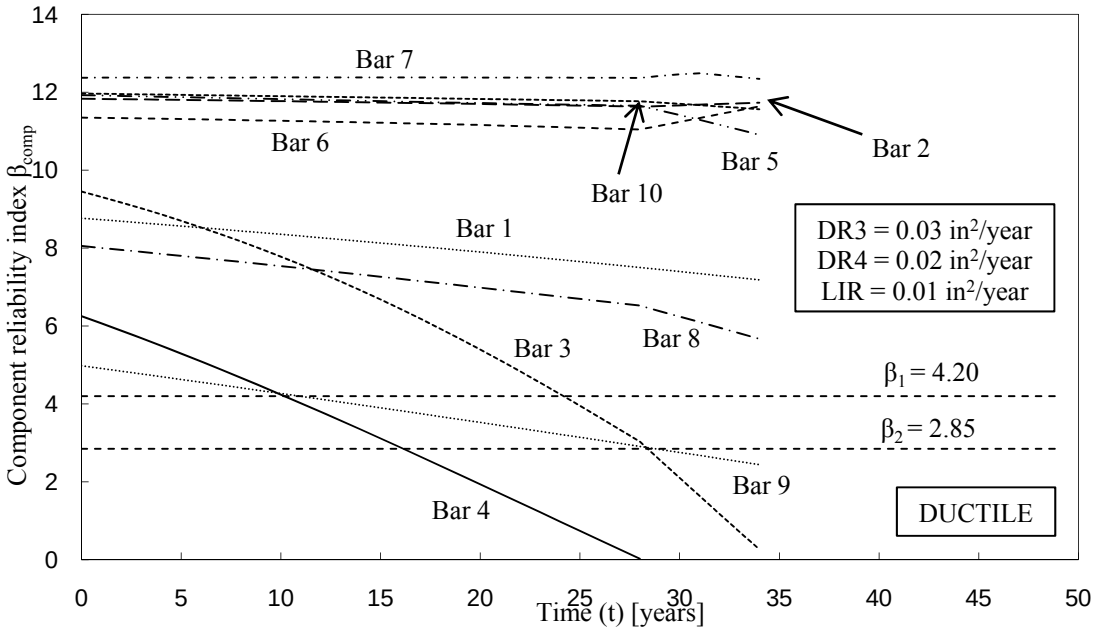

Figure 4.16 Effect of deterioration on bars 3 and 4 and load increase on the time-variant component reliability index β

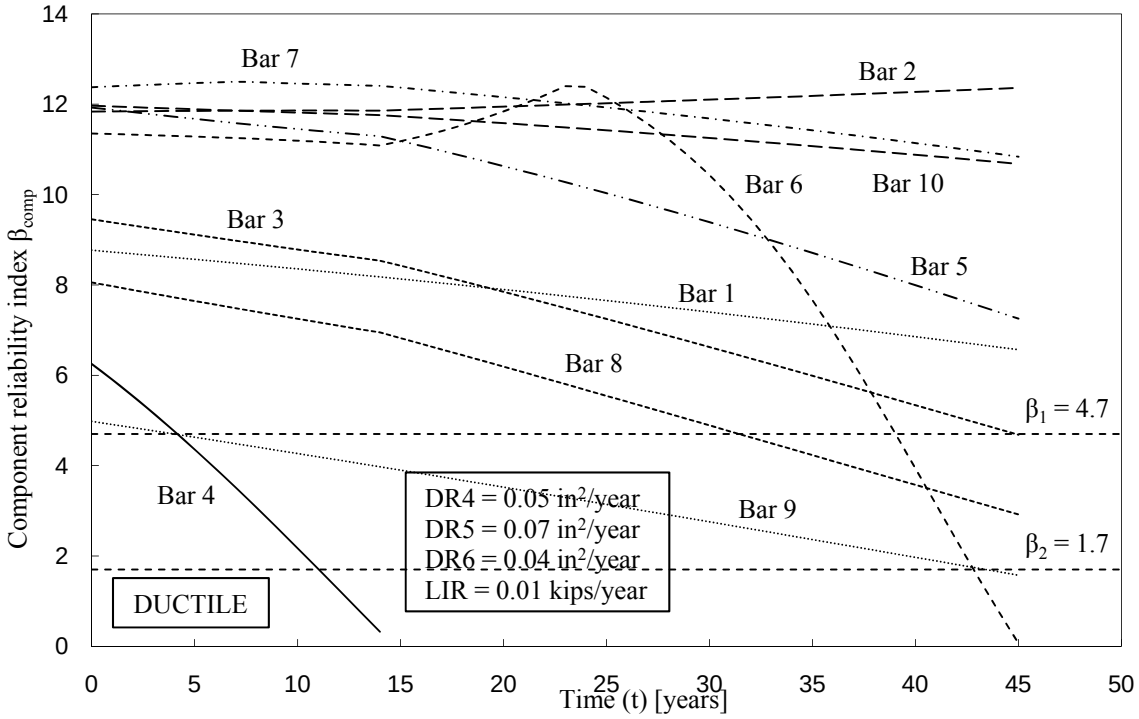

Figure 4.17 Effect of deterioration on bars 4, 5 and 6 and load increase on the time-variant component reliability index β

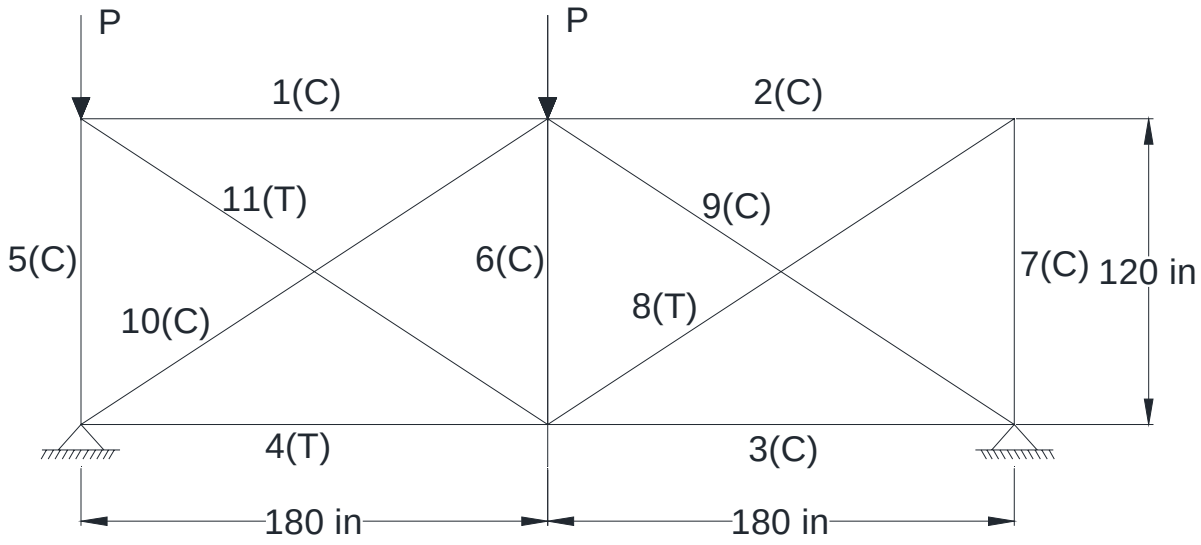

Figure 4.18 11 bar truss example applied with two vertical loads

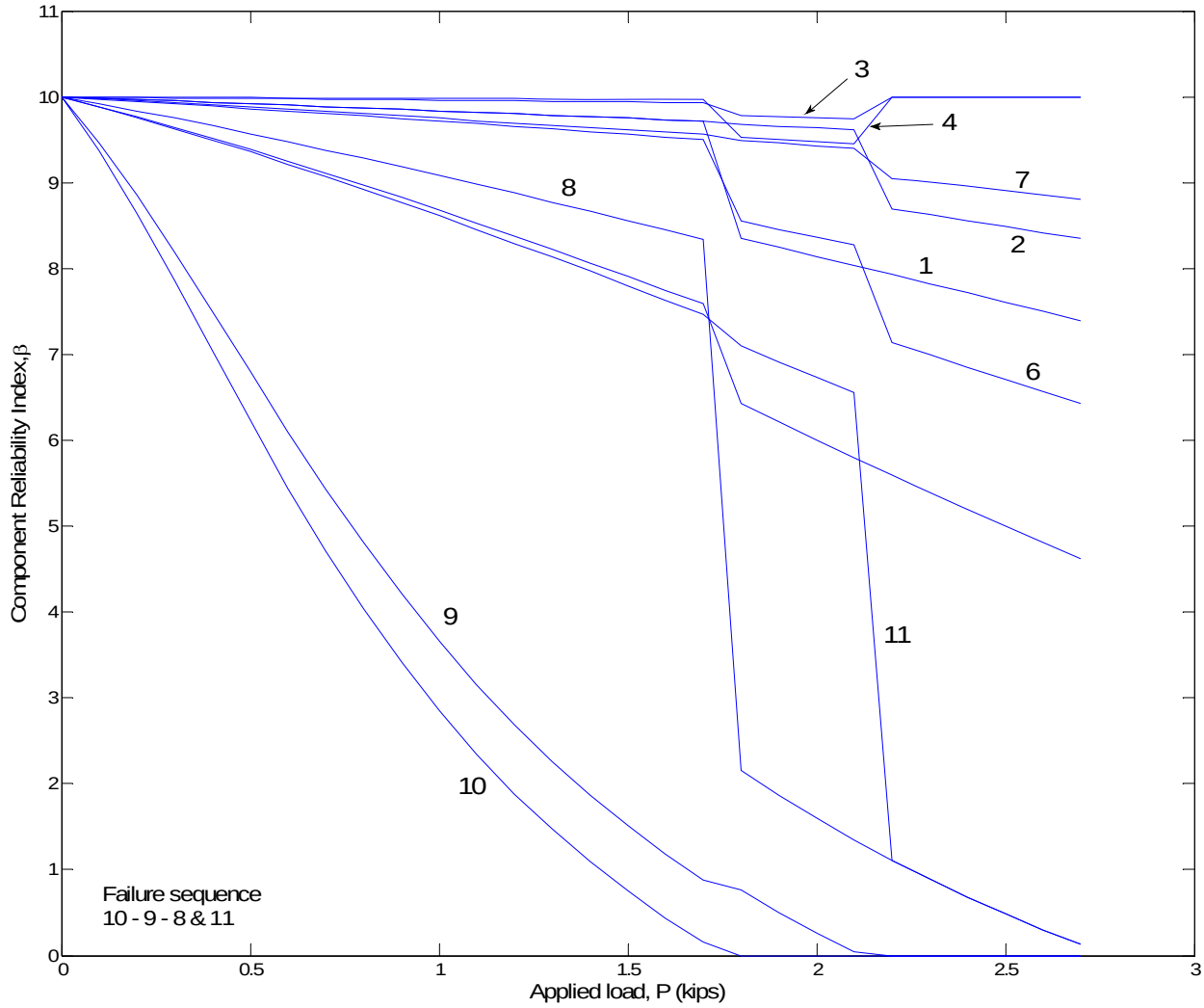

Figure 4.19 Component reliability index versus mean value of load applied on undamaged nondeterministic 11 bar truss example- Brittle Components

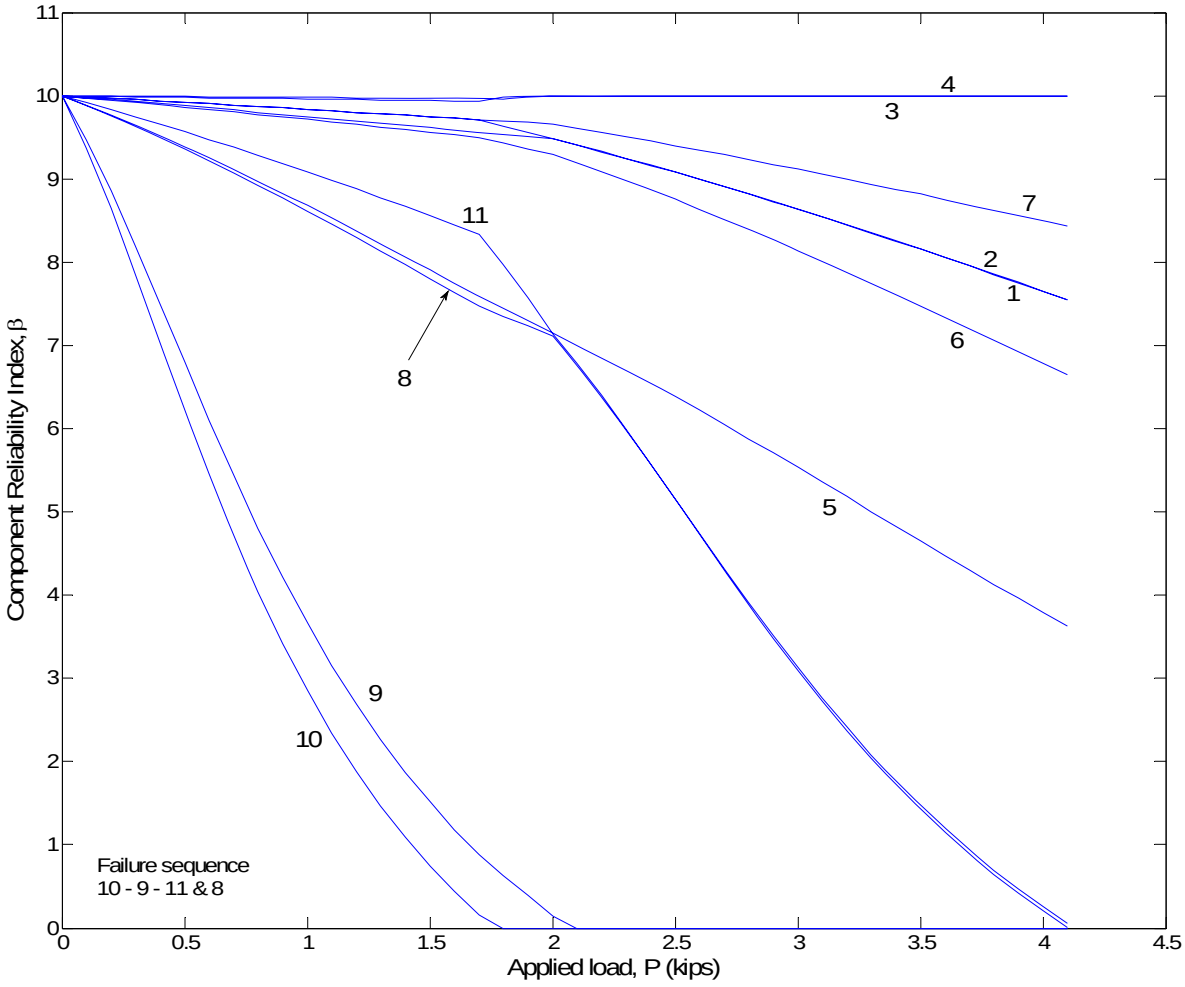

Figure 4.20 Component reliability index versus mean value of load applied on undamaged nondeterministic 11 bar truss example – Ductile Components

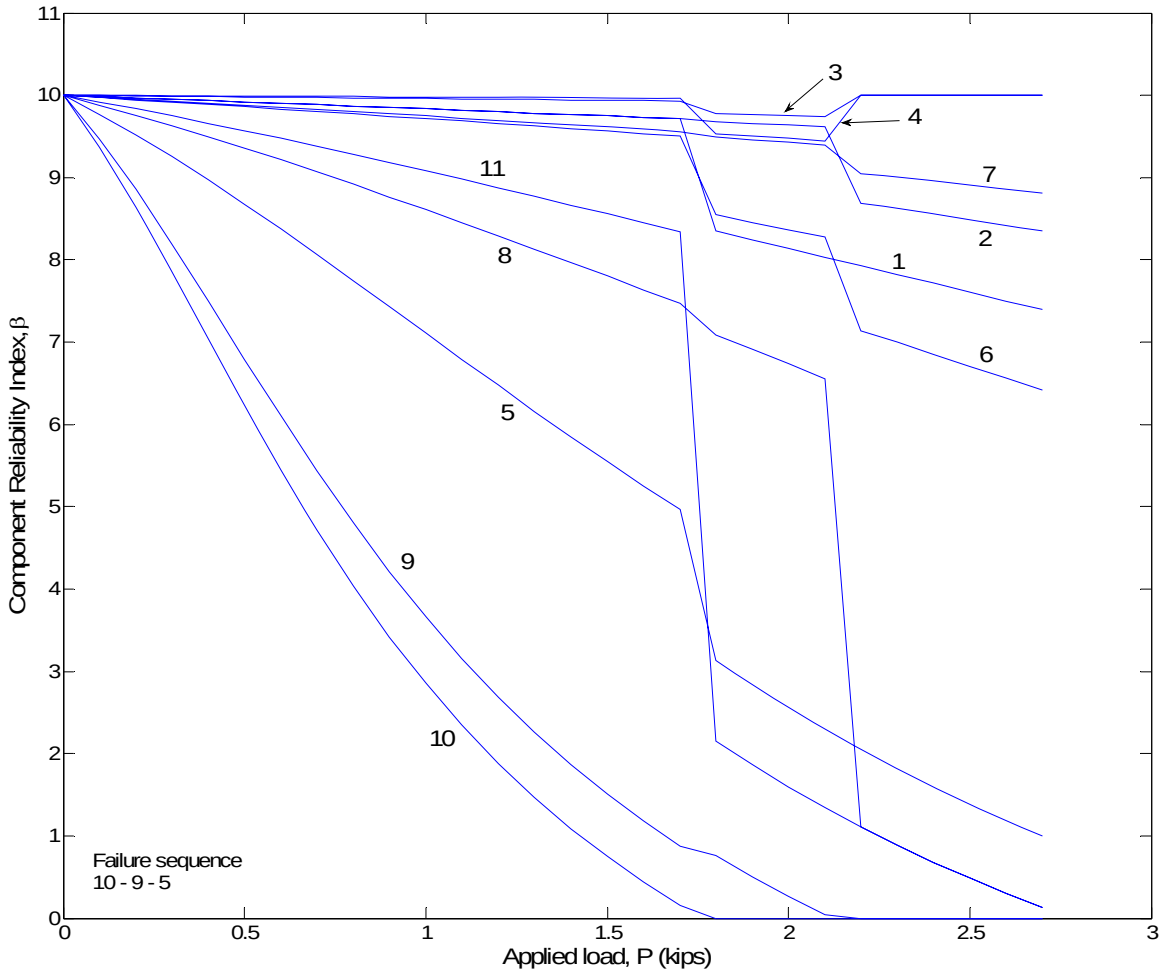

Figure 4.21 Component reliability index versus mean value of load applied on "moderate damaged" of member 5 on nondeterministic ten-bar two-story truss example – Brittle Components

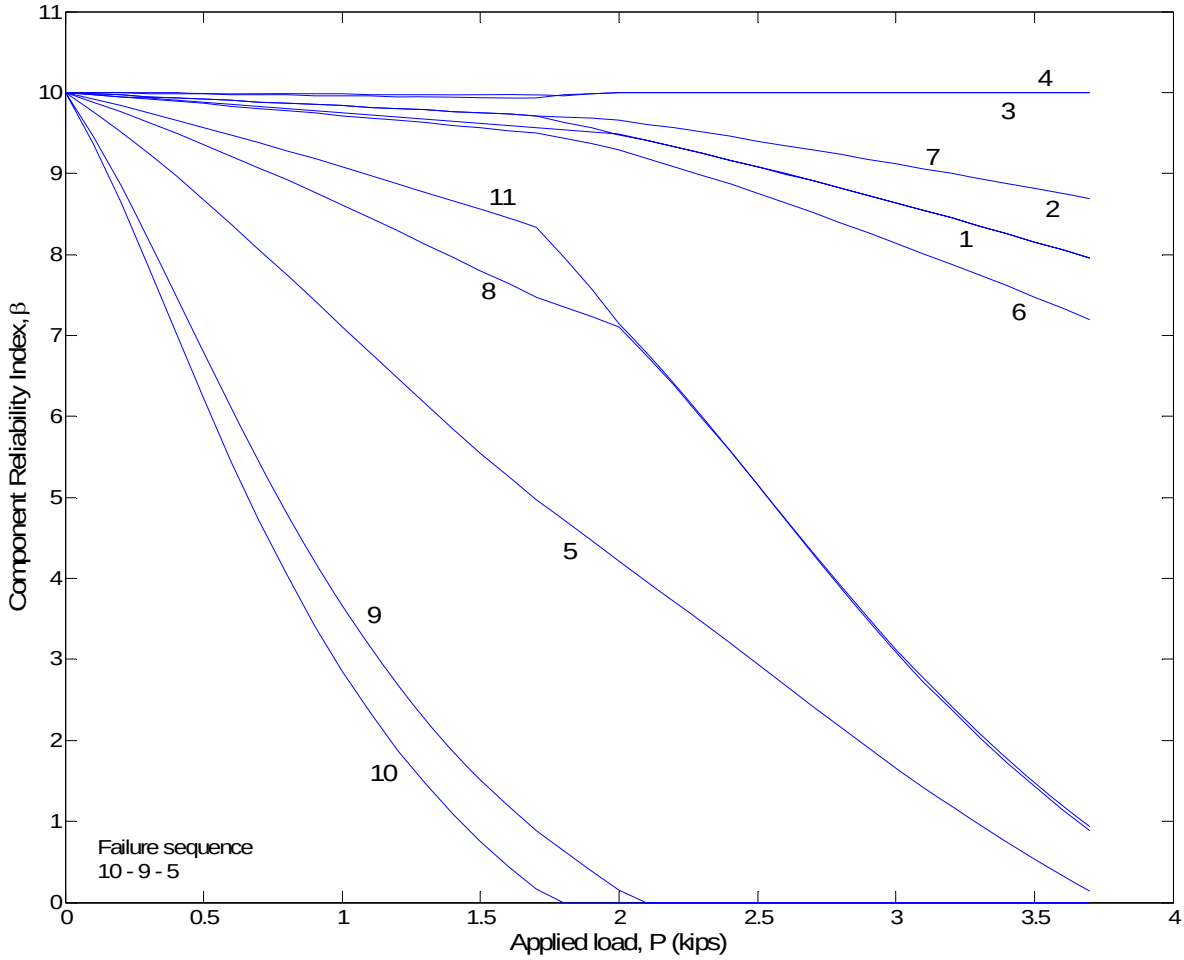

Figure 4.22 Component reliability index versus mean value of load applied on "moderate damaged" of member 5 on nondeterministic 11 bar truss example – Ductile Components

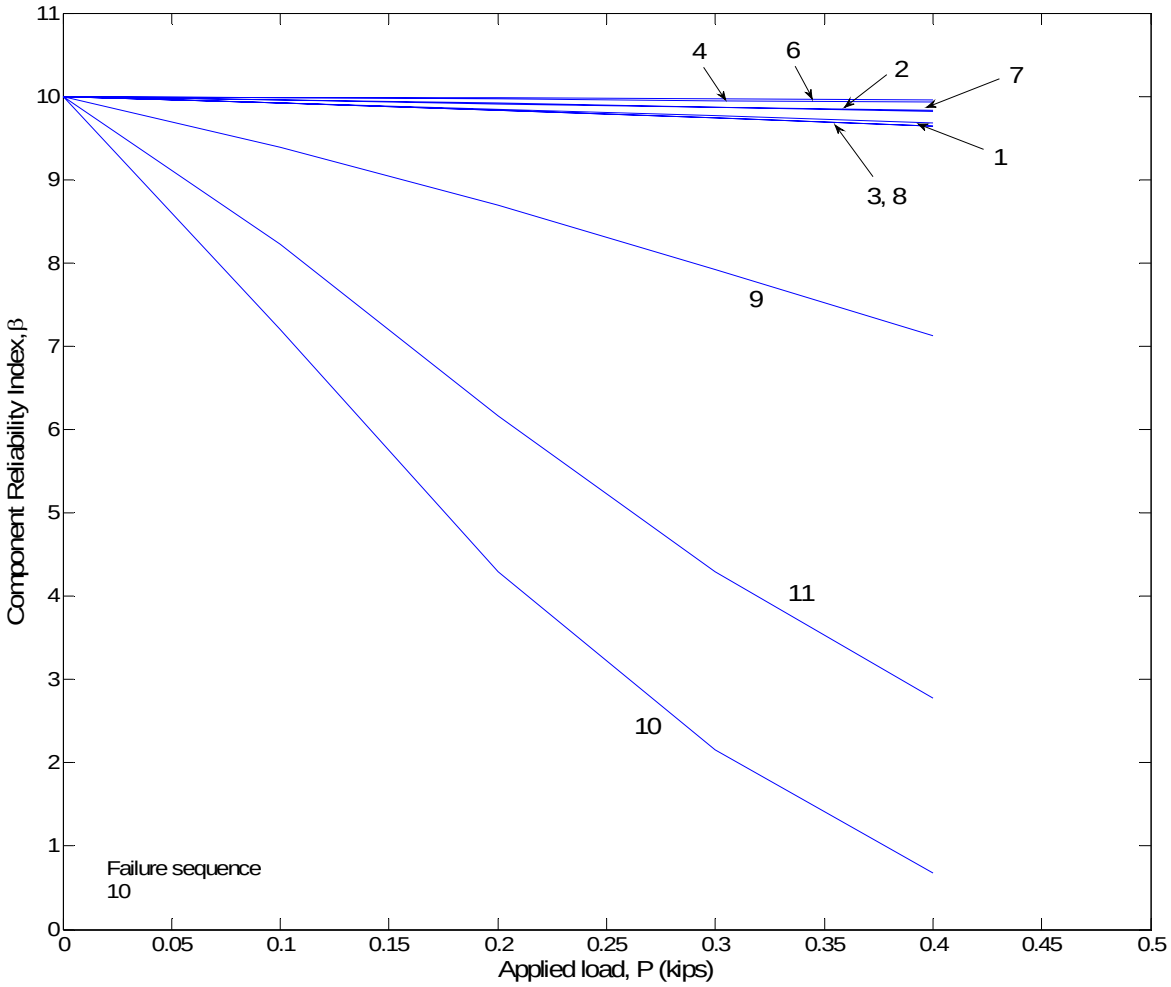

Figure 4.23 Member reliability index versus mean value of load applied on nondeterministic. 11 bar truss with brittle components- "complete" damage of member 5

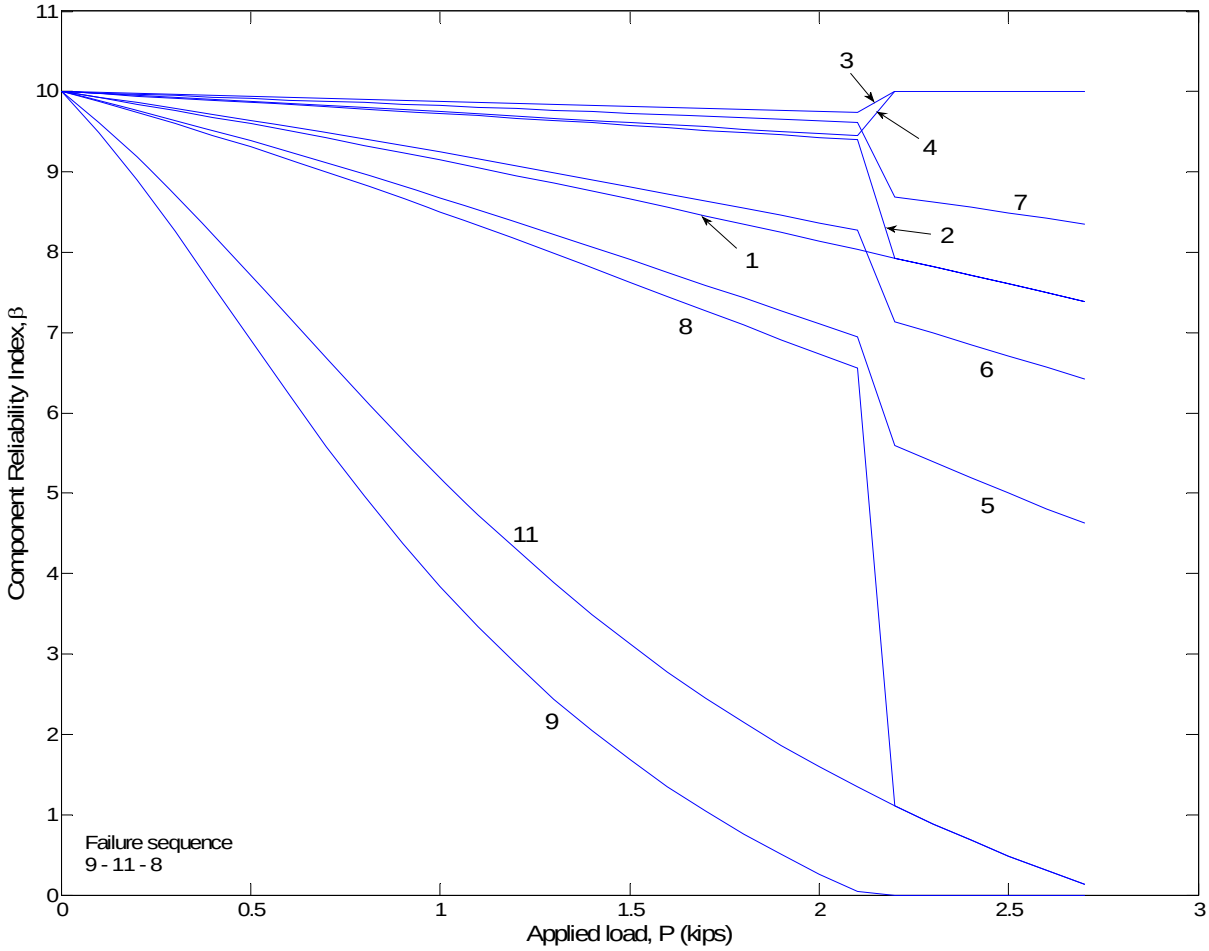

Figure 4.24 Member reliability index versus mean value of load applied on nondeterministic. 11 bar truss with brittle components- "complete" damage of member 10

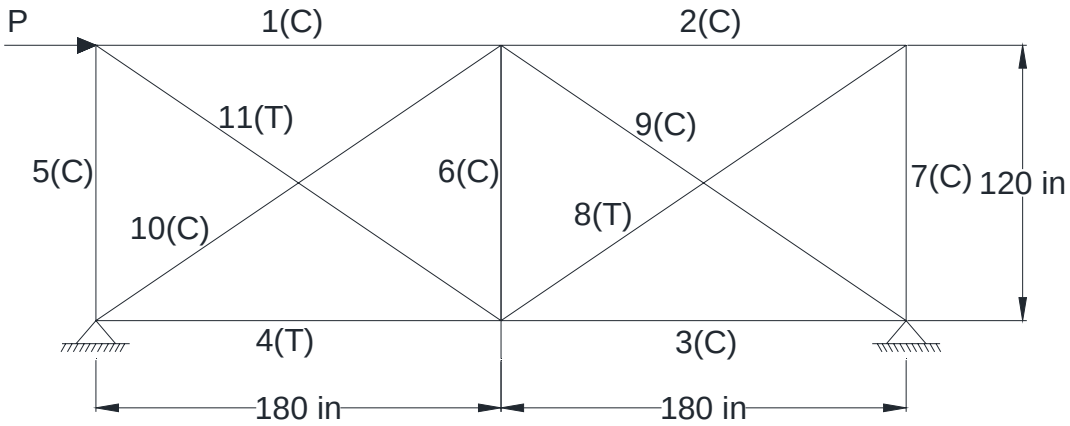

Figure 4.25 11 bar truss example applied with one horizontal load

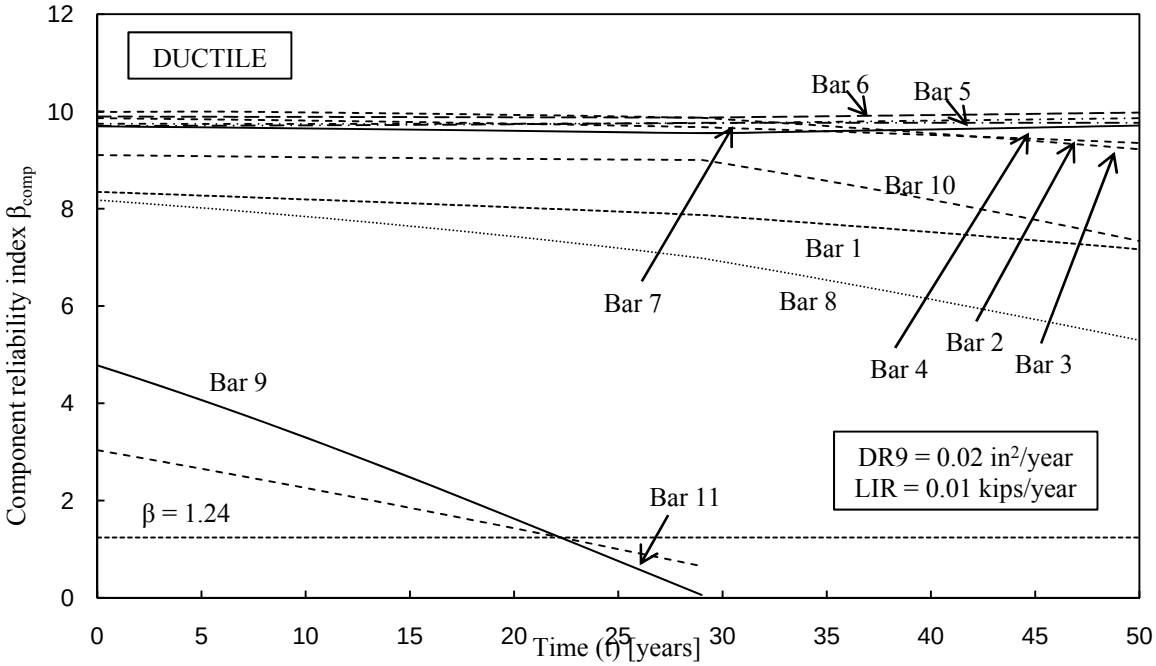

Figure 4.26 Effect of deterioration on bar 9 and load increase on the time-variant component reliability index β

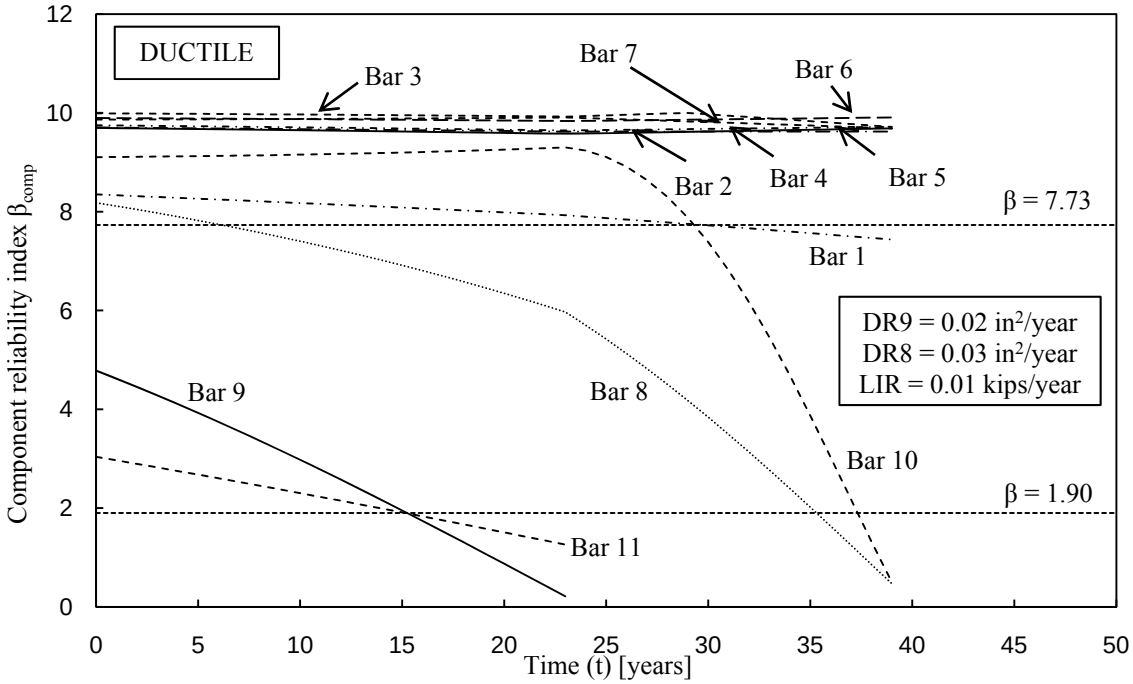

Figure 4.27 Effect of deterioration on bars 8 and 9 and load increase on the time-variant component reliability index β

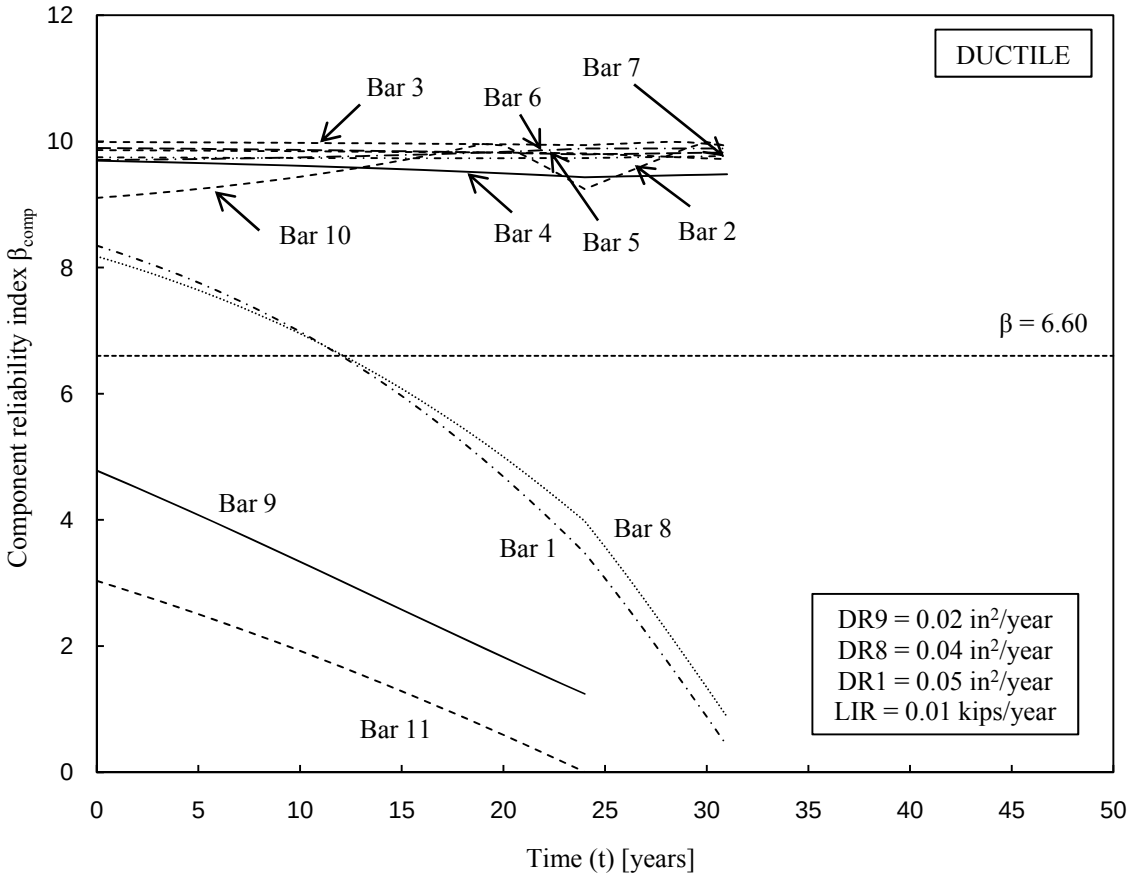

Figure 4.28 Effect of deterioration on bars 1, 8 and 9 and load increase on the time-variant component reliability index β

Table 4.1 Intact member forces for load case 1: (When P=1, unit: kip)

Bar No.	1	2	3	4	5	6	7	8	9	10
Force	-1.414	-0.036	0.893	-1.107	0.152	0.152	-0.072	0.893	-1.414	-0.036

Table 4.2 Member forces for load case 2: (When P=1, unit: kip)

Bar No.	1	2	3	4	5	6	7	8	9	10
Force	0.471	0.149	-0.113	-0.446	-0.312	0.160	0.036	0.220	-0.471	-0.185

Table 4.3 Member forces for load case 3: (When P=1, unit: kip)

Bar No.	1	2	3	4	5	6	7	8	9	10
Force	-0.943	0.185	0.780	-1.554	-0.160	0.312	-0.036	1.113	-1.886	-0.149

Table 4.4 Information for the two situations considered

	Time-independent				Time-dependent			
	Bar 1 to 7		Bar 8 to 11		Bar 1 to 7		Bar 8to 11	
	T	C	T	C	T	C	T	C
A (in^2)	1	1	0.25	0.25	1	1	0.25	0.25
μ_{Fy} (ksi)	20	10	20	10	10	5	10	5
σ_{Fy} (ksi)	2	1	2	1	1.6	0.8	1.6	0.8
c.o.v (Fy) (ksi)	0.1	0.1	0.1	0.1	0.1	0.1	0.1	0.1

Table 4.5 Intact member forces: (When P=1, unit: kip)

Bar No.	1	2	3	4	5	6	7	8	9	10
Force	2.250	0.763	-0.737	-2.250	-0.491	0.008	0.885	-0.918	0.902	-0.901

Table 4.6 Categories of member damage states

1	Intact member	No reduction	Damage factor = 0
2	Slight damage of a member	25% reduction in load capacity	Damage factor = 0.25
3	Moderate damage of a member	50% reduction in load capacity	Damage factor = 0.50
4	Severe damage of a member	75% reduction in load capacity	Damage factor = 0.75
5	Complete damage of a member	total reduction in load capacity	Damage factor = 1.00

CHAPTER 5

FATIGUE RELIABILITY ASSESSMENT USING MONITORING DATA

5.1 Introduction

Bridge structures subjected to various loads during their design life experience strength deterioration. Fatigue is one of the primary reasons for the failure of structural components. Due to unexpected increase of traffic, uncertainties in environmental and mechanical stressors, errors made during the construction or fabrication, fatigue crack initiation will probably propagate which may induce fracture at the end (Kwon and Frangopol, 2010). For steel bridge structures experiencing cyclic loads, prediction and decisions of assessment and maintenance should be made steadily based on structure performance. Therefore, the concept of reliability has to be used.

Structural reliability concentrates on probabilistic description of phenomena and application to code-oriented safety design. Its concept has been used in the industry and specially emphasized in the academic field. To estimate fatigue reliability of the structure, resistance and load effects considered as random variables have to be evaluated. The sum of the elapsed cycles demanded for a fatigue crack initiation and crack propagation from subcritical dimensions to the critical size are the two major reasons to determine the fatigue lives of structural components. The fatigue reliability is evaluated based on the S-N curves provided in the AASHTO Specifications and field monitoring data. AASHTO Specifications provides the classification information for AASHTO Category of the structural detail, from which fatigue resistance of structural components can be decided.

The history of loading afforded by the structure is obtained by field monitoring data.

Two methods are utilized to estimate fatigue reliability of the structure using measured data associated with monitoring systems. One method (Frangopol *et al.*, 2008) is based on predictive models with the resistance and load effects normally distributed, two predictive models are established based on whether the measured effective stress range will be less than one-half of the constant amplitude fatigue (CAF) threshold during the structure's design life; the other method (Kwon and Frangopol, 2010) is applying PDFs (probability density function) of several distribution types based on field monitoring data into the predictive models. For the determination of parameters of different distribution types, fatigue detail coefficient A and equivalent stress range S_{re} are two essential parameters. To consider reliable fatigue assessment performance under uncertainty, A and S_{re} are both defined as random variables. Fatigue is a phenomenon that is very complex and subject to a great deal of uncertainty. The uncertainties introduced due to external factors, such as fatigue loading and environmental conditions, and internal factors such as the fatigue capacity of details make deterministic fatigue analyses less reliable in estimating the fatigue lives of details in steel bridges (Chung, 2004). The information to determine the parameters of random variables for the estimation of fatigue reliability is obtained from AASHTO Specifications and field monitoring data. Fatigue reliability analysis for the second method can be conducted by using the reliability softwares CalREL and RELSYS.

5.2 Fatigue

The metals under the action of cyclic load will experience fatigue in a three

continuous stages (crack initiation, crack propagation and fracture). The most common type of structures which are susceptible to fatigue cracking is steel bridges.

Material fatigue strength can be tested under cyclic stresses. The fatigue resistance above the constant amplitude fatigue threshold, in terms of cycles, is inversely proportional to the cube of the stress range.

Figure 5.1 shows nominal fatigue resistance for Categories A to E based on AASHTO Specifications. This is a graph of the magnitude of a cyclic stress S_{re} against the logarithmic scale of cycles to failure N. In high-cycle fatigue situations, materials performance is usually characterized by an S-N curve. S-N curves are derived from samples of the material which is characterized by a testing machine applying a regular sinusoidal stress can also count the number of cycles to failure. The S-N curve graph can be used to predict total fatigue life including both crack initiation and crack propagation.

In 1945, Miner states that if there are k different stress levels and the average number of cycles to failure at the *i*th stress, S_i, is N_i, then the damage fraction, D, is:

$$\sum_{i=1}^{k} \frac{n_i}{N_i} = D \tag{5.1}$$

where n_i is the number of cycles accumulated at stress S_i, D is the fraction of life consumed by exposure to the cycles at the different stress levels. In general, when the damage fraction reaches 1, failure occurs.

5.3 Field monitoring data

Field monitoring data plays a very important role in fatigue life assessment of bridges. For long-term monitoring system, strain gages are installed to automatically record and

store the data on the hour, as well as when heavy vehicles cross the bridge. External factors, such as the effects of sustained load, temperature, environmental conditions, and bridge's performance under live load effects, can all be assessed by using the information provided by the monitoring system.

Stress range histogram data can be developed from the continuous time-history data collected during the long term monitoring, thus equivalent stress range and average daily truck traffic are obtained. Equivalent stress range can be estimated approximately by using the moment ranges from calculation. The parameters computed from PDFs are used in the reliability analysis.

5.4 Application to Commodore Barry Bridge

5.4.1 Introduction

A long span bridge is analyzed to determine its structural reliability based on field monitoring data. The Commodore Barry Bridge is a cantilever bridge that spans the Delaware River from Chester, Pennsylvania, to Bridgeport, in Logan Township, New Jersey, USA (Wikipedia, http://en.wikipedia.org/wiki/Commodore_Barry_Bridge). It is the fourth longest cantilever truss bridge in the world and the longest one in the United States. Owned by the Delaware River Port Authority (DRPA), the bridge was originally opened to traffic in 1974. The bridge includes five traffic lanes and currently serves an annual traffic flow of more than six million vehicles of which heavy truck vehicles take up a significant percentage. The bridge with a total bridge length of 13912 feet has a main span length of 1644 feet and side spans of 822 feet. Figure 5.2 shows the overview of the bridge. (Catbas et al., 2008).

5.4.2 Monitoring program

A long-term monitoring program was implemented in order to measure the in-situ live load stresses in the truss members. There were more than 1000 electroslag welds over the bridge. Based on the test results, previous analysis done by research staffs and faculty found out there were eight critical welds having the potential for fatigue crack growth. AECOM (formerly known as DMJM Harris) and the ATLSS Center of Lehigh University were both contracted by DRPA to reassess the potential for fatigue crack propagation. (Hodgson et.al, 2008)

The basic identification information for eight previously identified electroslag is described in the Table 5.1. Figures 5.3 and 5.4 show a 3-D graphic view of the Pennsylvania back span and the New Jersey back span of the bridge indicating the truss members with critical welds. Figures 5.5 to 5.7 show the detailed location of the critical members in the north and south truss respectively in a 2-D format.

The monitoring program was implemented in two phases. Phase 1 monitoring started on October 17, 2007. Stress-time history data was not collected continuously during this period. Phase 2 monitoring commenced on November 28, 2007 until December 7, 2007. Data was collected continuously from all the sensors with a rate of 10 Hz during this period. The data in Phase 2 was used to build the stress-range histograms used in the reliability assessment. Detailed information is available in ATLSS Report 08-04 (Hodgson et al, 2008).

A threshold was established that only the data value above the threshold can be recorded. Due to a large amount of spurious signals in the data collected in Phase 1, the

data from Phase 2 was finally utilized for fatigue reliability analysis of this example. It is assumed that the measured stress during the monitoring period is applicable.

5.4.3 Reliability assessment for fatigue behavior based on monitoring measurements

5.4.3.1. Reliability method integrated with monitoring data

The approach utilized was investigated by Frangopol, Strauss and Kim (2008a). First-order reliability method (FORM) and Second-order reliability method (SORM) are two methods to calculate the structural reliability. The limit state function used in this approach is described as:

$$g(X) = R - Q = 0 \tag{5.2}$$

where $X = \{X_1, X_2, \dots, X_n\}^T = vector\ of\ random\ variables$. g(X) = 0 = limit state, g(X) < 0 = failure state. The reliability index is defined as

$$\beta = \frac{\mu_R - \mu_Q}{\sqrt{\sigma_R^2 + \sigma_Q^2}} \tag{5.3}$$

where μ_R and μ_Q is the mean of resistance and load effect respectively, σ_R and σ_Q is the standard deviation of the resistance and load effect, respectively.

Integrated with monitoring into structural reliability, the limit state function can be expressed as:

$$g(X) = R - M = 0 \tag{5.4}$$

where M is the monitored load effect.

The reliability index can be defined as

$$\beta = \frac{\mu_R - \mu_M}{\sqrt{\sigma_R^2 + \sigma_M^2}} \tag{5.5}$$

where μ_M and σ_M are the mean and standard deviation of monitored load effect, respectively. Due to the arrangement of sensors on various locations of the structure and the fact that monitoring data could be negative or positive, the possibility of misinterpretation does exist. For this reason, the reliability index associated with sensor *i* can be modified as

$$\beta = \frac{\mu_R - \mu_{M_i}}{\sqrt{\sigma_R^2 + \sigma_{M_i}^2}} \tag{5.6}$$

where μ_{M_i} and σ_{M_i} are the mean value and standard deviation of monitored load associated with sensor *i*. In this example, the recorded maximum value of load effect during the entire monitoring period is considered as a random variable. The relation between mean and standard deviation is defined as

$$\sigma_{M_i}^o = \mu_{M_i}^o \cdot \frac{\sigma_R}{\mu_R} \tag{5.7}$$

The corresponding reliability index is

$$\beta_i^o = \frac{\mu_R - \mu_{M_i}^o}{\sigma_R \sqrt{1 + \left(\frac{\mu_{M_i}^o}{\mu_R}\right)^2}} \tag{5.8}$$

A large amount of measurements have to be verified via establishment of mechanical models, this process in general contains substantial errors. Even errors have to be taken into account in the interpretation of results from the monitoring system. Uncertainties $e_s(\%)$ generated by three types of errors associated with the sensors can be considered into the reliability index computation by defining the factor (Frangopol et al. 2008a)

$$f_s = 1 + e_s \tag{5.9}$$

The component reliability index of sensor i including e_s is defined as:

$$\beta_{i,e}^{o} = \frac{\mu_R - \mu_{M_i}^{o} \times f_s}{\sigma_R \sqrt{1 + \left(\frac{\mu_{M_i}^{o}}{\mu_R}\right)^2}} \tag{5.10}$$

5.4.3.2. Fatigue reliability assessment

The fatigue reliability of the Commodore Barry Bridge under traffic load will be investigated in accordance with AASHTO 2007. The seven members with critical welds are considered a Fatigue Category B per the AASHTO LRFD Specifications (AASHTO 2007) with a fatigue threshold of 16 ksi. Only one of the eight members (Number 244) was tested to have rejectable flaws and cannot be considered as Category B.

Two strain gages A and B were installed at each tested electroslag weld of the member. One gage was installed one inch away from the edge of the weld, the other gage was installed one inch away from the edge of the member. Field monitoring data has been collected for both gages for each member. Based on the data obtained from field testing, it is found that the data from strain gages A_448 and B_448 are not included in the analysis due to excessive noise in the data. (Hodgson et.al, 2008)

According to AASHTO 2007, it is considered as infinite lifetime, in terms of fatigue, if investigated detail of design stress range is provided less than one-half of the constant amplitude fatigue (CAF) threshold. From Figure 5.8, the constant amplitude fatigue (CAF) threshold for Category B is 16 ksi. The mean and standard deviation of effective stress range and number of cycles for each member are in Table 5.2. As Figure 5.8 shows that

the effective stress range with descending branch is only effective when it is above the one-half of the CAF threshold. According to the data provided by Table 5.2, since the assumption is made that effective stress range and the number of cycles per day are constant over the lifetime, the fatigue lifetime of the bridge is infinite. Two predictive models are made based on the established CAF threshold for Category B.

Predictive Model I:

The fatigue life for the bridge in is infinite, which indicates that the measured effective stress range is less than one half of the constant amplitude fatigue (CAF) during its lifetime. The fatigue reliability will be assessed in accordance with descending stress range with increasing number of cycles until the corresponding number of cycles N_s to the CAF threshold is reached. The N_s for Category B is 3.93×10^{12}. If the number of cycles exceeds the specified N_s, the fatigue reliability is computed based on the constant amplitude fatigue (CAF).

Predictive Model II:

The fatigue life for the bridge is finite, which indicates that the measured effective stress range is larger than one half of the constant amplitude fatigue (CAF) during its lifetime. The fatigue reliability will be assessed in accordance with descending stress range with increasing number of cycles during the lifetime of the bridge. There is an assumption made for this model, that is, the number of cycles and the stress range increases by the same rate during the bridge's lifetime.

Table 5.2 provides the information of mean and standard deviation of effective stress range in different units and numbers of cycles for each seven members with critical welds.

Take sensor A_44 for example, Figure 5.9 shows the histogram created from sensor measurements of the number of cycles N versus the stress range for sensor A_44 located on member 44. Figure 5.10 shows increases in the number of cycles by three different rates: 3.5%, 4.5% and 5.5%. For all the increasing rates, the number of cycles approaches the specified number of cycles N_s 2.93×10^6 corresponding to the constant amplitude fatigue (CAF) threshold for Category B. So the reliability assessment will be performed with respect to the CAF limit when the number of cycles is larger than N_s in the Model I.

The component fatigue reliability integrated with monitoring sensor reading is assessed based on the reliability index $\beta^o_{i,e,f}$, which is obtained by the equation as follows:

$$\beta^o_{i,e,f} = \frac{\mu_f - \mu^o_{M_i} \times f_s}{\sqrt{\sigma_f^2 + \left(\sigma^o_{M_i}\right)^2}} \tag{5.11}$$

where μ_f = the allowed effective stress range regarding AASHTO guidelines with respect to the aforementioned predictive models I and II; $\sigma_f = v \times \mu_f$ stands for the standard deviation of the allowed effective stress range where the coefficient of variation $v = \frac{\sigma_R}{\mu_R} = 0.08$, $\mu^o_{M_i}$ = the mean of effective stress range associated with sensor *i*; and $\sigma^o_{M_i}$ = the standard deviation of effective stress range associated with sensor *i*; and f_s = factor assigned to sensor errors.

Predictive model I is assessed based on the mean effective stress range $\mu^o_{M_i}$ and the standard deviation $\sigma^o_{M_i}$ of sensor i. For predictive model II, $\mu^o_{M_i}$ has been increased by three various rates arranged from 3.5% to 5.5% per year and $\sigma^o_{M_i}$ keeps constant over the bridge's lifetime.

Figure 5.11 shows the component fatigue reliability index for member 44 with monitoring reading from sensor A_44 in the prediction of 50 years. Variance from the predicted reliability indices is caused by different effective stress ranges based on the assumptions made in the predictive model I and II. In Figure 5.11 which presents component fatigue reliability of member 44, the assumption is made that the measurements of physical quantities provided by the monitoring system have no error. Figure 5.12 shows component reliability index of member 44 for models I and II with assumed 0%, 5%, 20% and 35% sensor reading error.

From the reliability assessment results, monitoring system is used to record and store the data of daily traffic, a rainflow cycle counting is utilized after the data had been collected using a PC to run MATLAB. Noise signals from the data were removed by using the digital signal processing techniques. Effective stress range and number of cycles are two very crucial parameters in assessing the fatigue performance. The monitoring system is of great significance to acquire and update information of magnitude and frequency of the traffic load which is changing over the lifetime of the structure.

5.4.4. Summary

The approach used in the Commodore Barry Bridge is to investigate fatigue reliability for the members with critical welds in the lifetime of the structure with different assumptions made for two predictive models. The most critical member can be identified from the predictive reliability index values.

From the figures shown previously, the effective stress range and numbers of cycles play an important role to predict fatigue performance and traffic loads having been always changing during the lifetime of the structure, so the application of monitoring system can update the information of traffic loads by using the effective stress range and number of cycles on a time-variant base to improve the probabilistic prediction models.

In reality, the consideration of sensor errors should be included in the assessment of the structure. These errors are generated in the process of verifying a great number of measurements to idealize mechanical models and using redundant used sensors.

5.4.5 Reliability assessment for fatigue behavior using probability density functions of equivalent stress range

Since reliability index is one of primary indicators to evaluate and predict structural performance, resistances and applied load effect are both treated as random variables in the limit state function. The parameters, which decide the probability density function (PDF) of the random variables, are used in the reliability index calculation. The formulation of PDF can be based on the field monitoring data, which has been conducted by Kwon and Frangopol (2010). The procedures of this approach are explained as follows.

5.4.5.1 Estimation of structural members

Based on the inspection and research done by Hodgson, Professor Yen and Bowman (2008), seven of the eight members are considered as Category B with a fatigue threshold of 16 ksi according to AASHTO. The fatigue detail coefficient A, material constant and constant amplitude fatigue limit (CAFL) can be obtained from AASHTO Specification. The only one could not be estimated by AASHTO due to its existence of rejectable flaws.

5.4.5.2 Selection of probability density function (PDF)

The relation between stress range and number of cycles shown by Figure 5.1 is obtained based on the scattered data from numerous experiments. As indicated before, the S-N curves and Miner's rule are used to investigate structural total fatigue life. So consider the load effects, the evaluation of fatigue life must take into account of variable amplitude loadings, such as stress range (Kwon and Frangopol, 2010). The PDF providing parameters for the reliability analysis is formulated by one of the best fit three distribution types, which are lognormal, weibull and gamma distribution, respectively. The PDFs and moments for the corresponding distribution types are briefly introduced as below (Kwon and Frangopol, 2010):

(1) Lognormal distribution

PDF: $$f_S(s) = \frac{1}{(s-s_c)\cdot\zeta\cdot\sqrt{2\pi}} \cdot \exp\left[-\frac{1}{2}\cdot\left(\frac{\ln(s-s_c)-\lambda}{\zeta}\right)^2\right. \quad (5.13)$$

For $s - s_c > 0$

The mean and standard deviation of the stress range is

$$E(S) = \exp(\lambda + 0.5\cdot\zeta^2) + s_c \quad (5.14)$$

$$Var(S) = [E(S) - s_c]^2 \cdot [\exp(\zeta^2) - 1] \quad (5.15)$$

(2) Weibull distribution

PDF: $$f_S(s) = \frac{\beta}{\alpha}\cdot\left(\frac{s-s_c}{\alpha}\right)^{\beta-1} \cdot \exp\left[-\left(\frac{s-s_c}{\alpha}\right)^{\beta}\right. \quad (5.16)$$

For $s - s_c > 0$

The mean and standard deviation of the stress range is

$$E(S) = \alpha \cdot \Gamma\left(\frac{1}{\beta} + 1\right) + s_c \tag{5.17}$$

$$Var(S) = \alpha^2 \cdot \left[\Gamma\left(\frac{2}{\beta} + 1\right) - \left[\Gamma\left(\frac{1}{\beta} + 1\right)\right]^2\right] \tag{5.18}$$

(3) Gamma distribution

PDF: $f_s(s) = \frac{\lambda \cdot [\lambda \cdot (s - s_c)]^{k-1}}{\Gamma(k)} \cdot \exp[-\lambda \cdot (s - s_c)]$ (5.19)

For $s - s_c > 0$

The mean and standard deviation of the stress range is

$$E(S) = \frac{k}{\lambda} + s_c \tag{5.20}$$

$$Var(S) = \frac{k}{\lambda^2} \tag{5.21}$$

The equivalent stress range S_{re} derived from the m-th moment of the stress range for the distribution types are expressed as:

$$E(S^m) = \int_0^\infty s^m \cdot f_s(s) \cdot ds \tag{5.22}$$

$$S_{re} = \left[\int_0^\infty s^m \cdot f_s(s) \cdot ds\right]^{\frac{1}{m}} = [E(S^m)]^{\frac{1}{m}} \tag{5.23}$$

5.4.5.3 Construction of stress range bin histograms

The stress range bin histograms are constructed based on available monitoring data from six critical members. The data from strain gage 448 is checked to contain a big amount of noise, so member 448 is excluded from constructing stress range histograms. Tables 5.3 and 5.4 show the maximum recorded stress range S_{Rmax} and histogram presented with all cycles for six members with critical welds. Figures 5.13 to 5.15 present

stress range bin histograms for six critical members based on the data collected by rain-flow counting method from Tables 5.3 and 5.4. The fatigue lives of the six critical members are accordingly theoretically expected as infinite. The equivalent stress range S_{re}, which is one of the random variables, is calculated from stress range bin histogram, is described as

$$S_{re} = \left[\sum \frac{n_i}{N_{total}} \cdot S_{ri}^3\right]^{\frac{1}{3}} \tag{5.24}$$

or

$$S_{re} = \left[\int_0^{\infty} s^3 \cdot f_s(s) \cdot ds\right]^{\frac{1}{3}} \tag{5.25}$$

where n_i = number of observations in the predefined stress-range bin, N_{total} = total number of observations during the monitoring period, S_{ri} is the number of cycles for each stress range (Kwon and Frangopol, 2010).

Figure 5.16 represents the effect of different stress range cut-off levels on fatigue reliability of members installed with strain gages A_444 and B_302, respectively. It is shown that higher stress range cut-off level indicates more critical reliability index.

5.4.5.4 The selection of distribution type and estimation of its mean and standard deviation

Since Figures 5.13 to 5.15 presented the stress range histograms for six critical members, the live load effects at the sensor locations are recorded continuously during a certain period of time. The stress range cut-off threshold s_c = 0 is taken for the two-parameter PDFs which provides the parameters for further reliability assessment and

estimation of estimate equivalent stress range. Figures 5.19 and 5.20 present the distribution type fitting of stress range histograms for member 302 and 444 on the distribution types: Lognormal, Gamma, Weibull, respectively. It was researched by Kwon and Frangopol (2010) that Anderson-Darling test is a best fit to assess the probability of failure since it would receive more contributions from the tails of a distribution in terms of the logarithm of the probabilities. Figure 5.22 shows the comparison of three selected distribution types tested by goodness-of-fit test on a particular strain gage A_291. As shown, lognormal PDF is the best fit of the stress range data obtained from field monitoring. The fatigue life of the Commodore Barry Bridge will be investigated by using Lognormal PDFs in the further study.

5.4.5.5 Prediction of annual cumulative number of cycles

The value of Average Daily Truck Traffic (ADTT) for each critical member was computed based on total number of cycles during the monitoring period from inspection results obtained by Hodgson et al (2008). The annual traffic increase rate is assumed. The predicted cumulative number of cycles is computed as (Kwon and Frangopol 2010)

$$N(y) = 365 \cdot ADTT \cdot \int_0^y (1+\alpha)^y \, dy = 365 \cdot ADTT \cdot \frac{(1+\alpha)^y - 1}{\ln(1+\alpha)} \qquad (5.26)$$

where y is the number of years, α is the annual traffic increase rate. N is used as the only time-variant quantity in the prediction of reliability index.

Table 5.2 represents the ADTT estimated by the assumed PDFs at each strain gage. Figure 5.23 shows time-variant cumulative stress number of cycles for strain gages on each critical member.

5.4.5.6 Fatigue reliability analysis at system level

It requires a system reliability approach to estimate how all the members with critical welds make effect on the overall reliability of the bridge. The system reliability models are classified as three models including all the available estimated components: parallel system model (six components), series system model (six components), series-parallel system model (five components).

Model I: Parallel system model, which means the failure of all the connected components result in the failure of the bridge. The system reliability index decreases from 11.79 to 6.15 in an expected lifetime of 50 years.

Model II: Series system model, that is, any failure of the six members will result in the system failure. The reliability index results range from 6.77 to 1.77.

Model III: Series-Parallel system model, which the failure of any parallel part will result in the system failure. This bridge model can be simplified as a model containing five main components connected as series, critical members will be classified based on these five main parts to form a series-parallel model. As shown in Figures 5.5, 5.6 and 5.7, all the critical members are noticed to be located in the anchor span part. Only member 44 is not included in this model since only its failure cannot make the bridge fails. Figure 5.27 represents the system classification of the bridge. In the expected lifespan of 50 years, the system reliability index decreases rapidly from 10.28 to 4.32.

Figure 5.28 shows three system predictive models under the different assumptions. Figure 5.29 represents time-dependent system reliability indices for the three system

models in a 50-year expected time. It indicates that parallel system is the most reliable one among the three and series system is the least reliable one.

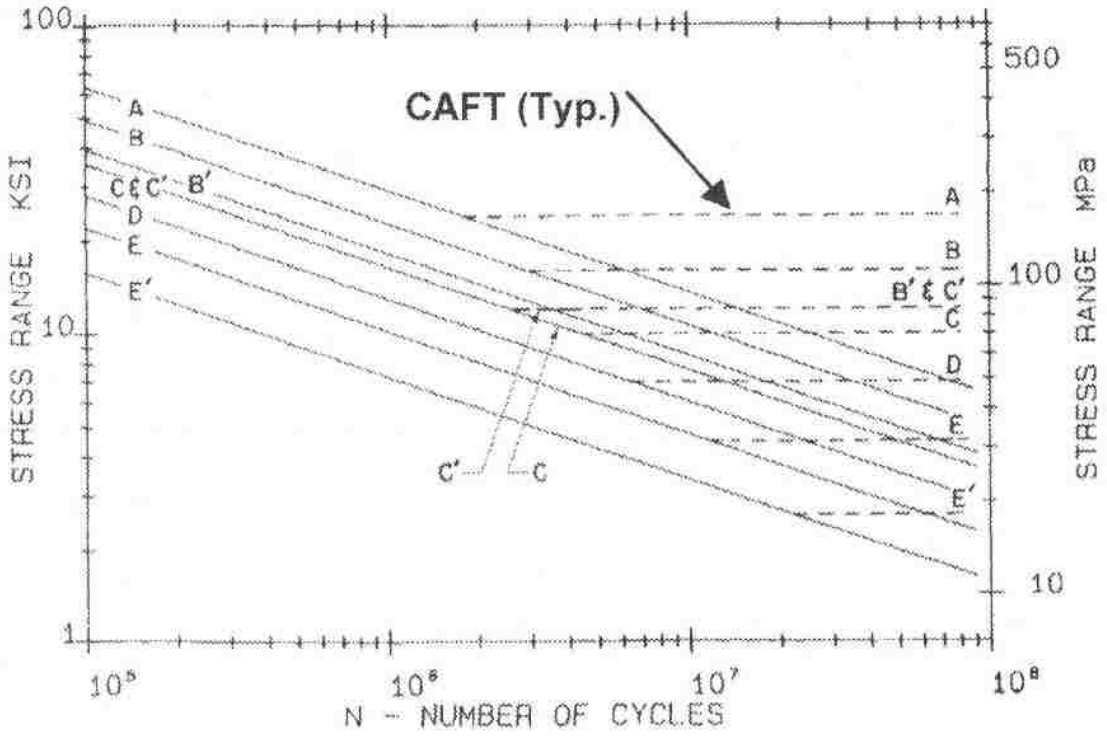

Figure 5.1 Stress Range Versus Number of Cycles (From AASHTO 2007)

Figure 5.2 Overview of the Commodore Barry Bridge (From Wikipedia, http://en.wikipedia.org/wiki/Commodore_Barry_Bridge)

Figure 5.3 Photographic view of Pennsylvania back span looking upstream showing instrumented truss members (green = upstream; yellow = downstream) (From Hodgson et. al, 2008)

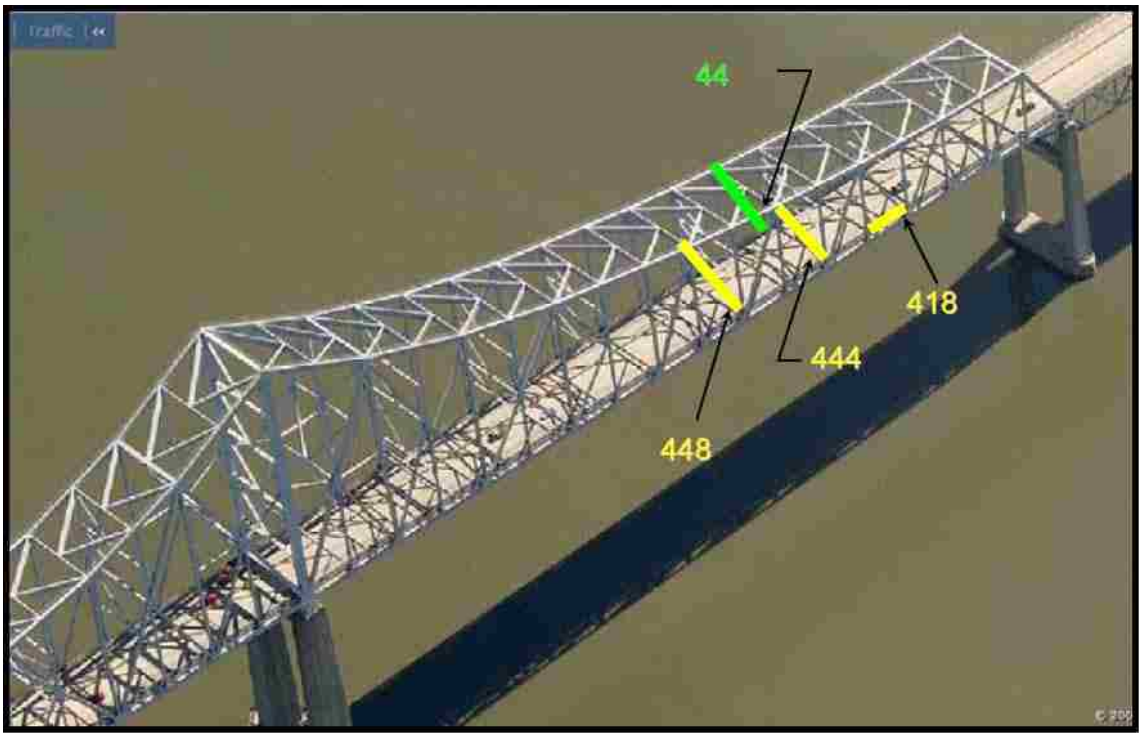

Figure 5.4 Photographic view of New Jersey back span looking upstream showing instrumented truss members (green = upstream; yellow = downstream) (From Hodgson et. al, 2008)

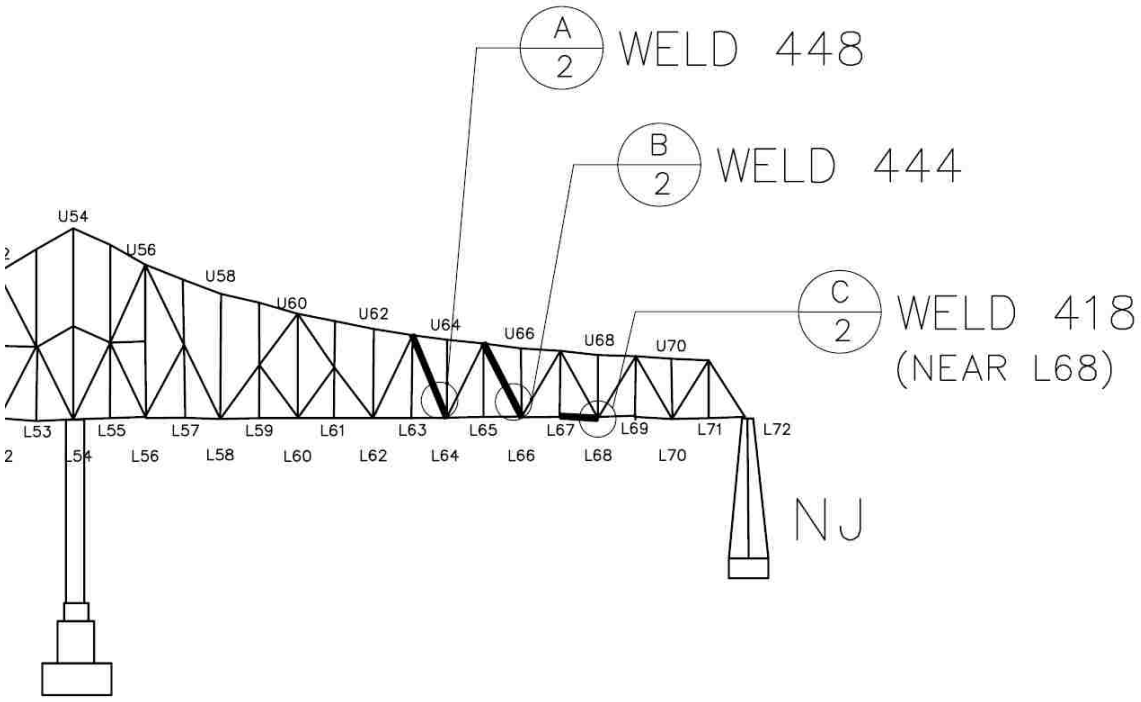

Figure 5.5 Detail of welds in the south truss (From Hodgson et. al, 2008)

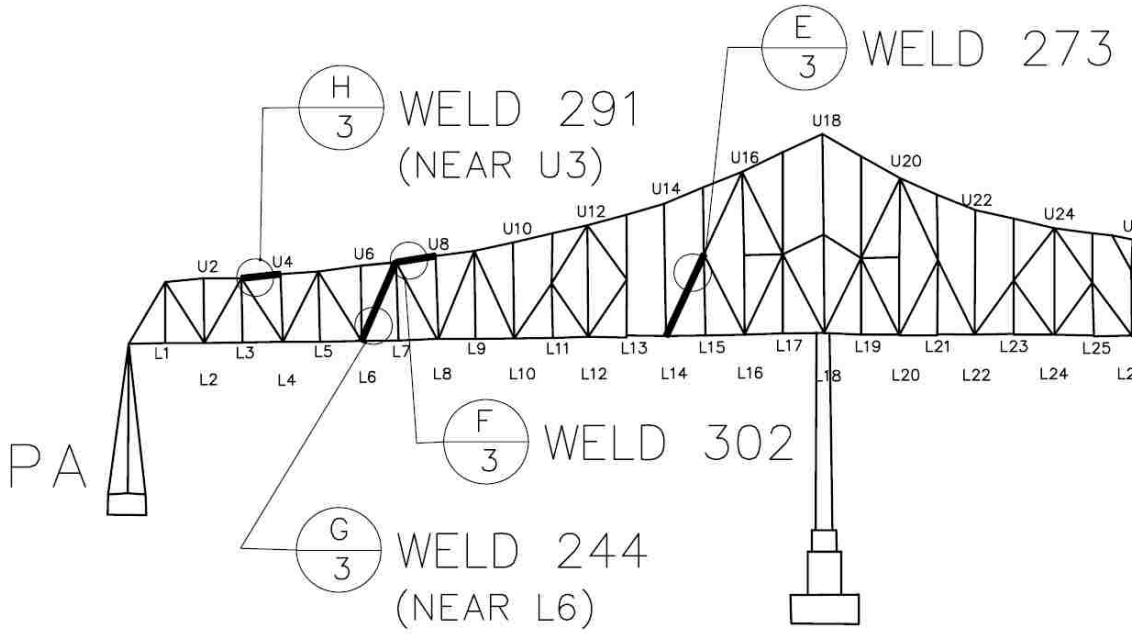

Figure 5.6 Detail of welds in the north truss (From Hodgson et. al, 2008)

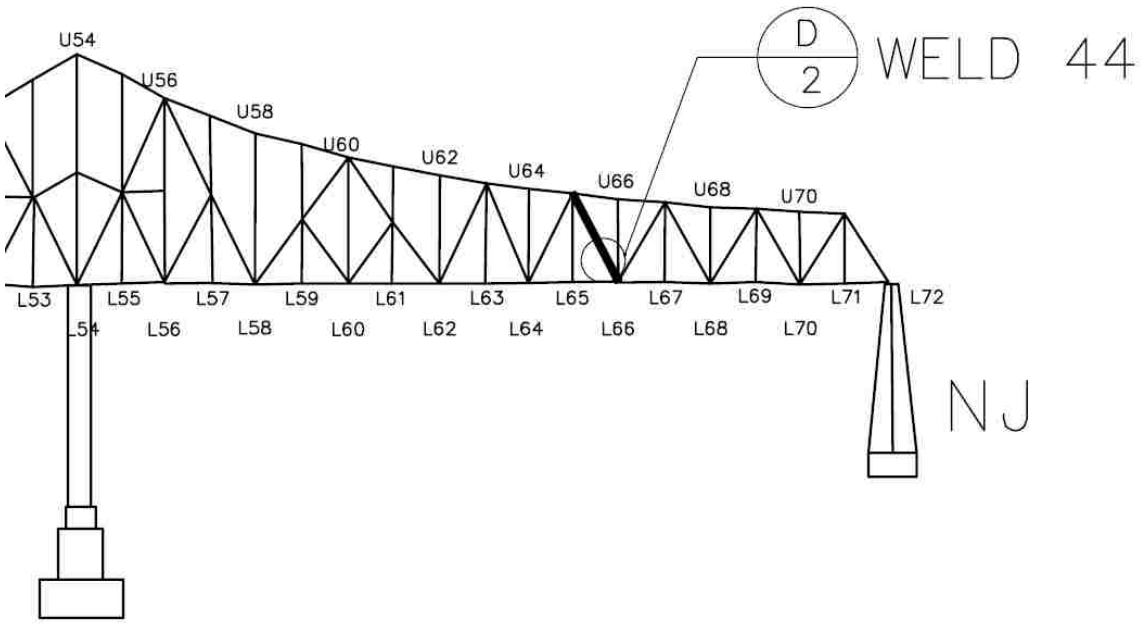

Figure 5.7 Detail of welds in the north truss (From Hodgson et. al, 2008)

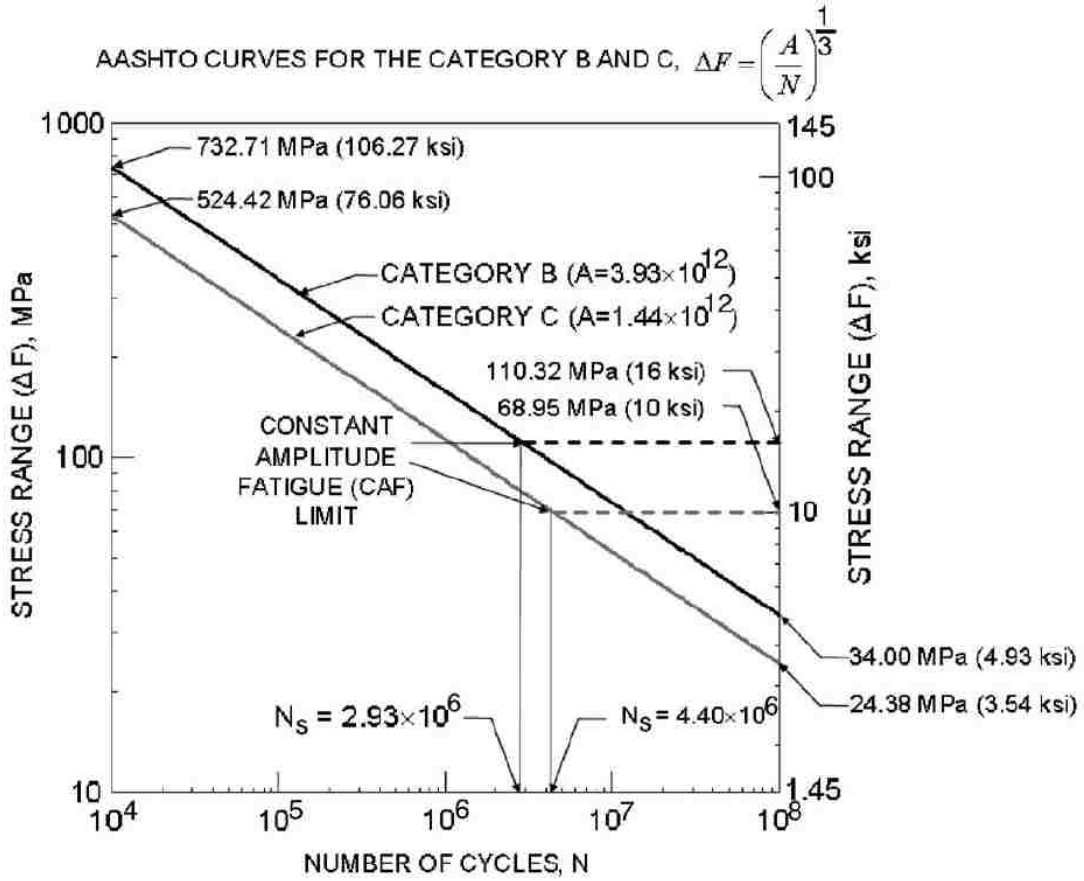

Figure 5.8 Stress range versus number of cycles (From Frangopol et.al, 2008)

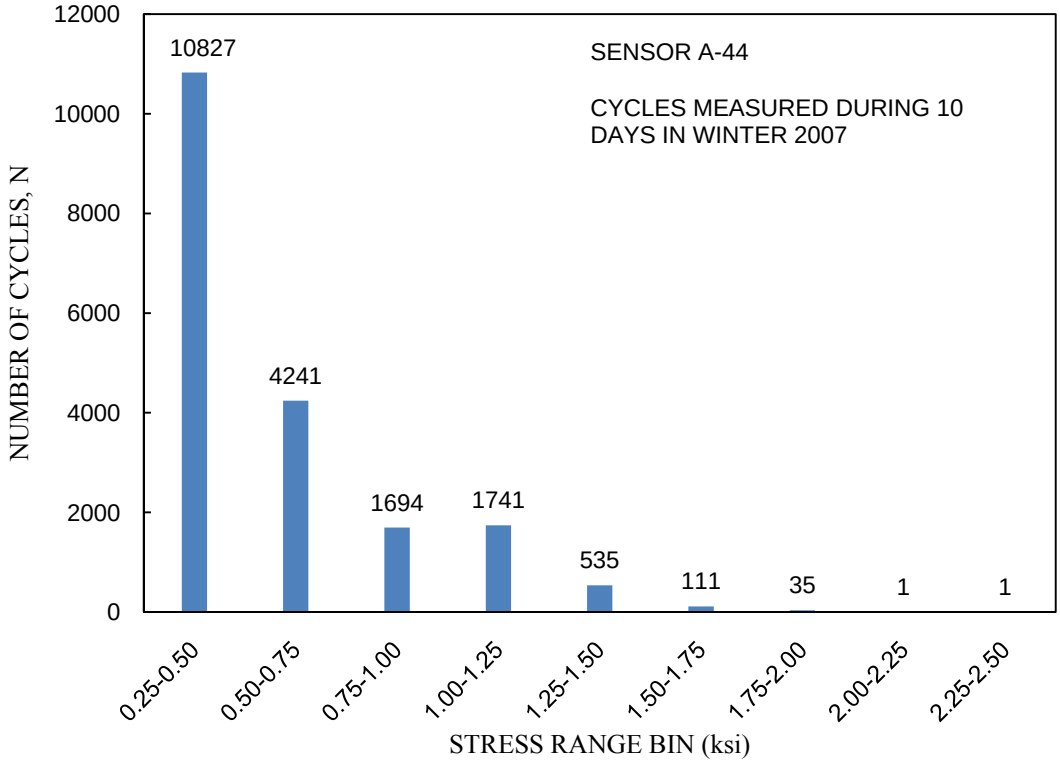

Figure 5.9 Stress range histogram of sensor A-44

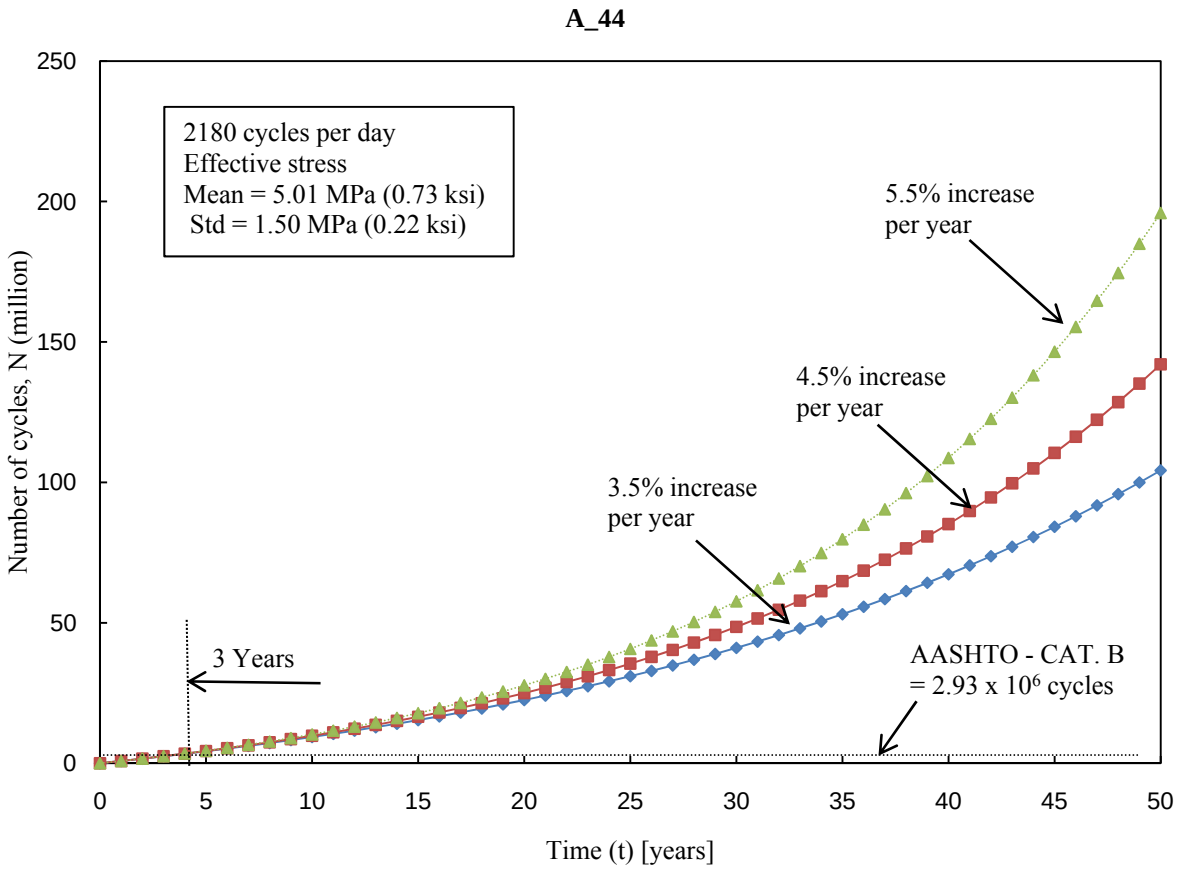

Figure 5.10 Increase in the number of cycles for the sensor A_44

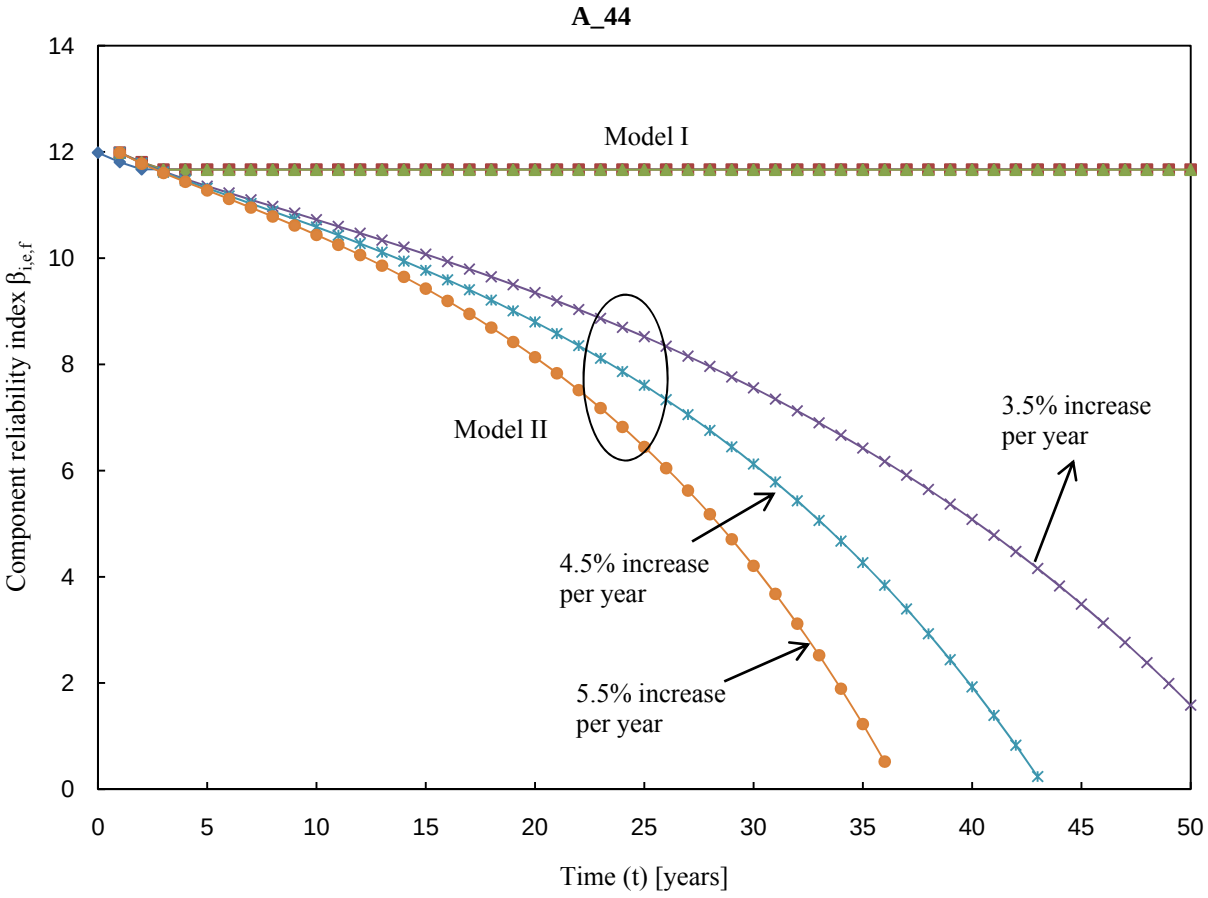

Figure 5.11 Fatigue reliability prediction for the sensor A_44

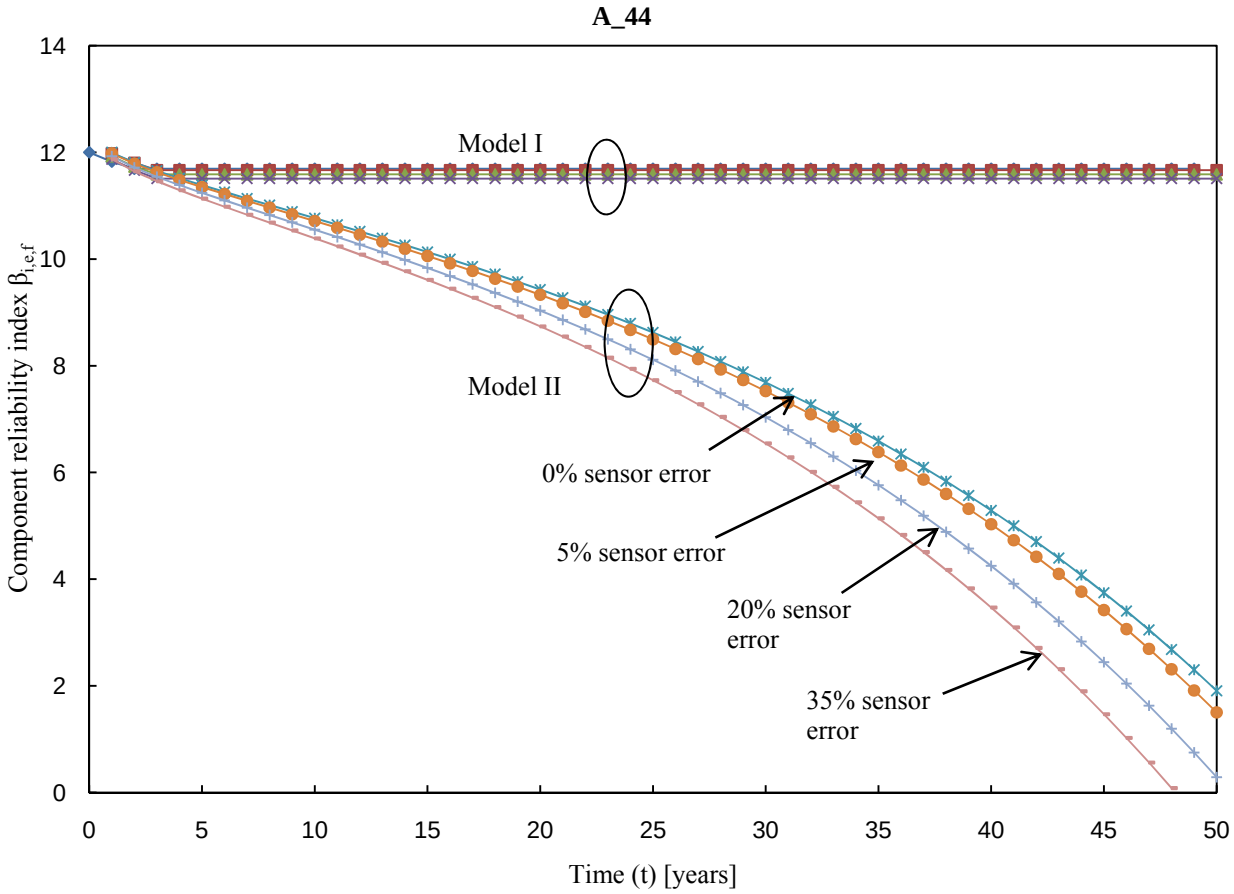

Figure 5.12 Sensor errors affecting the prediction models for the fatigue behavior of sensor A_44

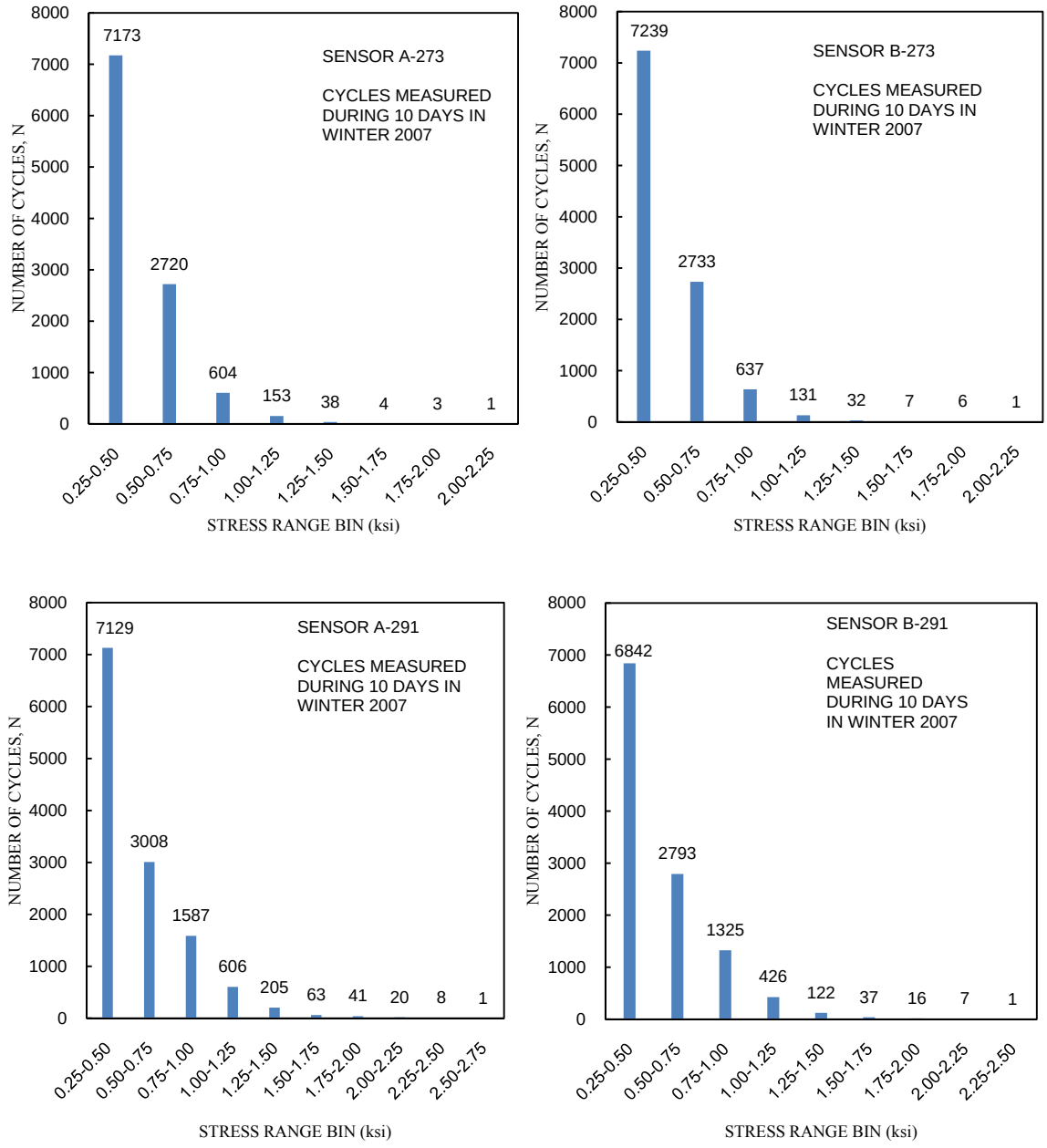

Figure 5.13 Stress range bin histogram for member 273 and 291

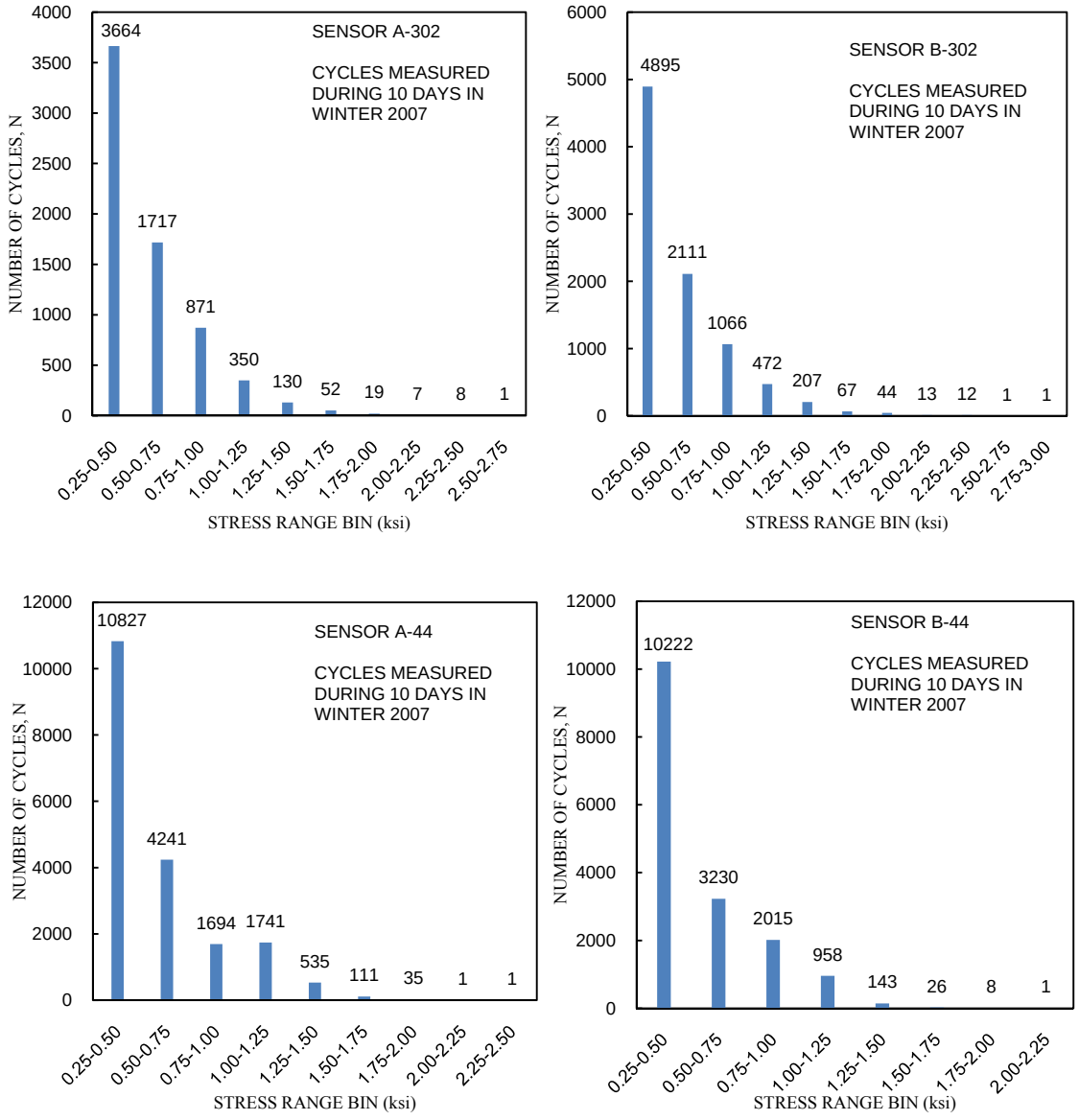

Figure 5.14 Stress range bin histogram for member 302 and 44

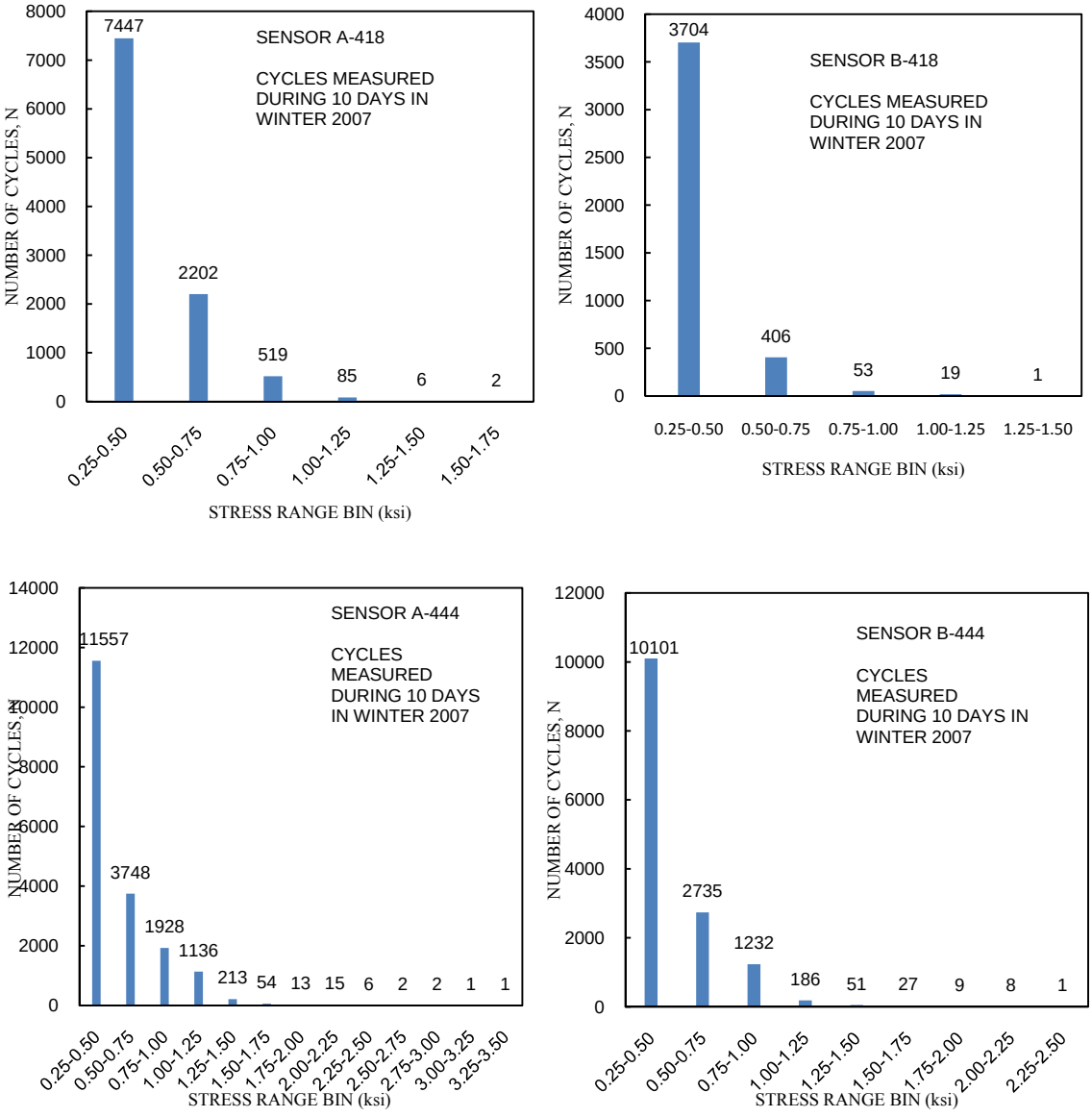

Figure 5.15 Stress range bin histogram for member 418 and 444

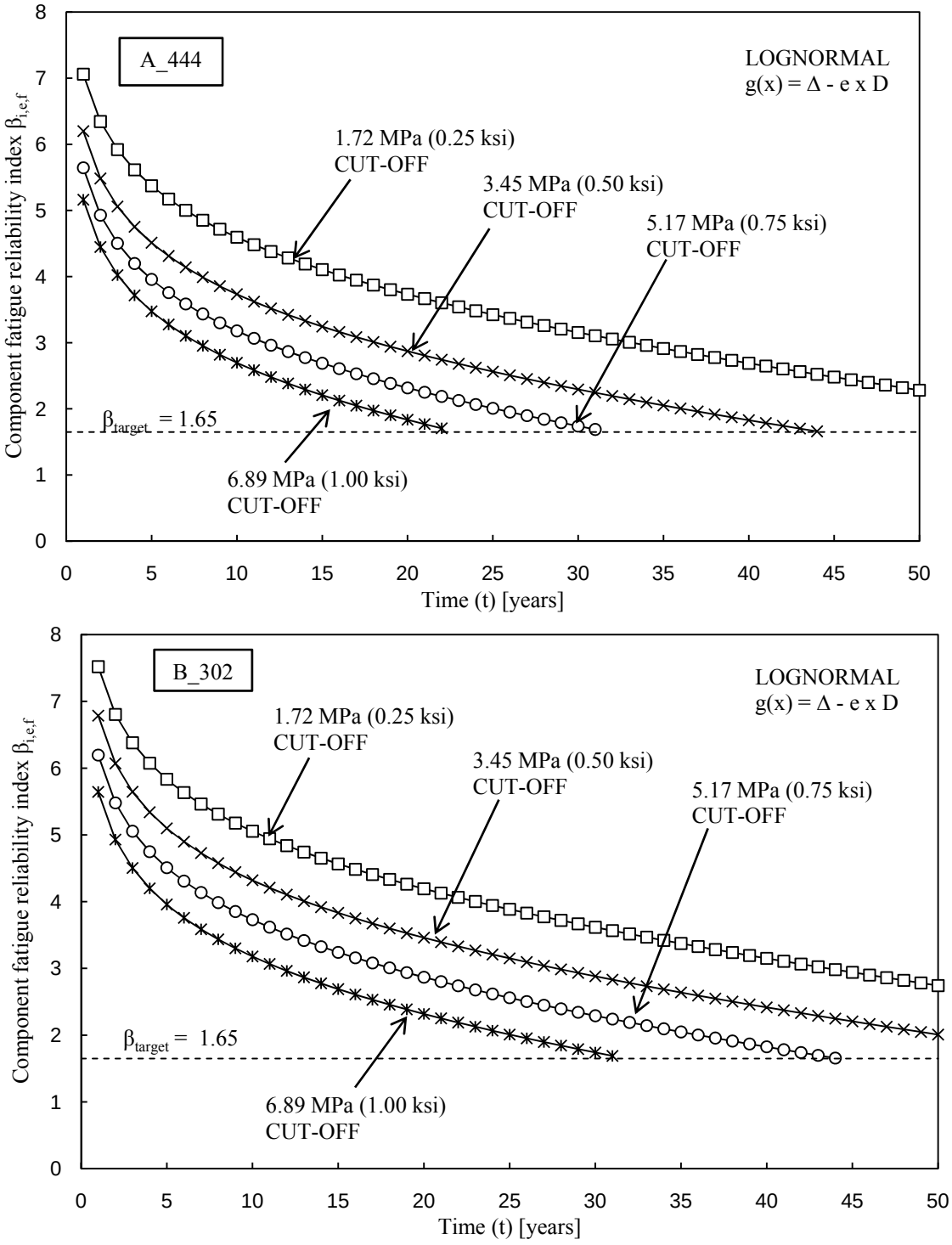

Figure 5.16 Effect of the predefined cut-off thresholds on fatigue reliability of A_444 and B_302

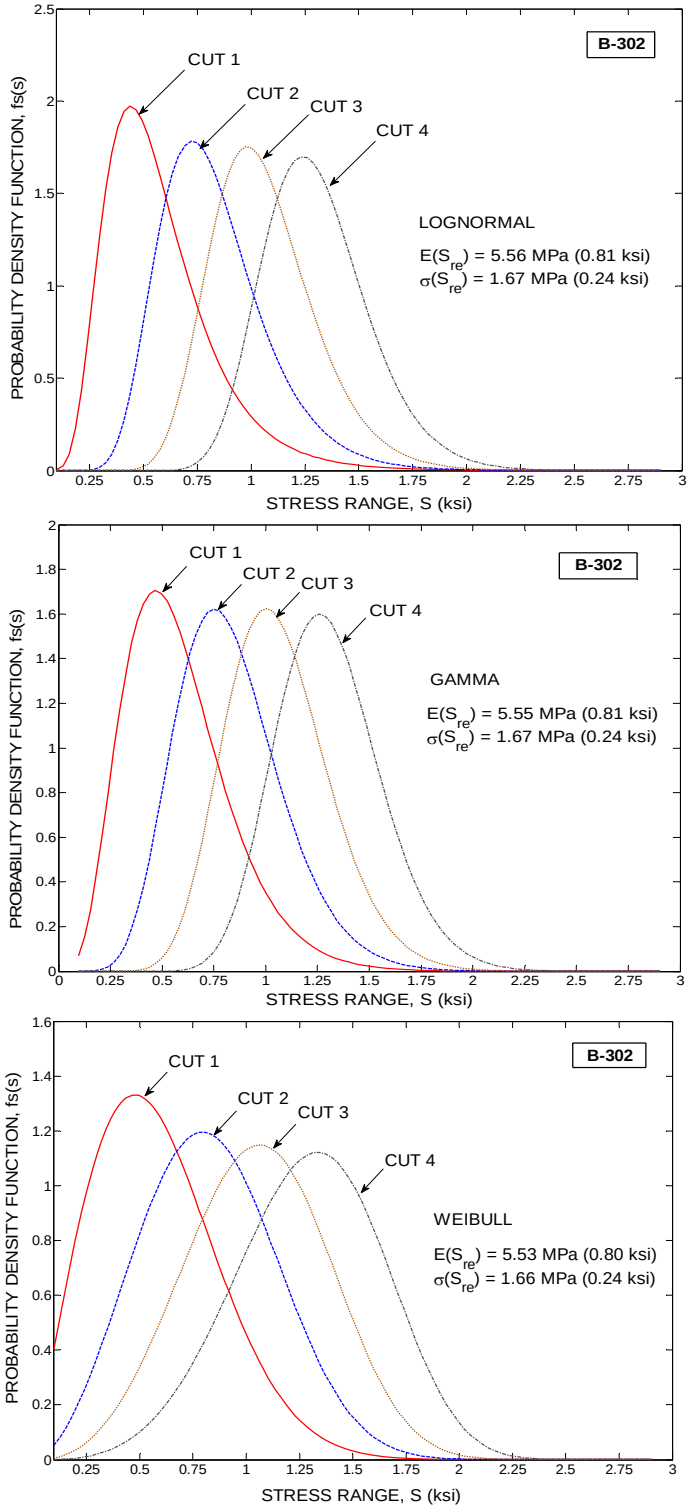

Figure 5.17 PDFs according to the predefined cut-off thresholds of strain gage B-302 for three distribution types

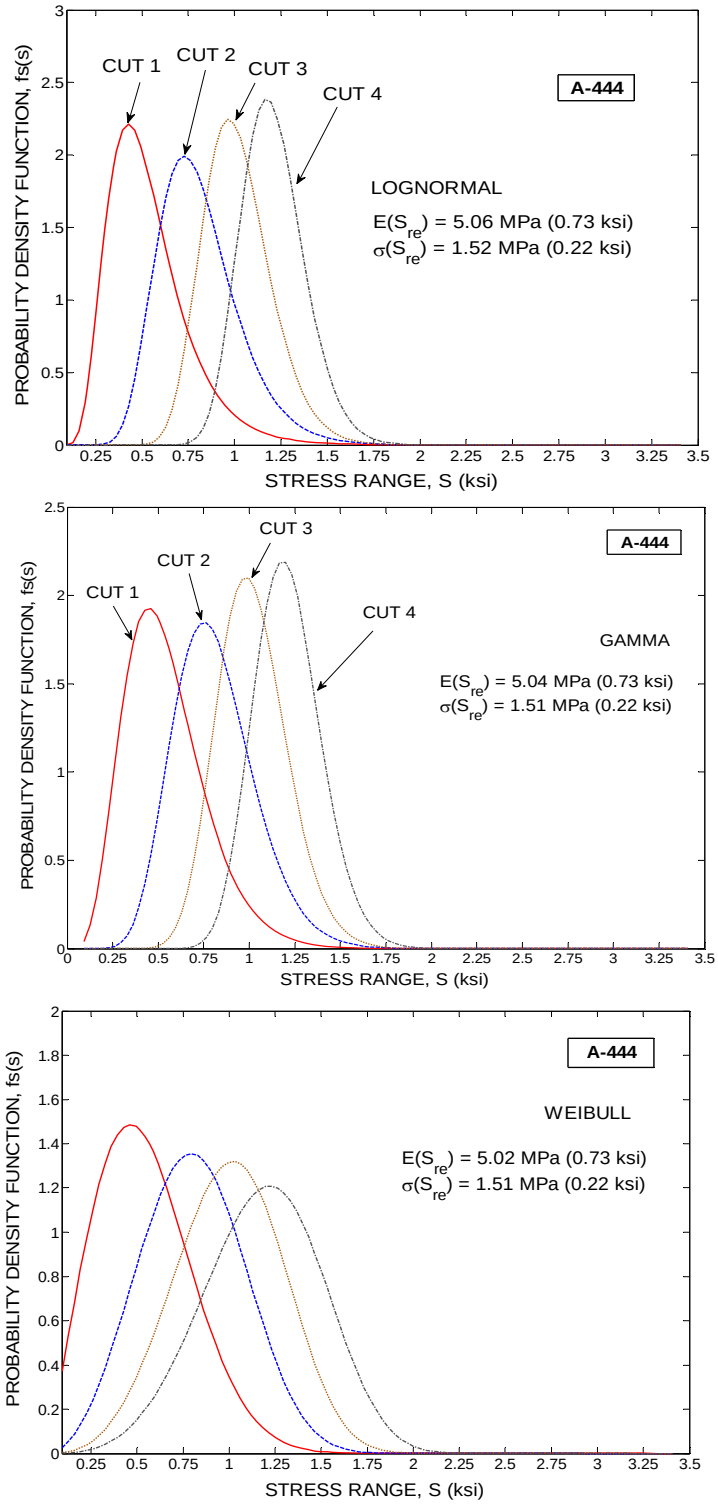

Figure 5.18 PDFs according to the predefined cut-off thresholds of strain gage A-444 for three distribution types

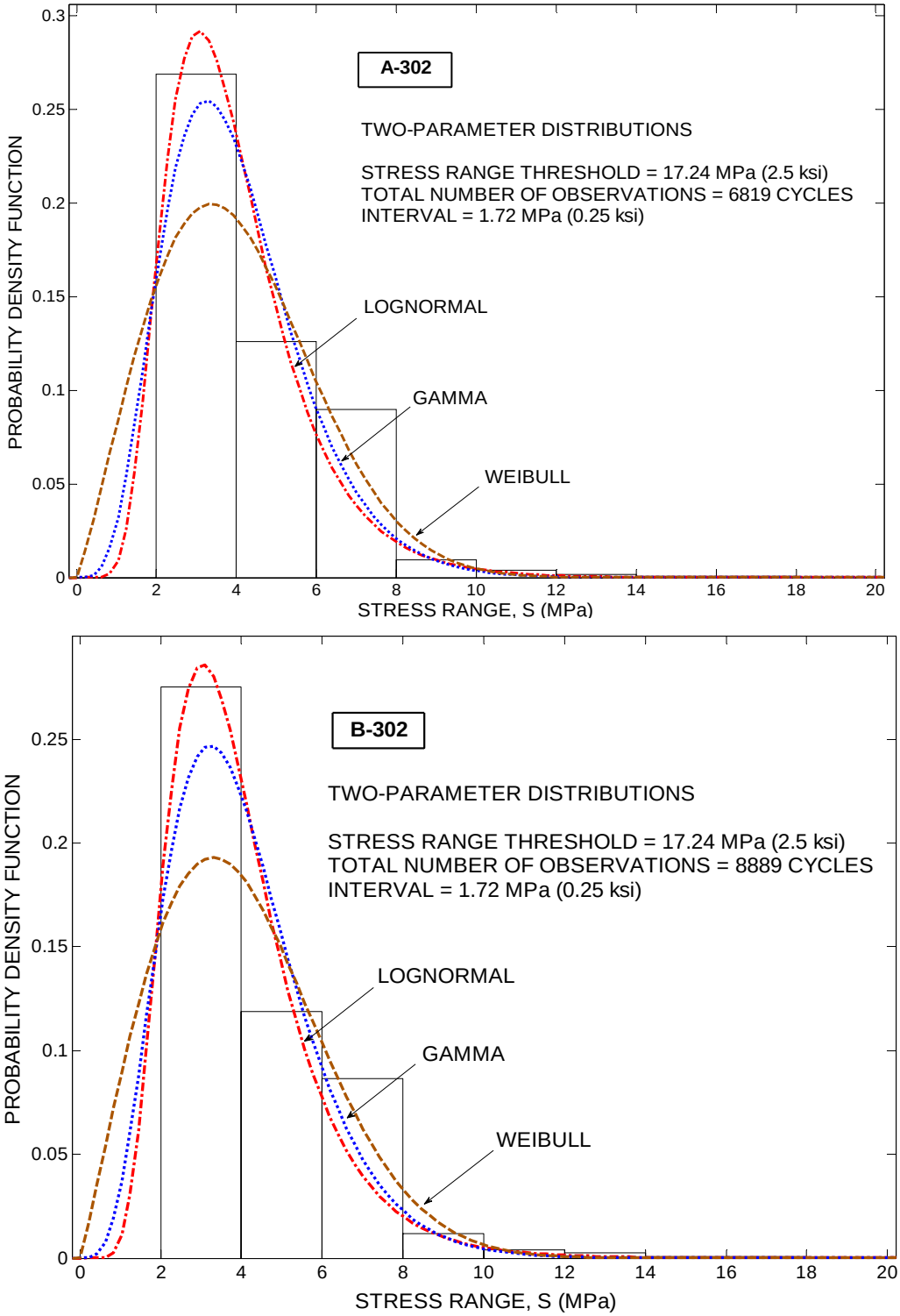

Figure 5.19 Stress-range bin histogram and PDFs at the member 302

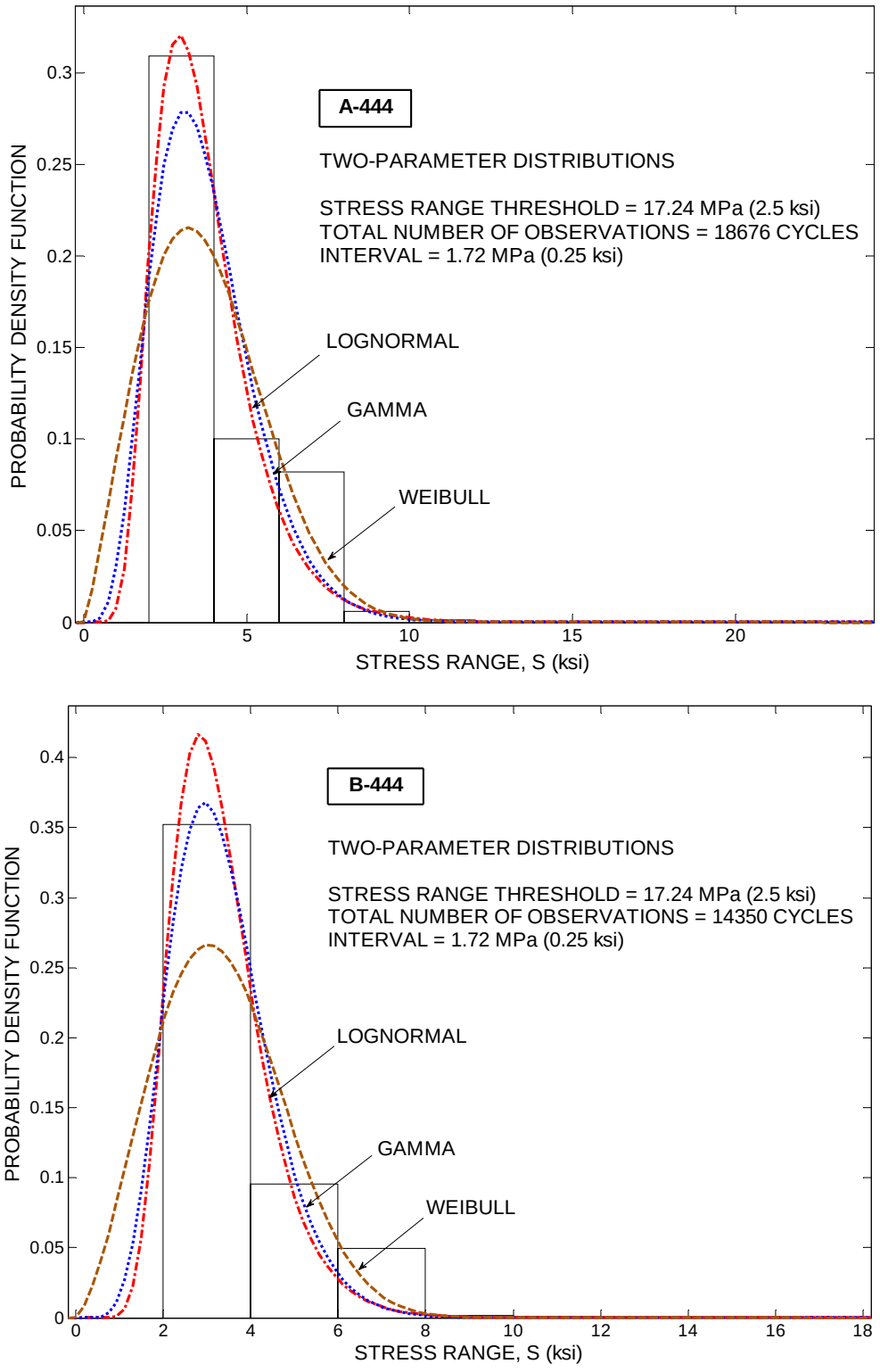

Figure 5.20 Stress-range bin histogram and PDFs at the member 444

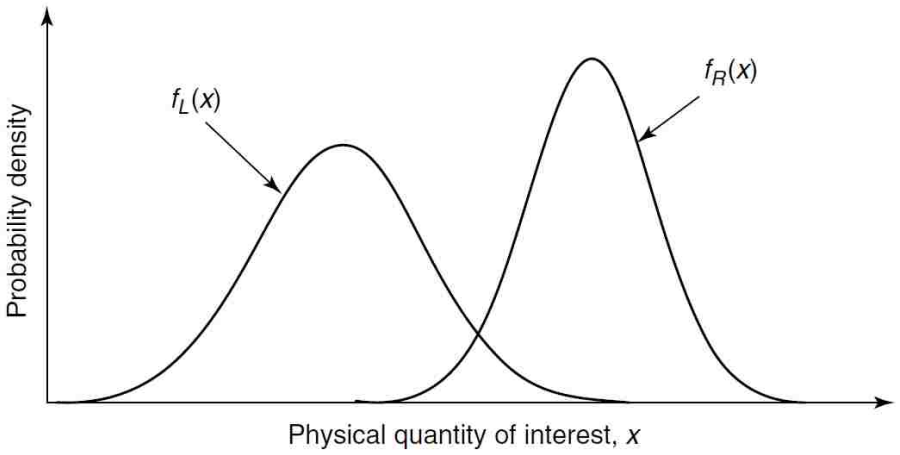

Figure 5.21 Probability density function of resistance and load effect (From Frangopol and Messervey, 2009)

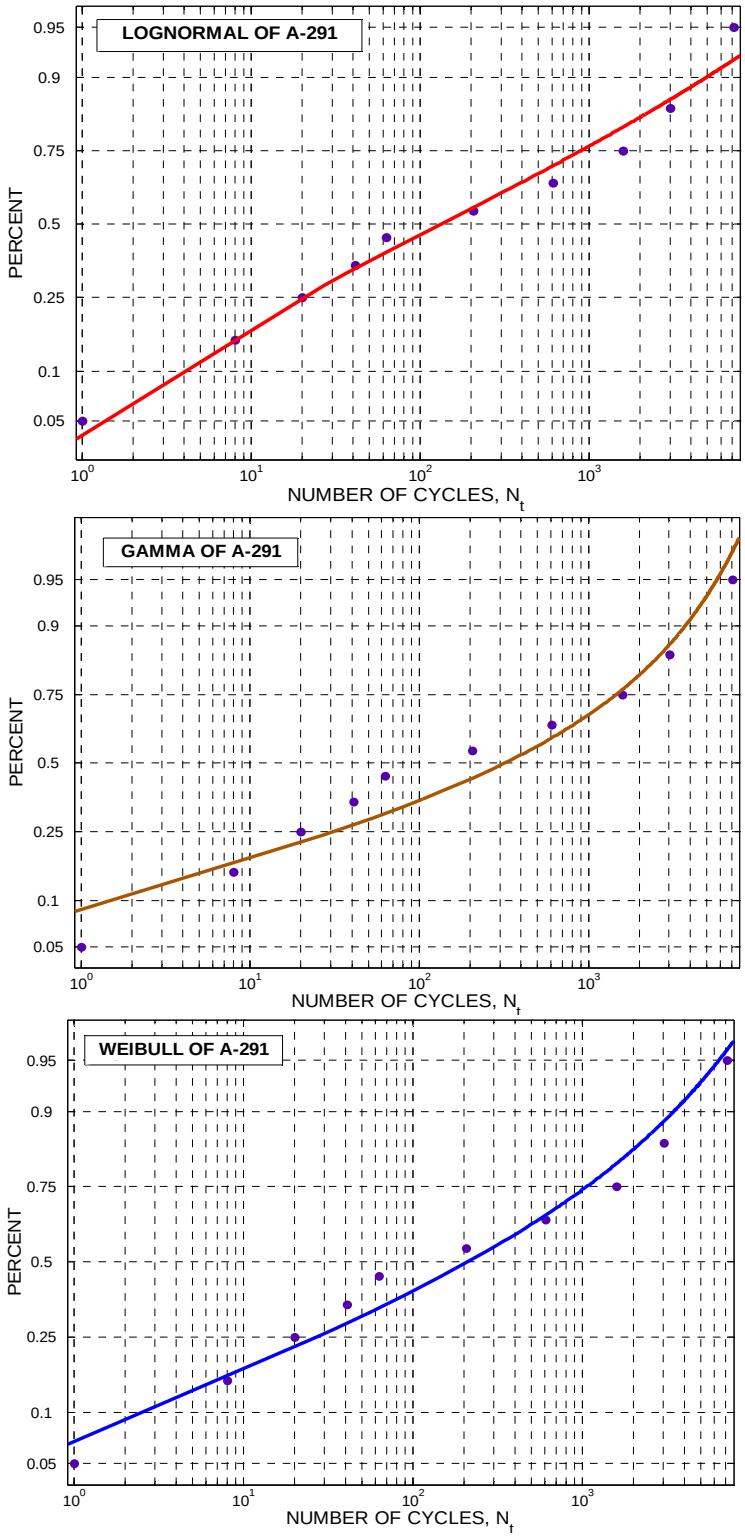

Figure 5.22 Goodness-of-fit tests on the strain gage A_291

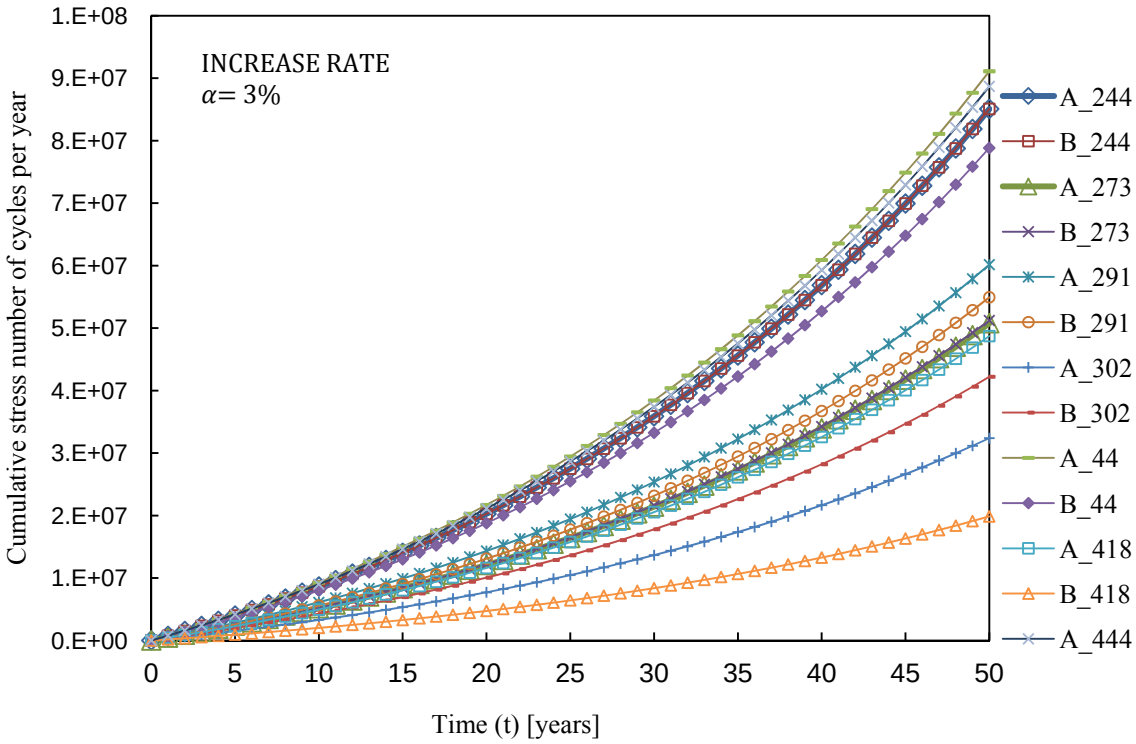

Figure 5.23 Time-variant cumulative stress numbers of cycles for each strain gage

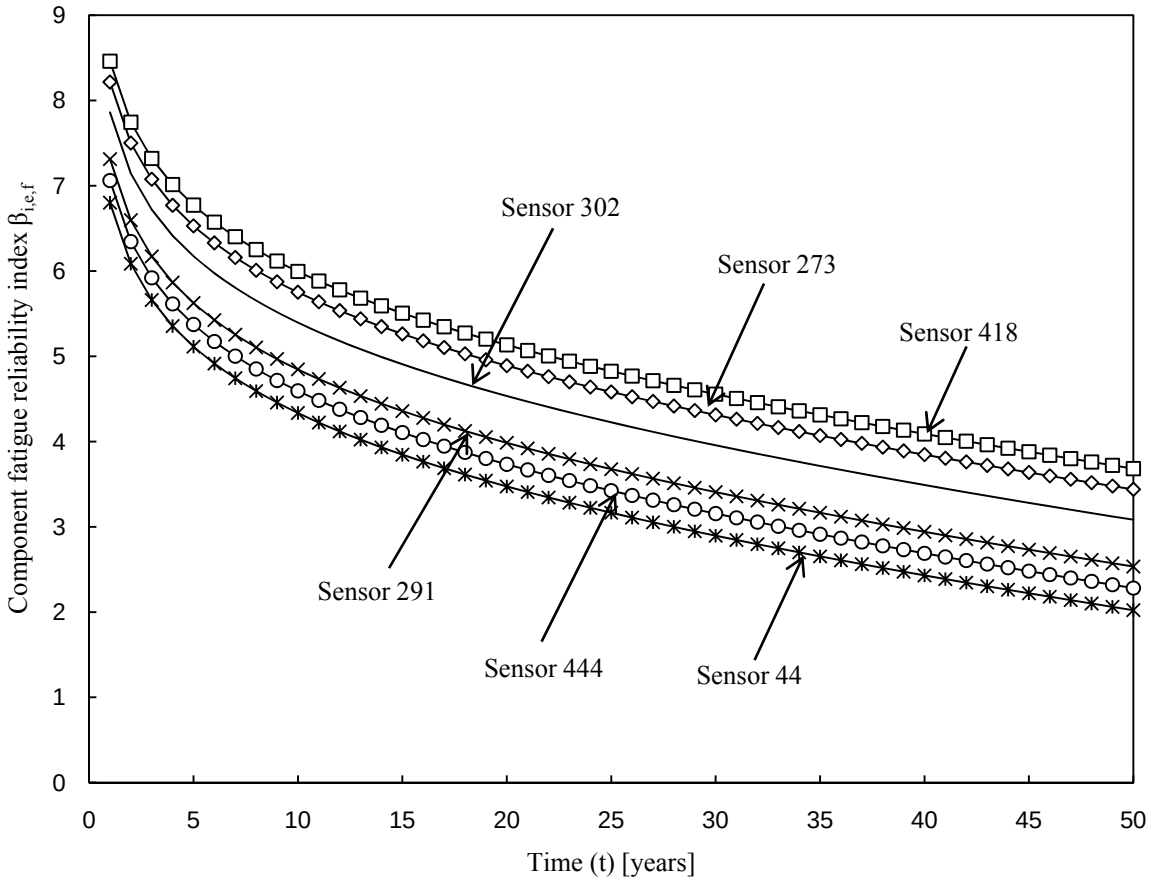

Figure 5.24 Fatigue reliability for six members with critical welds

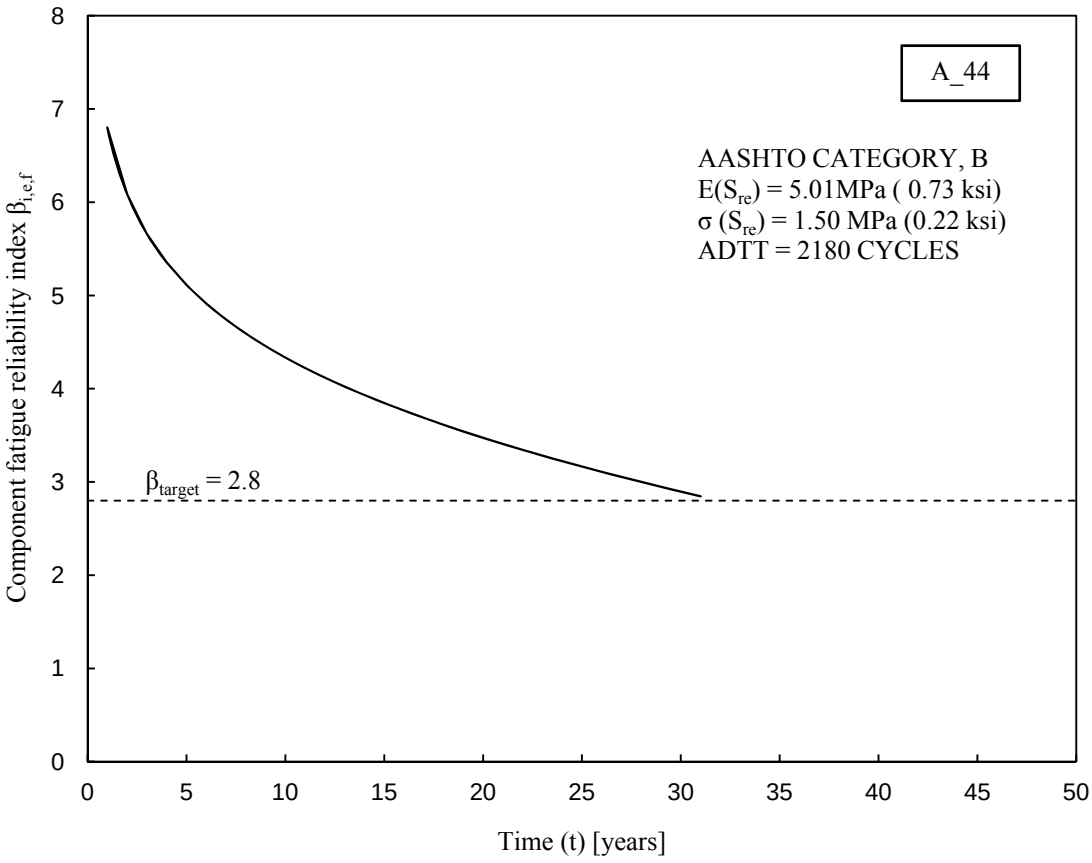

Figure 5.25 Fatigue reliability evaluation on sensor A_44

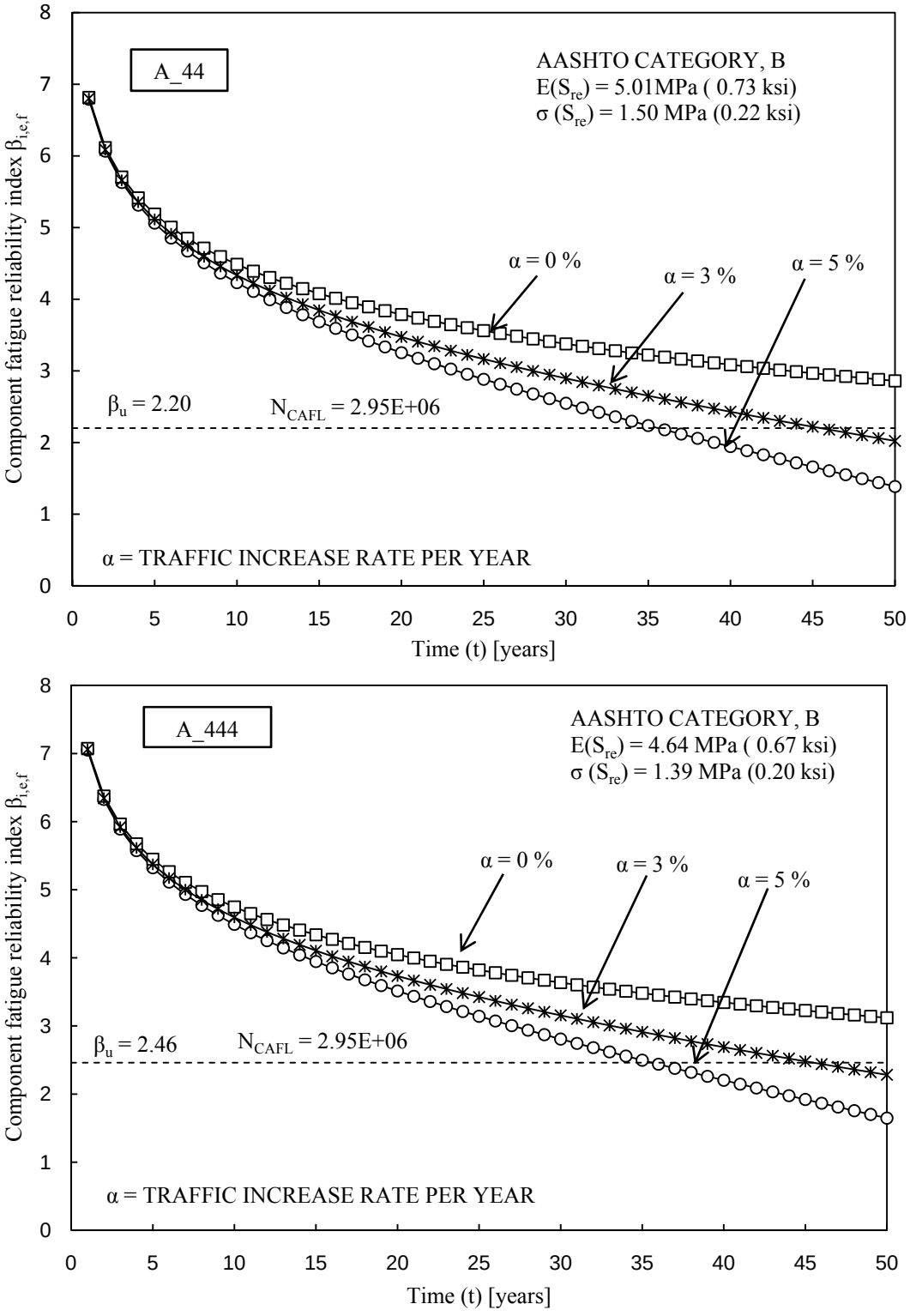

Figure 5.26 Fatigue reliability evaluation on sensor A_44 and A_444

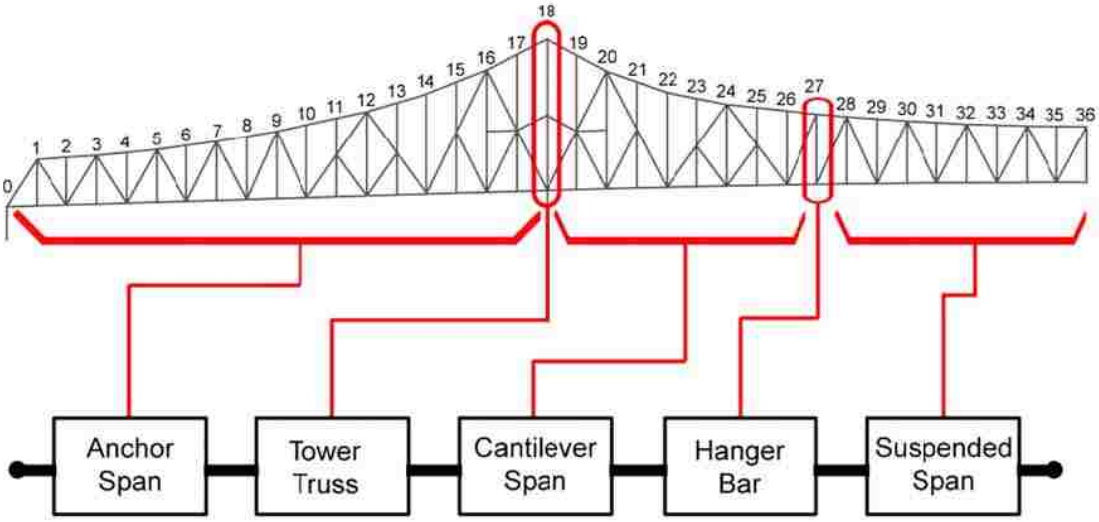

Figure 5.27 System classification for the bridge (From Catbas et.al, 2008)

Series System

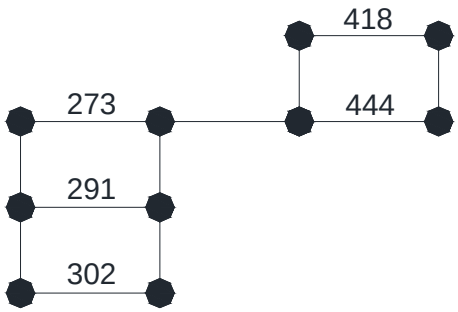

Series-Parallel System

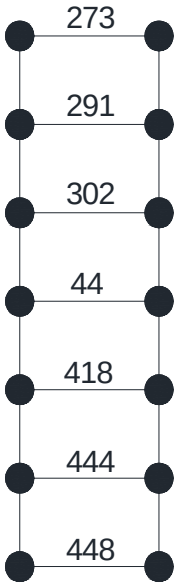

Parallel System

Figure 5.28 System models

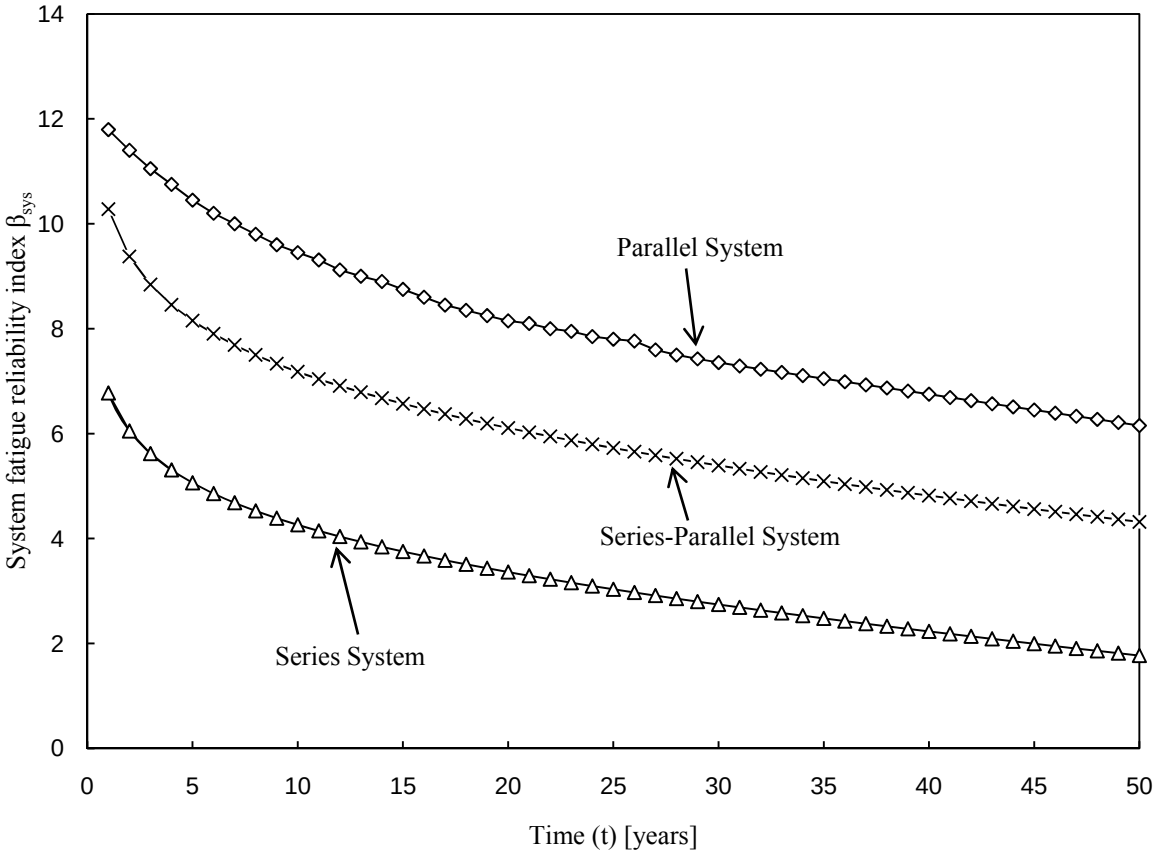

Figure 5.29 Fatigue reliability evaluations on three system models

Table 5.1 Summary of bars with critical welds (From Hodgson et.al, 2008)

Weld ID	Truss	Member Type	Span
44	North	Diagonal	NJ back span
244	North	Diagonal	PA back span
273	North	Diagonal	PA back span
291	North	Upper chord	PA back span
302	North	Upper chord	PA back span
418	South	Lower chord	NJ back span
444	South	Diagonal	NJ back span
448	South	Diagonal	NJ back span

Table 5.2 Summary of key stress range histogram parameters

Strain Gage Location	$S_{R,max}$ (ksi)	$S_{R,max}$ (MPa)	$S_{R,eff}$ (ksi)	$S_{R,eff}$ (MPa)	$\sigma_{R,eff}$ (ksi)	$\sigma_{R,eff}$ (MPa)	Number of cycles per day
A_44	2.5	17.24	0.73	5.01	0.22	1.50	2180
B_44	2.3	15.86	0.65	4.49	0.26	1.79	1887
A_418	1.8	12.41	0.52	3.57	0.16	1.07	1166
B_418	1.5	10.34	0.44	3.04	0.18	1.21	475
A_444	3.5	24.13	0.67	4.64	0.20	1.39	2122
B_444	2.5	17.24	0.57	3.95	0.23	1.57	1631
A_244	2.3	15.86	0.66	4.55	0.26	1.82	2036
B_244	2.3	15.86	0.64	4.41	0.26	1.77	2036
A_273	2.3	15.86	0.55	3.81	0.17	1.14	1215
B_273	2.3	15.86	0.55	3.81	0.22	1.52	1226
A_291	2.8	19.31	0.70	4.86	0.21	1.46	1440
B_291	2.5	17.24	0.65	4.49	0.26	1.79	1315
A_302	2.8	19.31	0.72	4.98	0.22	1.49	775
B_302	3	20.69	0.74	5.10	0.22	1.53	-

Table 5.3 Stress range histogram for Pennsylvania back span members (From Hodgson et.al, 2008)

Stress Range (ksi)		Number of Cycles							
Min	**Max**	**A_244**	**B_244**	**A_273**	**B_273**	**A_291**	**B_291**	**A_302**	**B_302**
0.00	0.25	354175	357572	495999	504554	405940	419762	466277	491246
0.25	0.50	10862	11380	7173	7239	7129	6842	3664	4895
0.50	0.75	3789	3412	2720	2733	3008	2793	1717	2111
0.75	1.00	1866	2091	604	637	1587	1325	871	1066
1.00	1.25	1163	861	153	131	606	426	350	472
1.25	1.50	193	133	38	32	205	122	130	207
1.50	1.75	36	31	4	7	63	37	52	67
1.75	2.00	6	7	3	6	41	16	19	44
2.00	2.25	1	2	1	1	20	7	7	13
2.25	2.50	0	0	0	0	8	1	8	12
2.50	2.75	0	0	0	0	1	0	1	1
2.75	3.00	0	0	0	0	0	0	0	1
3.00	3.25	0	0	0	0	0	0	0	0
3.25	3.50	0	0	0	0	0	0	0	0
3.50	3.75	0	0	0	0	0	0	0	0
3.75	4.00	0	0	0	0	0	0	0	0
4.00	4.25	0	0	0	0	0	0	0	0
4.25	4.50	0	0	0	0	0	0	0	0
4.50	4.75	0	0	0	0	0	0	0	0
4.75	5.00	0	0	0	0	0	0	0	0
S_{Rmax} (ksi) =		2.25	2.25	2.25	2.25	2.75	2.50	2.75	3.00

Table 5.4 Stress range histogram for New Jersey back span members (From Hodgson et.al, 2008)

Stress Range (ksi)		Number of Cycles					
Min	**Max**	**A_44**	**B_44**	**A_418**	**B_418**	**A_444**	**B_444**
0.00	0.25	357844	364660	488200	493156	355623	369753
0.25	0.50	10827	10222	7447	3704	11557	10101
0.50	0.75	4241	3230	2202	406	3748	2735
0.75	1.00	1694	2015	519	53	1928	1232
1.00	1.25	1741	958	85	19	1136	186
1.25	1.50	535	143	6	1	213	51
1.50	1.75	111	26	2	0	54	27
1.75	2.00	35	8	0	0	13	9
2.00	2.25	1	1	0	0	15	8
2.25	2.50	1	0	0	0	6	1
2.50	2.75	0	0	0	0	2	0
2.75	3.00	0	0	0	0	2	0
3.00	3.25	0	0	0	0	1	0
3.25	3.50	0	0	0	0	1	0
3.50	3.75	0	0	0	0	0	0
3.75	4.00	0	0	0	0	0	0
4.00	4.25	0	0	0	0	0	0
4.25	4.50	0	0	0	0	0	0
4.50	4.75	0	0	0	0	0	0
4.75	5.00	0	0	0	0	0	0
S_{Rmax} (ksi) =		2.50	2.25	1.75	1.50	3.50	2.50

Table 5.5 Summary of deterministic and random variables for fatigue reliability assessment

Parameter	Notation	Distribution type	Source
Fatigue detail coefficient	A	Lognormal (25.0291, 0.3316)	AASHTO Specifications,Chung [5], and Keating and Fisher [20]
Equivalent stress range	S_{re}	Lognormal	Field monitoring data
Miner's critical damage accumulation index	Δ	Lognormal LN (1.0, 0.3)	Wirsching [24]
Measurement error	e	Lognormal LN (1.0, 0.03)	Frangopol et al. [18]
Material constant	m	Normal (3.0, 0.01)	AASHTO Specifications [1]
Average daily truck traffic	ADTT	Deterministic	Connor et al. [8,9] Field monitoring data

CHAPTER 6

STRUCTURAL RELIABILITY ASSESSMENT AND PERFORMANCE PREDICTION USING THE STATISTICS OF EXTREMES

6.1 Introduction

Long term Structural Health Monitoring (SHM), which makes a time-based continuous history of structural responses under the live load effects at specific locations, can update and provide the information of structural aging and deterioration process in real time. However, long term monitoring is not cost-effective. The data compression and selection of quality data is time-consuming. To further aid in handling the collected data, the characteristics of statistics of extremes should be realized to use in the condensation process. The features of extreme values are of great significance in many engineering applications. In the field of civil engineering, the monitoring data can be used to update established finite element models and track structural performance over time. For reliability based structural safety evaluation, the probability that resistances are larger than applied loads is highly relevant to the extreme values.

The application of statistics of extremes integrated with field monitoring data will be used in the I-39 Northbound Wisconsin River Bridge which is a five span continuous steel girder bridge. The monitoring period of this bridge was 95 days which is long enough to collect certain amount of data for the extreme value extraction. The controlled load test consists of crawl tests and dynamic tests has been conducted to measure the

maximum stress of structural members, while the uncontrolled load test is conducted to record stresses at sensor locations under the live loads. Both the data acquisition and length of the monitoring period are applicable for the following study.

In the performance function, live load considered as a random variable needs further investigation to improve the accuracy of the models. Messervey (2009) summarizes several compelling advantages of SHM technologies: First, based on the more complete up-to-date data, the existing models and code provisions can be more accurate. Second, monitoring data providing real traffic condition avoid a lot of efforts and also improve the accuracy. The third advantage leveraging SHM is to specialize the study from a general level to a local level, that is, for a specific bridge performance assessment. The fourth advantage is the established models can be updated and changes are tracked over the structural lifetime span if the monitoring based live load distribution is defined. The last advantage of SHM technology is the continuous monitoring data may be available to use to warn decision makers if the target threshold levels are approached (Messervey, 2009).

This chapter indicates the method of integrating the extreme values and monitoring data to simplify and improve the accuracy of prediction on bridge safety evaluation based on a reliability analysis. There is a big amount of data recorded during the monitoring period, but only daily maximum values are considered to use in the analysis. A specific sample size and timeframe are used in the transformation of defining the distribution for large sample size in a long period. Once the distribution of live loads can be determined, the method of identifying the aleatoric or epistemic uncertainty based on monitoring data

will be applied in the bridge reliability assessment.

6.2 Theoretical background (A review of Messervey (2009))

The study of extreme values statistics in this chapter is to predict live load effects in the reliability estimation. Daily maximum stress values will be initially collected as the resource of extreme values being estimated, a determination on the optimum length of timeframe will be made. Due to the collection of only maximum values, the amount of data for analysis has been tremendously reduced. Messervey (2009) investigates an approach using the features of extreme values from live load stress including the uncertainty of errors in the structural lifetime performance evaluation.

Assume X is the initial random variable with known initial distribution function Fx(x). There are sample sizes of n are taken from the sample space of X. Each sample is indicated as a set of observations (x_1, x_2, …, x_n) which means the first, second,…, *n*th observed values. Each observed value is a random variable and random variables (X_1, X_2,…, X_n) are extreme values obtained from samples of observations (x_1, x_2, …, x_n). The maximum values of random variables (X_1, X_2,…, X_n) are also random variables, which can be described as

$$Y_n = \max(X_1, X_2, X_3, \dots, X_n) \tag{6.1}$$

Y_n's probability distributions can be applied in the transformation of probability distribution, which means the largest value from samples of size n taken from random variables (X_1, X_2,…, X_n) are also random variables whose probability distributions may be derived from the initial variate X.

If the distribution of random variables (X_1, X_2,…, X_n) has an exponentially decaying upper tail, its cumulative distribution function and the probability density function of the distribution of the extremes Y can be explained respectively as

$$F_{Y_n}(y) = [F_x(y)]^n \tag{6.2}$$

$$f_{Y_n}(y) = n[F_x(y)]^{n-1} f_x(y) \tag{6.3}$$

Equations (6.2) and (6.3) express that the distribution of the extreme values Y is only relevant with distribution of initial variate X and the number of sample size n. With its asymptotic characteristic, the distribution can be transformed from one timeframe to another if the extreme phenomenon can be defined in a specific timeframe. There are three asymptotic distribution types classified by the tail behavior of the initial PDFs: (1) Type I for the largest value which is the double exponential form is well known as the Gumbel distribution; (2) Type II the single exponential form is often referred to as the Fisher-Tippett distribution; (3) Type III the exponential form with an upper or lower bound is well known as the Weibull distribution. Compare these three distribution types, only the PDF of the largest value from Gumbel distribution will keep the same shape as that of the initial value, the location of its PDF will change when the most probable value of Y_n varies. Researchers conducting a reliability analysis can leverage this asymptotic behavior to consider the time effect of any recurring live load with the transformation defining the distribution of the most likely maximum value (Messervey, 2011).

The use of extreme value statistics is already well established in the design and

assessment of highway bridges for the calibration of load factors, resistance factors, load combination factors and the treatment of design trucks (Ghosen et al. 2003, Ghosn and Moses 1986). The application of extreme value statistics utilizing structure specific data in a probabilistic analysis can consistently account for uncertainties at the local level and develop essentially what could be termed a 'bridge-specific' code (Enevoldsen 2008). The extreme distribution is formed based on picking maximum values from on-site monitoring data. The selection of the most appropriate distribution type can be determined by using the approach goodness-of-fit. Compared with other two asymptotic distributions, the Gumbel distribution has two more advantages: one is the EVD parameters determining the distribution can be decided from the mean and standard deviation of the maximum values of recorded data avoiding complicated numerical calculations or tables; the other one is the factor determining the shape of PDF distribution is constant, so the transformation of the PDF of the maximum live load from current state to its end of lifetime 75^{th} year only needs a simple shift without any shape change. Advantages of characterizing a monitoring based live load include ensuring that live load parameters are reflective of modern truck weights, passing from a general to a structure specific analysis, and replacing the difficult modeling of a traffic simulation that incorporates vehicle speeds, vehicle spacing, and multiple lane side-by-side truck occurrences (Messervey 2011). The practical example will use the method specific to the Type I EVD for reliability analysis.

In order to obtain greater accuracy, more information is needed and characterizing a monitoring based distribution is very sensitive to the available on site monitoring data.

Messervey(2007) conducted research on characterizing monitoring based EVDs and their use in a reliability analysis. In this research, why to choose type I EVD distribution and how to determine its parameters is based on simulations.

The transformation of type I Gumbel distribution is identified by picking up maximum monitoring data, which has been researched to quantify in improving efficiency and accuracy of the transformation. The cumulative distribution function (CDF) and probability density function (PDF) defined for the double exponential type I Gumbel distribution is explained respectively as

$$F_{Y_n}(x) = \exp\left(-e^{-\alpha_n(x-u_n)}\right) \tag{6.4}$$

$$f_{Y_n}(x) = \alpha_n e^{-\alpha_n(x-u_n)} \exp\left(-e^{-\alpha_n(x-u_n)}\right) \tag{6.5}$$

Where n means the number of times the initial distribution X is sampled, α_n is the shape factor, u_n is the characteristic value. The mean value μ_{Y_n} and standard deviation σ_{Y_n} of maximum values Y_n are used to define the parameters of the type I Gumbel EVD

$$\alpha_n = \frac{\pi}{\sqrt{6}\sigma_{Y_n}} \tag{6.6}$$

$$\mu_n = \mu_{Y_n} - \frac{\gamma}{\alpha_n} \tag{6.7}$$

Where $\gamma = 0.5772$ is Euler's number. If the considered number of samples is infinitely large, the distribution obtained via "peak picking" will match the asymptotic transformation of the initial distribution defined as (Ang and Tang, 1984)

$$\mu_{Y_n} = \mu_x + \frac{\ln(n)}{\alpha} \tag{6.8}$$

For the Gumbel distribution, the standard deviation and shape factor are constant and there is no need to transform these quantities using equations.

There are three findings from Messervey (2009): First, the variability of both the mean and standard deviation parameters is approximately equal,

$$\sigma_{\mu_{Y_n}} \approx \sigma_{\sigma_{Y_n}} \tag{6.9}$$

Second, according to the Central Limit Theorem, the variability of both parameters is inversely proportional to the number of maximum values using the standard deviation of the underlying distribution

$$\sigma_{\mu_{Y_n}} = \frac{\sigma_X}{\sqrt{m}} \tag{6.10}$$

$$\sigma_{\sigma_{Y_n}} = \frac{\sigma_{Y_n}}{\sqrt{m}} \tag{6.11}$$

Where m is the number of observations of the maximum value.

Third, the assumption is made as follows

$$\sigma_{Y_n} \approx \sigma_X \tag{6.12}$$

So the variability of both Gumbel EVD parameters can be estimated directly from monitoring data as

$$\sigma_{\mu_{Y_n}} = \sigma_{\sigma_{Y_n}} = \frac{\sigma_{Y_n}}{\sqrt{m}} \tag{6.13}$$

By using transformation calculations and picking up maximum values, the extreme value distribution can be predictable for a sufficient number of n observations. However, the simulation will be more complicated than a single known distribution in consideration of changes in daily traffic, side-by-side truck occurrence, vehicle speed, wind load, temperature, and extreme events. The appropriate observation timeframe and suitable number of observations should be determined to investigate the changes in structural performance by changing distribution parameters. More reasonable results can be obtained by balancing the selection of the observation period and number of observations during the period, the structural future performance can be predicted by repeating the process. In some cases, the study may be constrained for limited amount of monitoring data. A method considering both the availability of amount of data and uncertainty is presented in the application example.

6.3 Numerical example

6.3.1 Description of I-39 Northbound Wisconsin River Bridge

The I-39 Northbound Bridge was built in 1961 in Wausau, Wisconsin, USA. The bridge carries the northbound traffic of the interstate I-39. According to Mahmoud et al., it is a five span continuous steel plate girder bridge. The alignment of the horizontal curved girders is symmetric with respect to the mid-point of the third span. The bridge spans are: 30.40m (109.6 ft) for the lateral spans, 42.64m (139.9 ft) for the second and fourth spans, and 42.67m (140 ft) for the middle span. The total length of the bridge is

188.81m (619.45 ft). The horizontal curved bridge has two northbound traffic lanes with four steel plate girders spacing at 2.74m (9.0 ft) equally. The built-up steel girders are a combination of the top and bottom flange plates and a typical 132.1 cm (52 in.) high web plate. The steel flange plates vary from 38.1 cm (15 in.) to 45.7 cm (18 in.) in width, and 3.175 cm (1.25 in.) to 4.445 cm (1.75 in.) in thickness. The steel used in the girders is M270 Grade 50 W with the nominal yield strength of 345 MPa (50 ksi). The bridge was opened to traffic in 1961, and carries the average daily traffic (ADT) from 2165 to 14,500 during the period from 1964 to 2001. (Wisconsin department of transportation.2002).

6.3.2 Monitoring Program

The monitoring program was operated between July and November 2004 by researchers from ATLSS Center. The objectives of this program are (Mahmoud et al. 2005): First, assessing the serviceability of the bridge by conducting a complete fatigue evaluation of various fatigue prone details. Second, estimating remaining fatigue life of the details in question. Third, monitoring the overall behavior and the global response of the bridge for a period of up to 3 or 4 months. There were 24 resistance strain gauges fully temperature compensated by applying the recommended thermal expansion coefficients for structural steel and two linear variable differential transformers installed at 24 locations on the bridge. The controlled load tests including crawl test [speed up to 8 km/h (5 mph)] and dynamic tests [speed up to 108 km/h (65 mph)] were performed between 9 a.m. and 11 a.m. on July 28, 2004, by employing two triaxle dump trucks with the gross vehicle weights of 296.5 kN (67.2 kips) and 329.2 kN (74.6 kips), respectively. The monitored strain data from the uncontrolled load tests were extensively collected and

investigated during the period of 95 days from July 29 to November 3, 2004. It should be noted that all the monitored strain data used in this study are converted into the stress data under the assumption that these strain data follow Hooke's law. The details about the monitoring are reported in Mahmoud et al. (2005). (Liu, M., Frangopol, D.M. and Kim, S. 2009b).

6.3.3 Monitoring data collection and selection

Twenty four strain gages and two Linear Variable Differential Transformers (LVDT) are selected to collect data. The long term monitoring program commenced on July 29, 2004 until November 3, 2004, for a total of approximately 95 days. For each sensor, 82 days of data are available to use. A predefined stress limit was used to minimize the volume of recorded data from the stress-time-history files. So the data history is not continuous. Two test trucks were used to do the controlled load test including a series of crawl and dynamic tests. A logger used to collect data is a high speed, multi-channel, 16-bit system configured with digital and analog filters to assure noise-free signals. Table 6.1 shows the statistical information of daily maximum live load stress for the four estimated strain gages. (Mahmoud et al., 2005)

The study focuses on data recorded from four strain gages installed in span 2 at four girders respectively. Daily maximum data during the whole monitoring period is selected for the application of the statistics of extremes. Figure 6.1 shows the structural response of strain gage CH_19 on July 29, 2004. It is shown that the maximum stress which is nearly 40 MPa occurred around 7:05pm at night. In this way, the daily extreme stress

values for strain gages CH_17, CH_18, CH_19 and CH_20 are selected to find most critical members for reliability analysis. Figure 6.2 represents the top view of the bridge and detailed sensor locations.

6.3.4 EVD parameter determination and observation timeframe optimization

The four girders which are installed with strain gages CH_17 to CH_20 will all be selected for the reliability analysis. The data provided in Table 6.2 can be applied to characterize the daily EVD for the four sensors, however, there is still the possibility that some longer observation timeframe is more appropriate to decrease the uncertainty of the characterization of the EVDs. Therefore, the new parameters for determining distribution of PDFs are created by picking up maximum stress values from a series of timeframe length (one day, two days, three days, six days, nine days and twelve days). Since new maximum values are verified by various timeframe lengths, corresponding EVDs can be defined by Equations (6.6) and (6.7). Mean value and standard deviation of daily maximum stress can be calculated from daily maxima record during monitoring period. Figure 6.3 shows distribution of PDFs for the selected timeframe lengths for the sensor CH_19 in span 2. It is seen that the shapes for 2 day and 3 day maxima EVDs experience large changes than daily maxima EVD, which indicates daily maximum values fluctuate routinely in a short period. The EVDs are better defined for longer timeframe, such as 6 days, 9 days and 12 days, the shapes for these timeframes are very similar. (Messervey, 2009)

Table 6.2 reports the EVD parameters on different timeframes for sensor CH_18. The 9 day length of timeframe is selected as the most appropriate timeframe length because it

has lower value of coefficient of variation than the others and maximizes number of available daily maxima observations. Another approach can be applied is to compare the experimental cumulative frequency with the CDF of an assumed theoretical distribution. Figure 6.4 displays empirical cumulative distribution function and the best fit Type I EVD for sensor CH_19 in span 2. It is seen that the selection of optimum timeframe of EVD is reasonable although the amount of extreme data is limited.

The lifespan of the bridge is defined as 75 years and the bridge was opened to traffic in 1961, so there are 32 years left since the year of 2004 when monitoring program started. Table 6.3 has the results for the 9 day and 32 year prediction parameters of the type I Gumbel distribution. Figure 6.5 shows the transformation from 1 day and 9 day timeframe to 32 year EVDs respectively. It also reports that the 32 year predicted EVD for 9 day timeframe of EVD has a smaller mean value and standard deviation than those of daily timeframe.

The 9 day EVDs for sensors CH_17 to CH_20 are illustrated in Figure 6.6. Sensor CH_17 has greater mean value than the other three sensors which means the girder installed with sensor CH_17 is afforded much more load than the other three girders. For sensor CH_20, it has the lowest standard deviation but similar mean value as sensor CH_19. The impact of the selection of 9 day maxima EVD as the optimum one is illustrated in Figure 6.7 which shows the transformation of daily maxima EVDs to 32 year EVDs for four investigated sensors. It is shown that sensor CH_17 has a much higher mean value for 9 day maxima than the other sensors and its mean of 32 year EVD is also the highest. The mean maximum stress values for the other three sensors are

nearly close prior to transform, but the variation of the means between these three sensors increases after the transformation due to different standard deviations which increase in proportional to the location factors.

6.3.5 Variation of parameters for EVDs

Since the 9 day timeframe is selected as the optimal choice for EVD, the variety of mean and standard deviation for 9 day EVD is estimated by observations. Figures 6.8 and 6.9 display how the mean and standard deviation will change with the number of observations, respectively. Both of these figures indicate that the mean and standard deviation fluctuate in the scale of observation times.

6.3.6 Two approaches applied in the reliability analysis

Two methodologies (Messervey, 2009) which are error-based and treating monitoring-based parameters as random variables can quantify the uncertainty of characterizing live load distribution.

6.3.6.1 Monitoring based distribution parameters as random variables approach

During the process of obtaining live load data, the occurrence of errors is very likely to happen. How to account for the uncertainty of error into live load defined as a random variable will make great effect on the value of the reliability index. The mean of the mean maximum stress value μ_{Y_n} in a selected timeframe is computed by Equations (6.7) and (6.8). The mean of its standard deviation σ_{Y_n} equals standard deviation of the maximum stress in the selected timeframe. Regarding to variability of mean μ_{Y_n} and standard deviation σ_{Y_n}, it is can be estimated by Equations (6.10) to (6.13) with the assumption that these two parameters are approximately equivalent when the parameters are

proportional to the amount of available monitoring data. Both the random variables μ_{Y_n} and σ_{Y_n} are treated as normally distributed, the parameters μ_{Y_n} and σ_{Y_n} defined as the parameters to determine the PDF distributions of EVDs are computed according to the Type I Gumbel distribution characterization, which can be used to transform the distribution to any timeframe.

The performance function of this approach is described as

$$g = R - L_{DS} - L_{DC} - L_L \tag{6.14}$$

$$L_L \begin{cases} \mu_{Y_n} \begin{cases} \mu_{\mu_{Y_n}} \\ \sigma_{\mu_{Y_n}} \end{cases} \\ \sigma_{Y_n} \begin{cases} \mu_{\sigma_{Y_n}} \\ \sigma_{\sigma_{Y_n}} \end{cases} \end{cases}$$

It is defined that the two parameters themselves are random variables with computed mean and standard deviation.

Because μ_{Y_n} and σ_{Y_n} are both random variables, the reliability index derived from this approach is also a random variable. A Monte Carlo simulation is conducted to incorporate the uncertainty of the two parameters into the reliability analysis. The simulation is conducted 2000 iterations to get 2000 values of the reliability indices. Figure 6.10 shows the histogram of the reliability index simulated from collected live load data in sensor CH_19.

6.3.6.2 Error based approach

In order to quantify the uncertainty of error related with the available monitoring data and selected observation timeframe separately, this approach considers the effect of error as two additional terms. The performance function for the bridge is described as

$$g = R - L_{DS} - L_{DC} - \left(L_L + \varepsilon_{obs} + \varepsilon_{timeframe}\right) \quad (6.15)$$

Where R indicates the member resistance, L_{DS} means the dead load caused by steel, L_{DC} means the dead load caused by concrete, L_L means the monitoring-based EVD live load, ε_{obs} is the error term associated with the available data, $\varepsilon_{timeframe}$ is the error term associated with timeframe of EVD. All the terms excluding L_L are assumed as normally distributed. The nominal steel strength as mentioned is 345 MPa (50 ksi), but probabilistic values have to be determined. Strauss et. al have done an extensive research to exam the steel yield strength, tensile strength and their correlation of the probabilistic models (Strauss A et. al, 2006) Based on the investigations from Strauss et al., the probabilistic descriptor for the I-39 Northbound Bridge is derived as having a mean value of 380 MPa (55.11 ksi) and a standard deviation of 26.6 MPa (3.86 ksi), which are symbolized as μ_R and σ_R. The mean values for dead load stress caused by steel and concrete are $\mu_{DS} = 116.3\ MPa$ and $\mu_{DC} = 108.8\ MPa$, respectively. The coefficients of variation for the resistance and dead load (concrete and steel included) are 0.07 and 0.04, respectively. So the standard deviations for resistance and dead load are computed as: $\sigma_R = 380 \times 0.07 = 26.6\ MPa$, $\sigma_{DS} = 116.3 \times 0.04 = 4.65\ MPa$, $\sigma_{DC} = 108.8 \times 0.04 = 4.35\ MPa$. Both the error terms are taken a mean value of zero which means the two error types have the same weighted average value zero indicating the same probability of overestimating or underestimating the magnitude of live load. The standard deviations of two error terms are computed as the product of the coefficient of variation and average daily maximum stress value μ_{Y_n}, which can be obtained by Equations (6.6) and (6.8). The coefficients of variation are assumed as 0.22 and 0.03, respectively, which

are derived based on Messervey's research. Table 6.4 reports all the random variables regarding to their distribution types, parameters in terms of mean and standard deviation, symbols and sources used in the error based approach.

6.3.6.3 Results

The reliability analysis is conducted on both component and system level. The system models are created based on the different failure modes: First, system model I - Series system, the most conservative one which assumes that any failure of the girder will induce system failure; Second, system model II – Series-Parallel system I, which is assumed any two girder fail will result in system failure; Third, system model III – Series-Parallel system II, assume the failure of any three girders will induce failure of the system. The three system models are presented from Figures 6.11 to 6.13.

6.3.6.3.1. Reliability analysis by using the first approach

For the component level analyzed by using the first approach, Figure 6.14 indicates the reliability indices for the four girders installed with sensors CH_17, CH_18, CH_19 and CH_20 from year 2004 until the end of its lifespan of 75 years. It is seen that the girder with sensor CH_17 has the lowest value of reliability index from the year of monitoring until the end of lifespan. The reliability indices of the other three girders are very close at the beginning, but the girder with sensor CH_20 decreases the most rapidly during the lifetime and the girder with sensor 18 is the most reliable one. Figure 6.15 shows the system reliability indices for the three models for the rest of its lifetime. Series-Parallel system II assuming the failure of any three girders has the highest reliability index value among the models during the lifetime, while the reliability index for series

system is much lower than the other two models. Figures 6.16 to 6.18 compare the component reliability indices of four girders with each system model, respectively. It is shown that the time-variant reliability index of series system is the same as the girder with sensor CH_17. As the most critical member with the lowest reliability index, the girder installed with sensor CH_17 should receive the monitoring priority. Figures 6.17 and 6.18 display system reliability indices of the two series-parallel systems are nearly the same as sensor CH_19 and CH_20.

6.3.6.3.2. Reliability analysis by using the second approach

Figures 6.19 and 6.20 show the time-variant reliability indices of the four girders estimated by the second approach during the rest of its lifetime on component and system level, respectively. The results obtained from the two figures are very close to the ones by the first approach. Figures 6.21 and 6.22 compare reliability indices estimated by using two approaches at the component and system level, respectively.

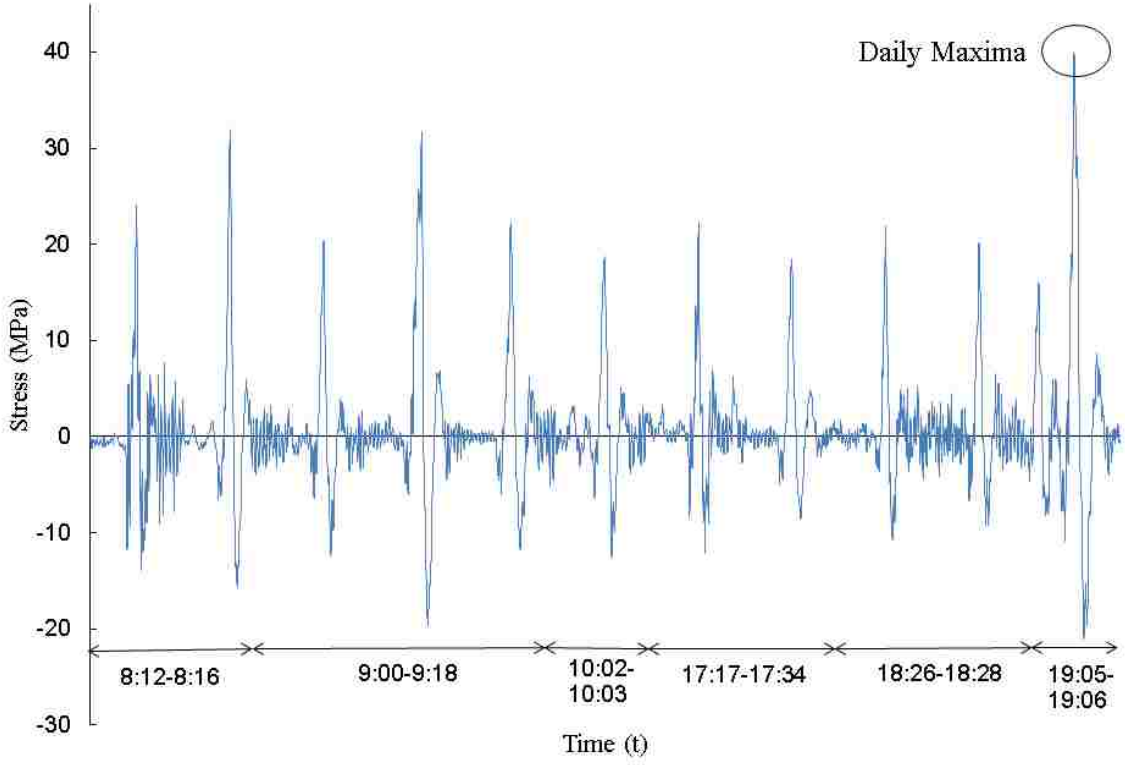

Figure 6.1 Structural response of strain gage CH_19 on July 29, 2004

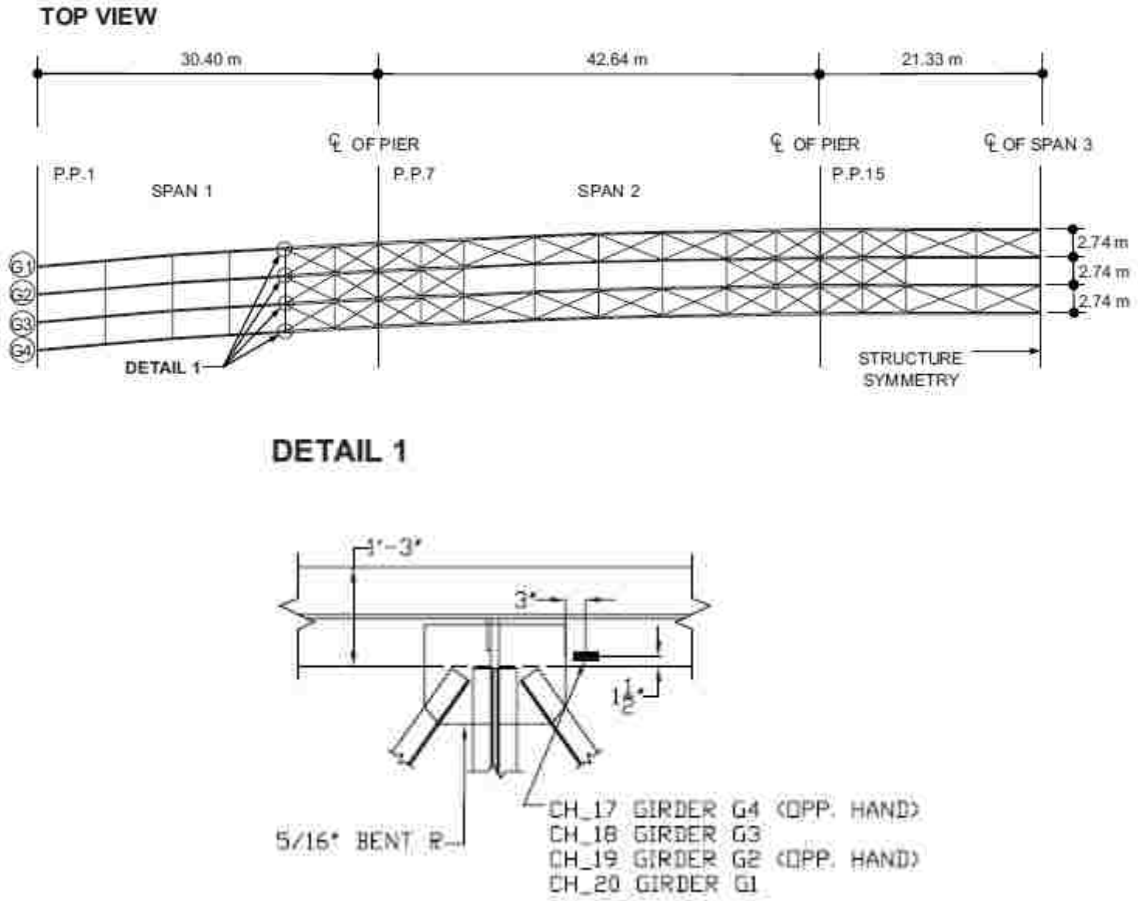

Figure 6.2 The top view and sensor locations on the I-39 Northbound Wisconsin River Bridge (From Mahmoud et al. 2005)

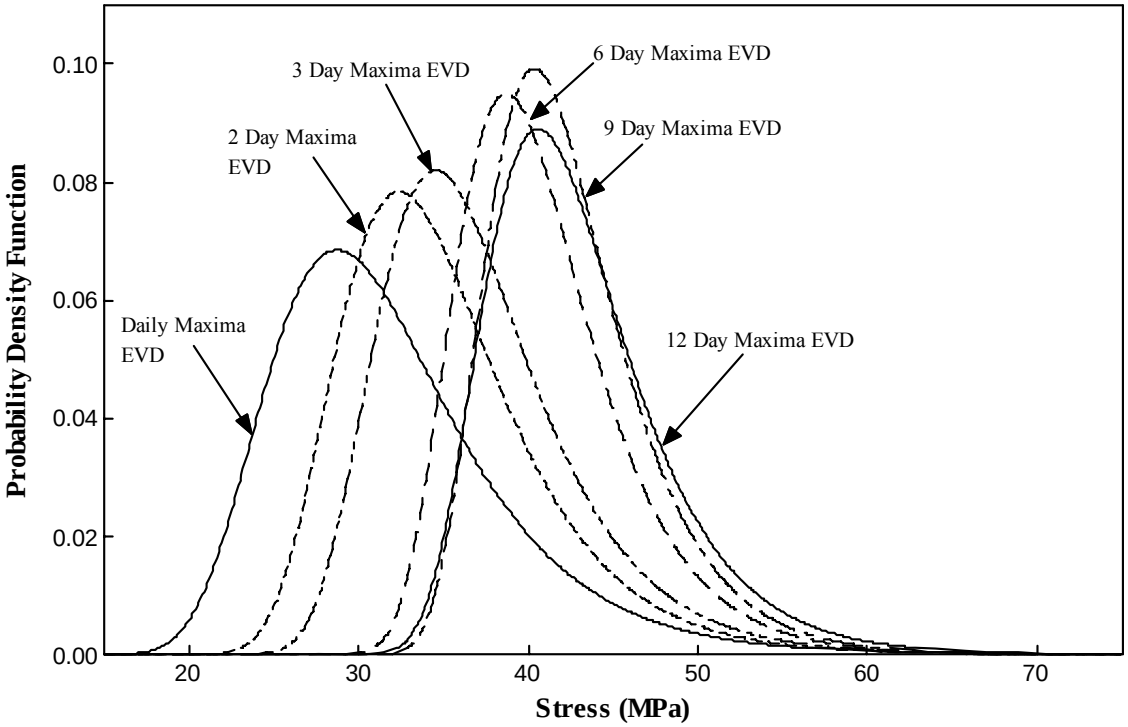

Figure 6.3 Distribution of PDFs for the selected timeframe lengths for the sensor CH_19

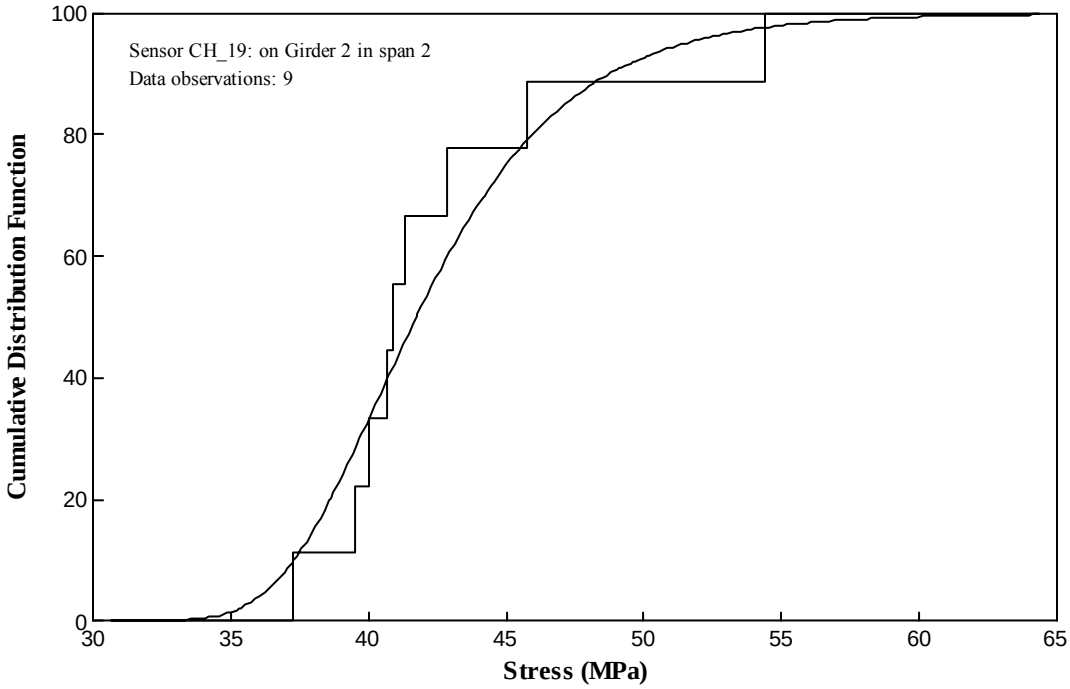

Figure 6.4 Empirical cumulative distribution function and the best fit Type I EVD for sensor CH_19

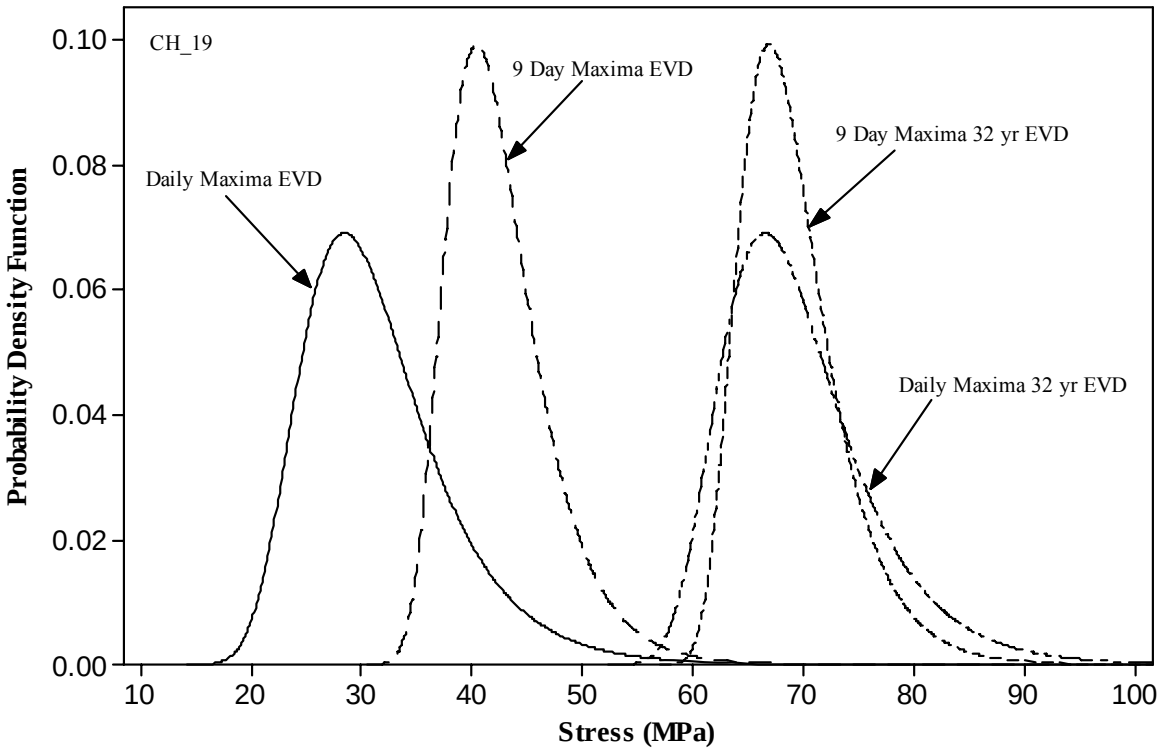

Figure 6.5 Simulation based daily and 9 day EVDs and their associated 32 yr EVD

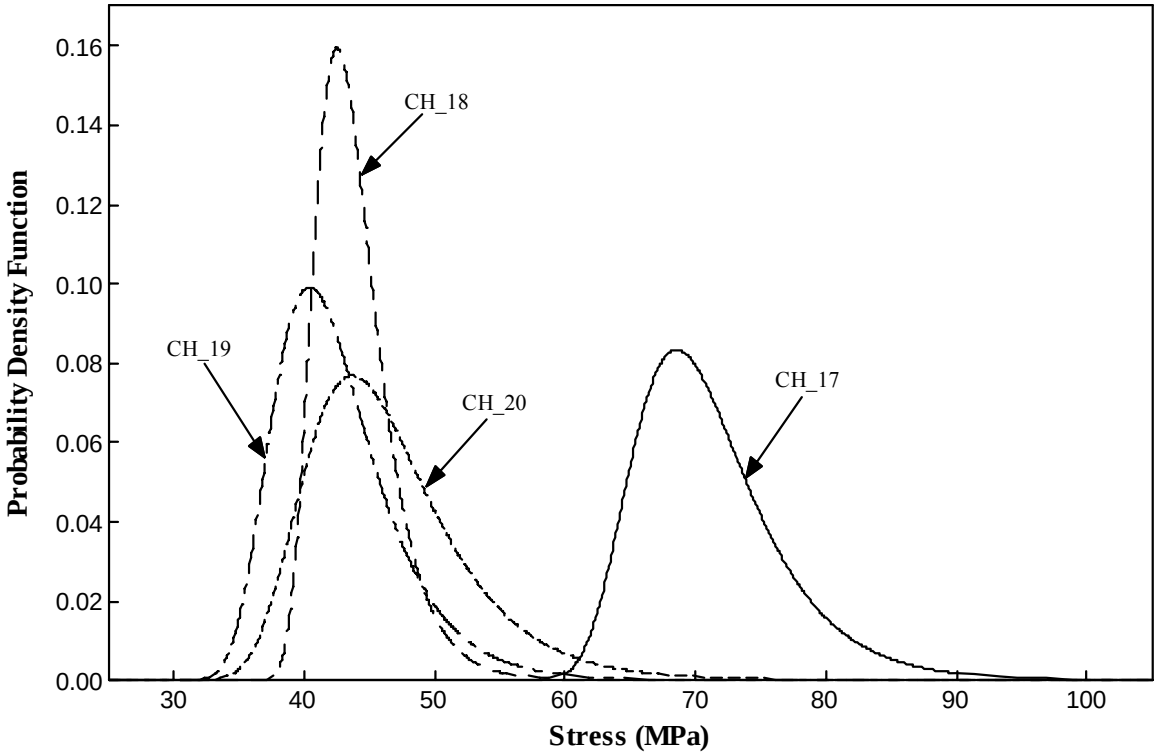

Figure 6.6 The 9 day EVDs for sensors CH_17 to CH_20

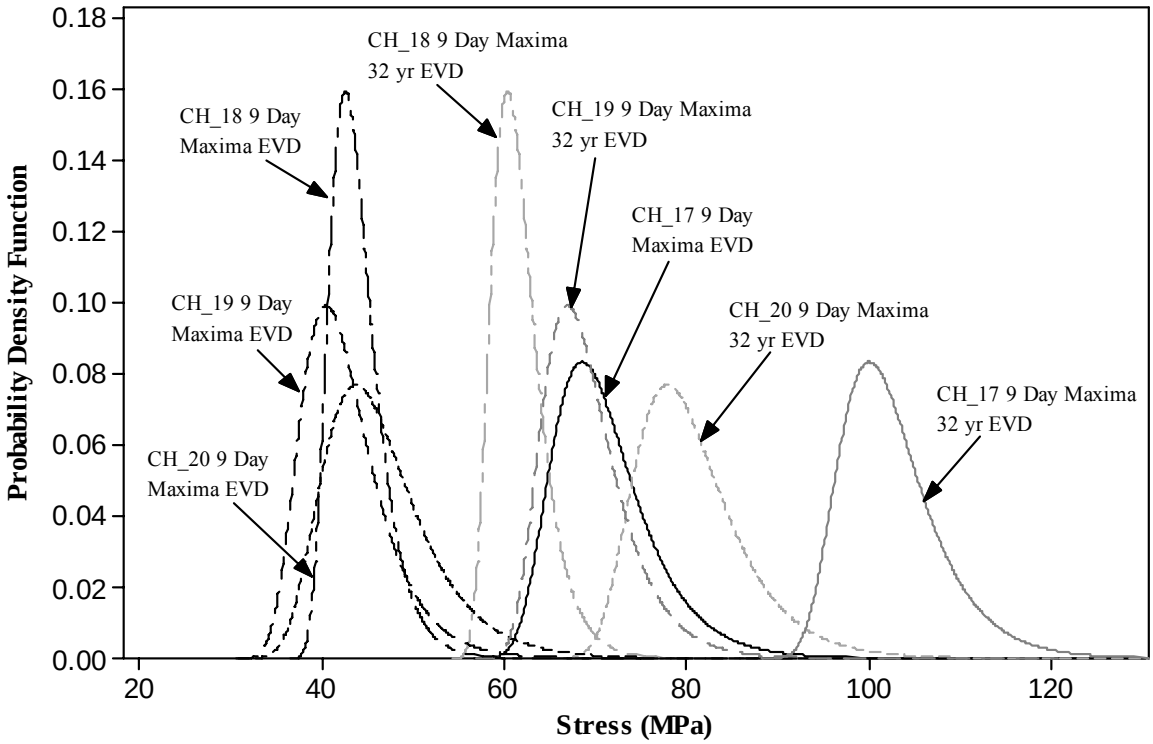

Figure 6.7 9 Day and associated 32 ys. EVDs for sensor CH_17, CH_18, CH_19 and CH_20

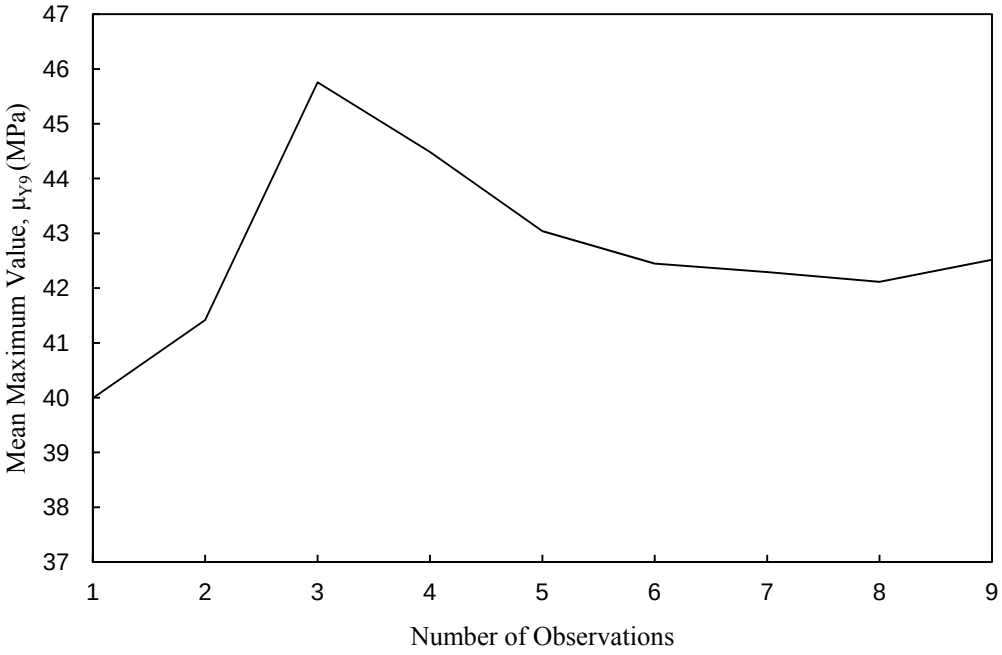

Figure 6.8 Mean of the maximum stress value vs. number of observations for sensor CH_19

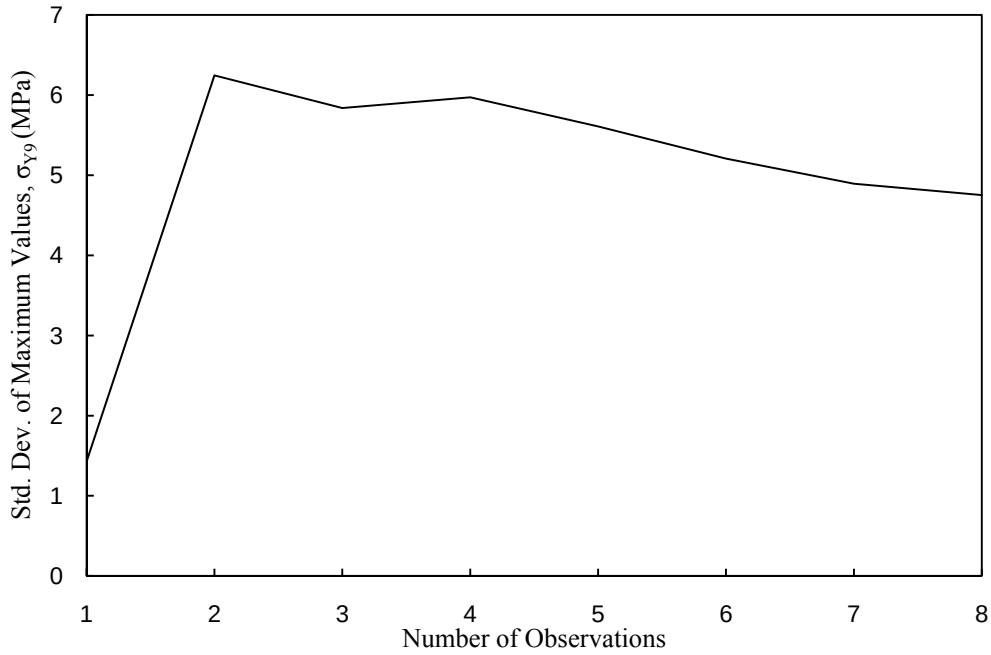

Figure 6.9 Standard deviation of the maximum stress value vs. number of observations for sensor CH_19

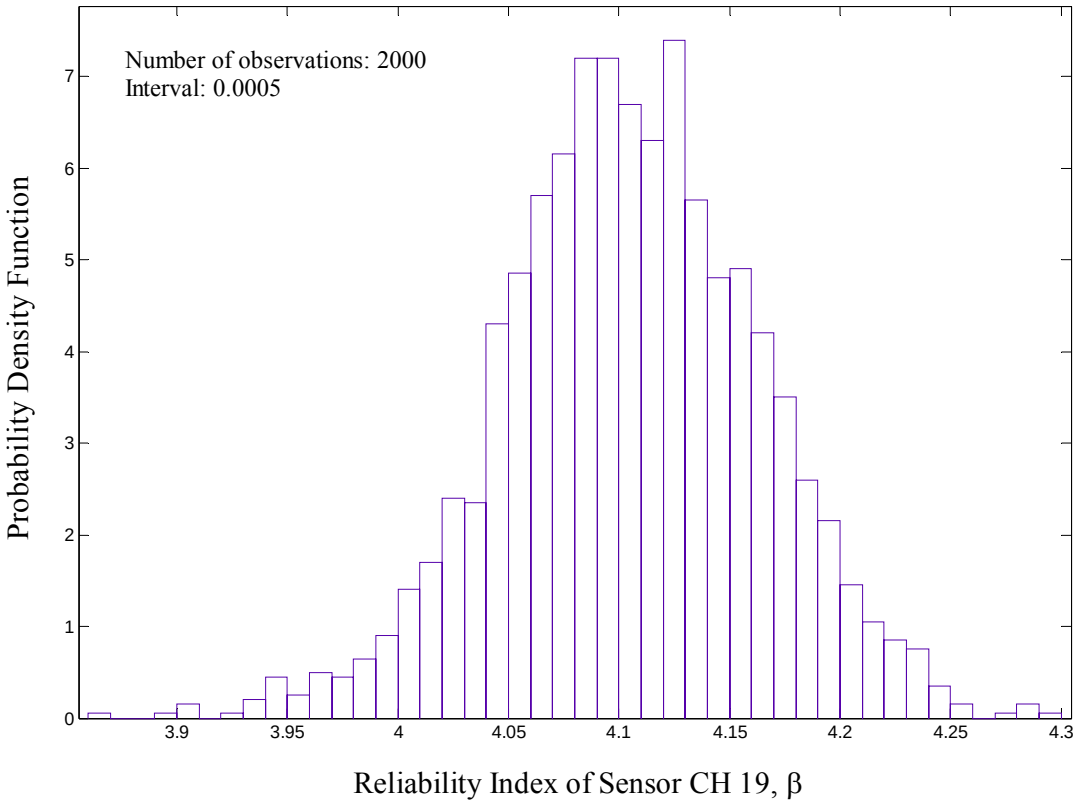

Figure 6.10 Reliability index distribution for sensor CH_19

Figure 6.11 System model I: series system

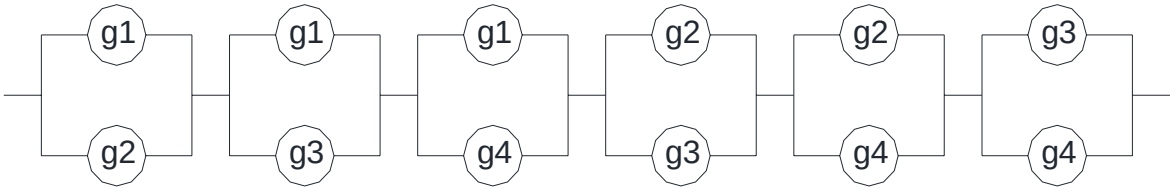

Figure 6.12 System model II: series-parallel system I

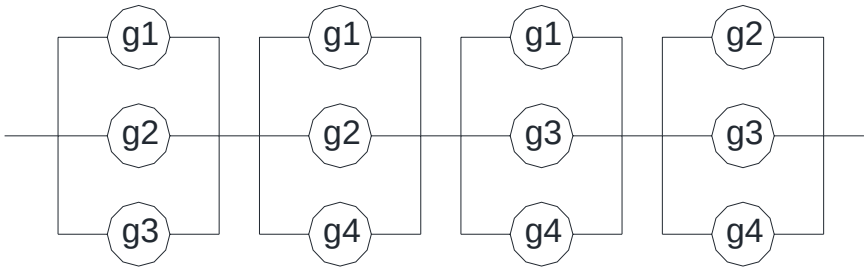

Figure 6.13 System model III: series-parallel system II

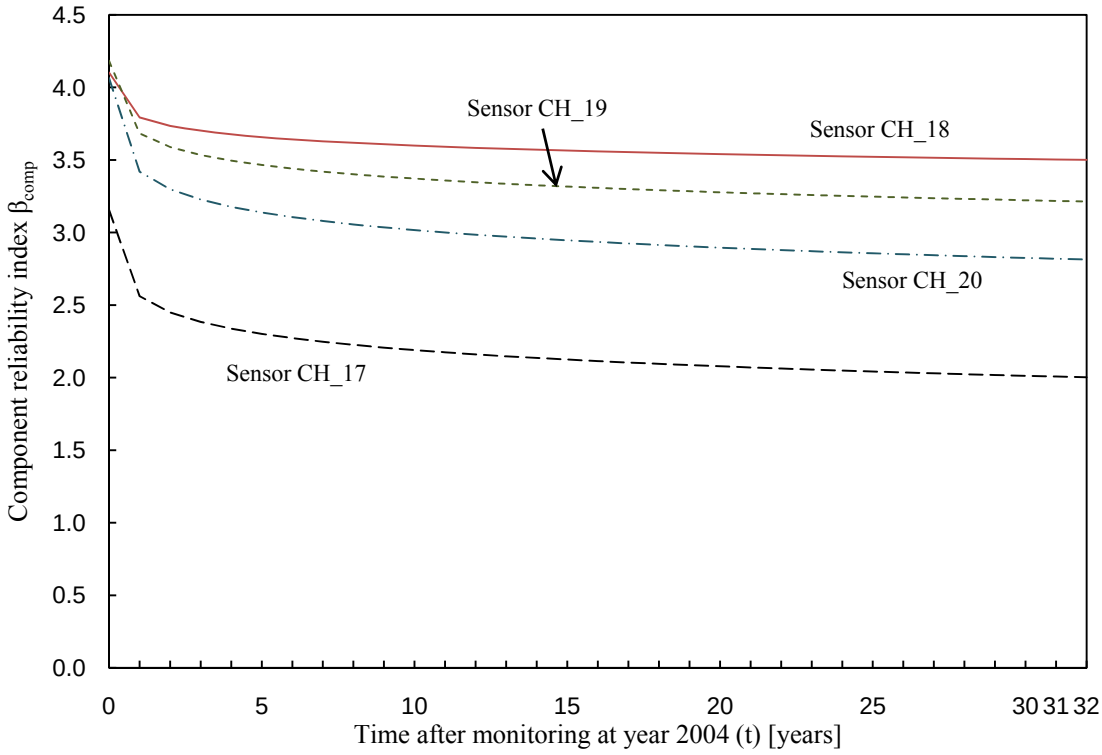

Figure 6.14 Component reliability evaluation by the first approach for sensors CH_17, CH18, CH_19 and CH_20

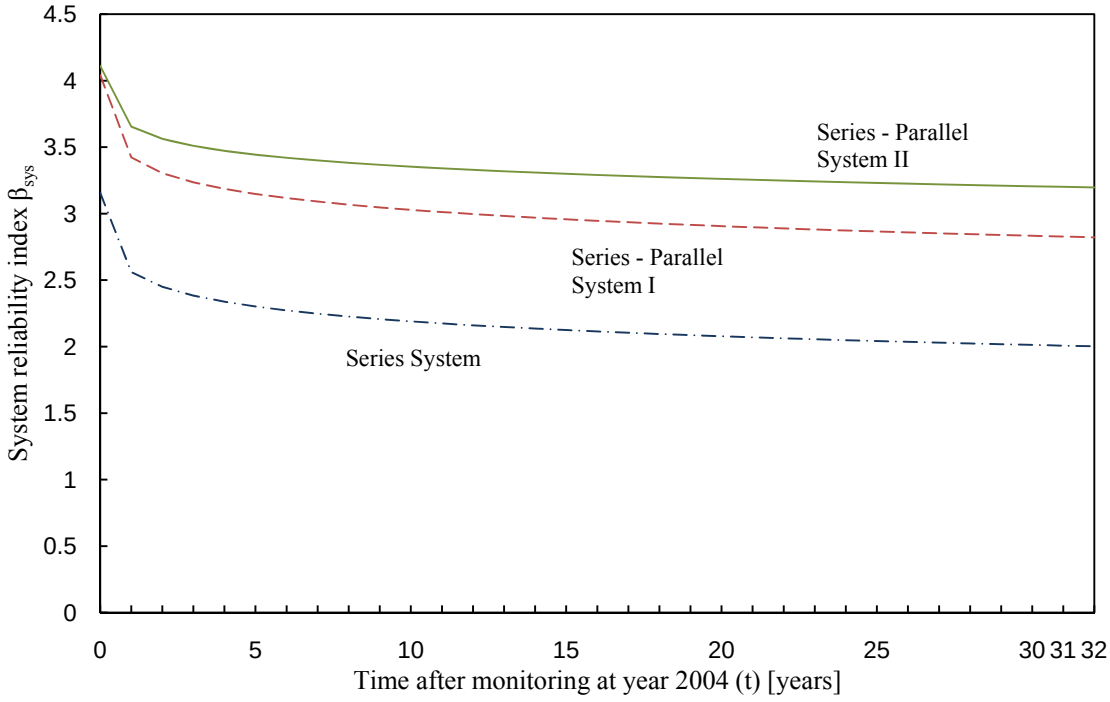

Figure 6.15 System reliability evaluation by the first approach for three system models

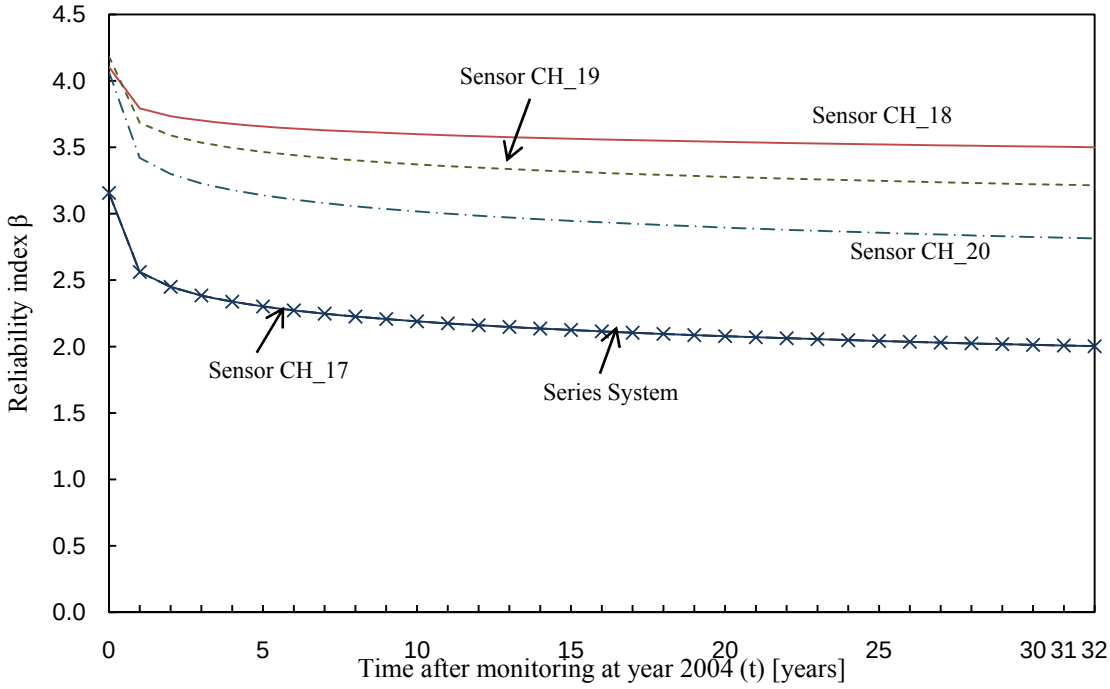

Figure 6.16 Component reliabilities of four sensors vs. series system reliability

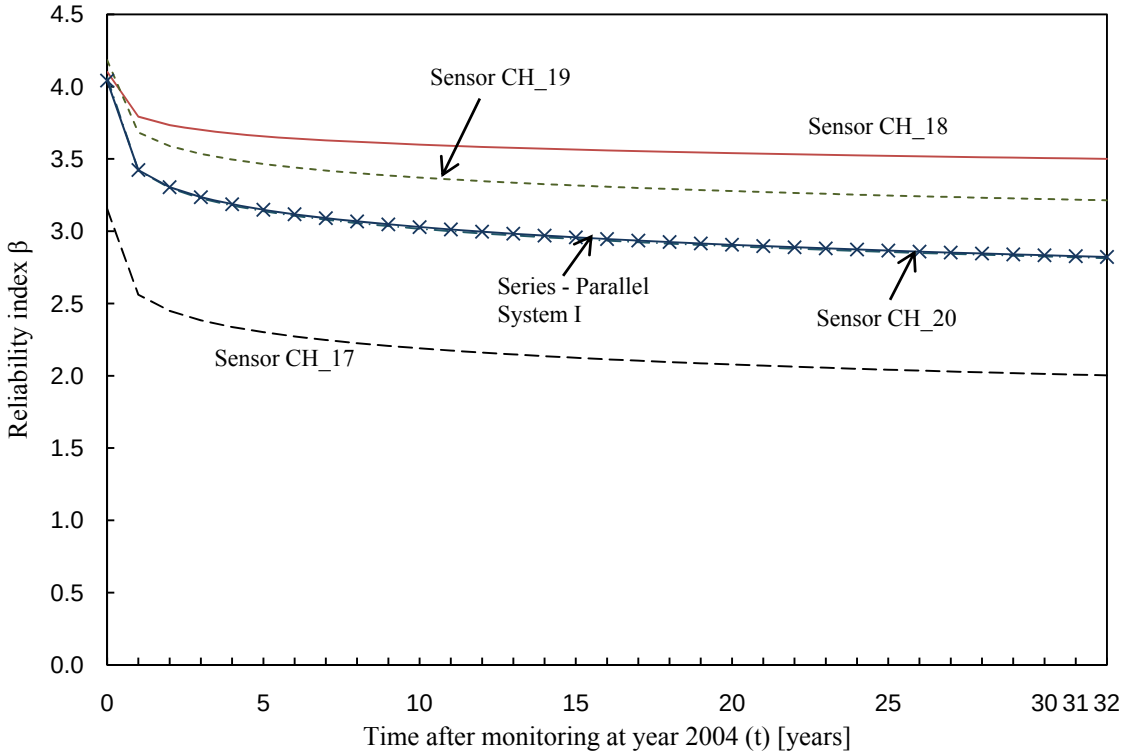

Figure 6.17 Component reliabilities of four sensors vs. series-parallel system I reliability

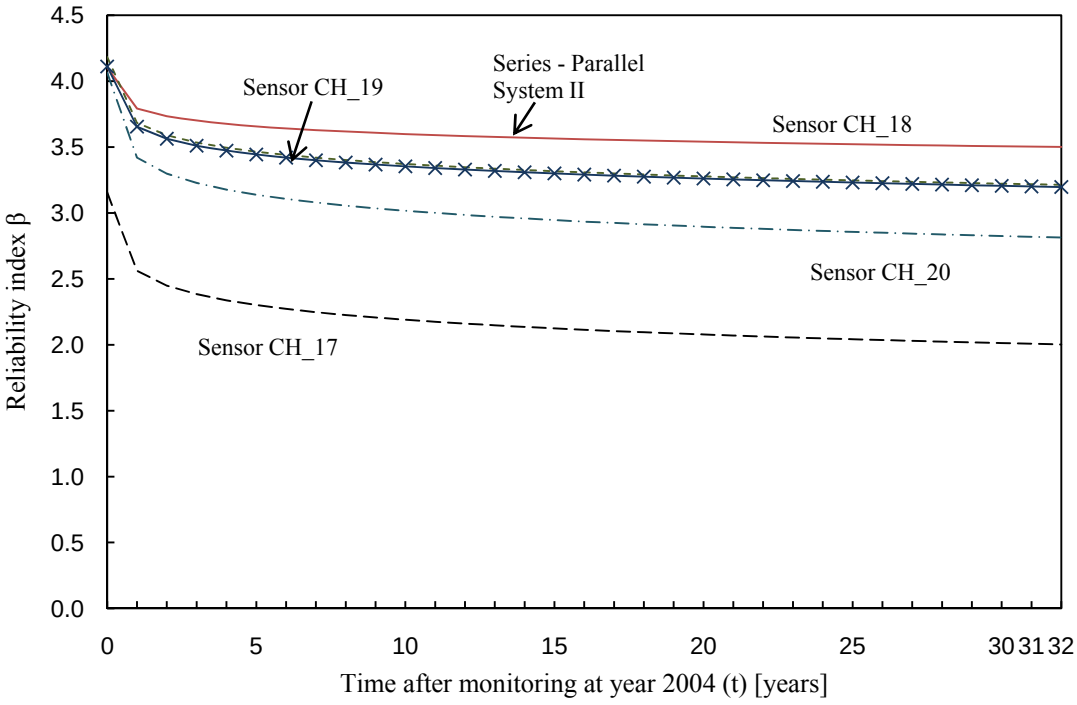

Figure 6.18 Component reliabilities of four sensors vs. series-parallel system II reliability

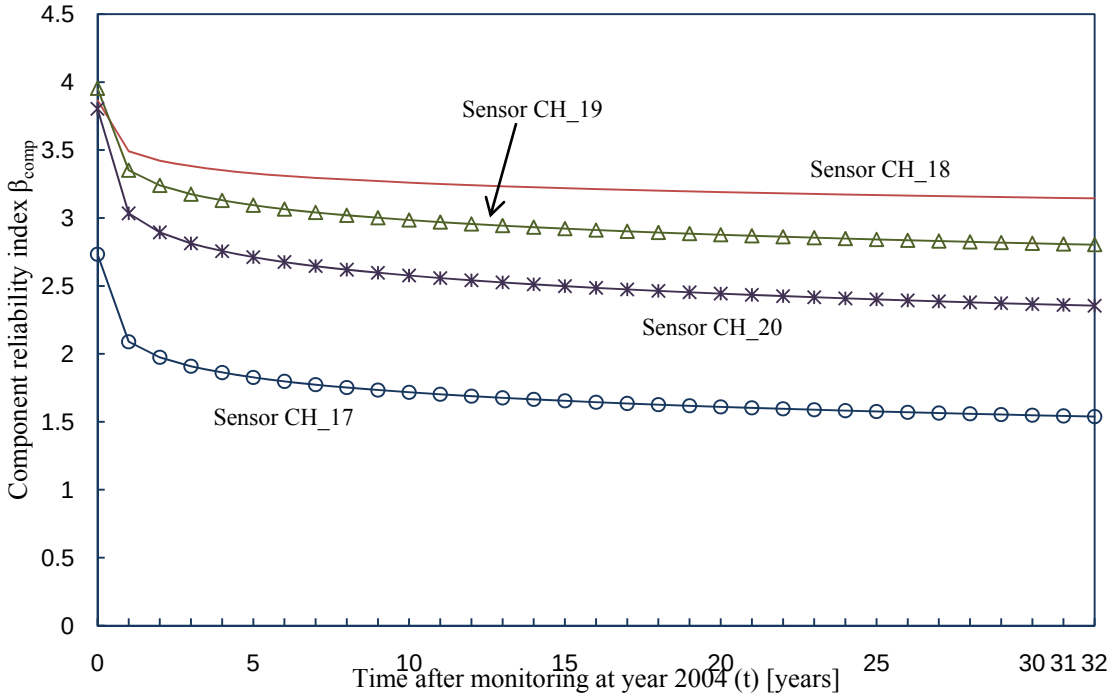

Figure 6.19 Component reliability evaluation by the second approach for sensors CH_17, CH18, CH_19 and CH_20

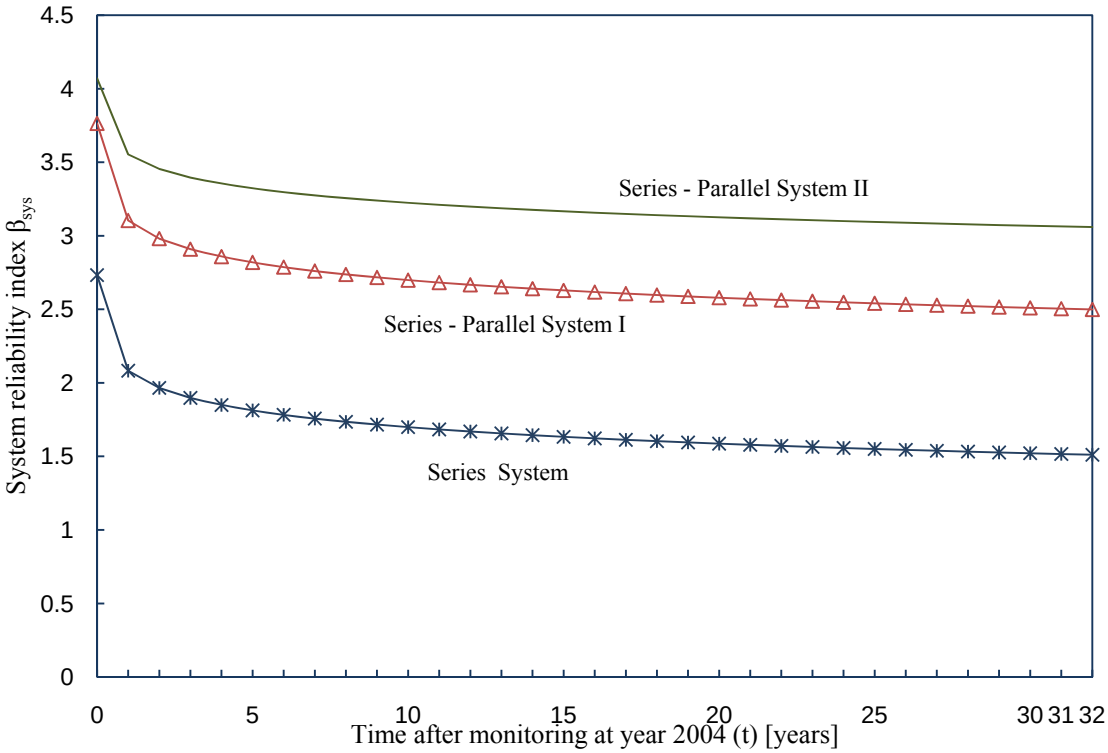

Figure 6.20 System reliability evaluation by the second approach for three system models

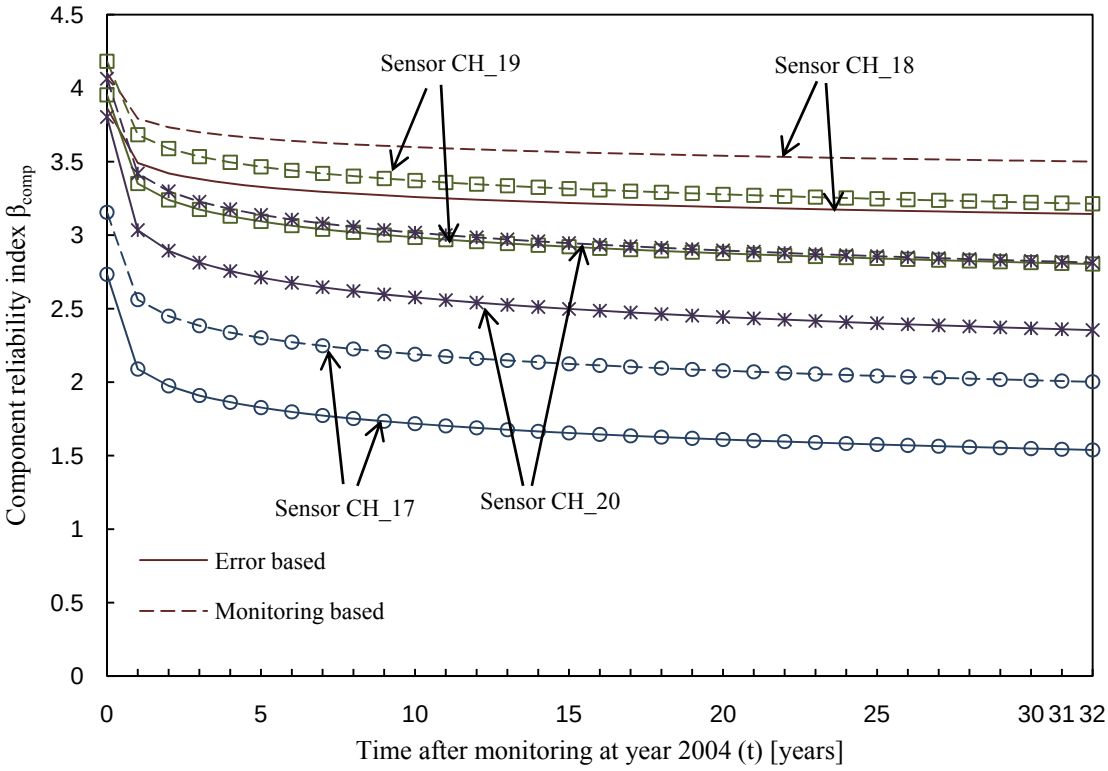

Figure 6.21 Comparison between two approaches on component level

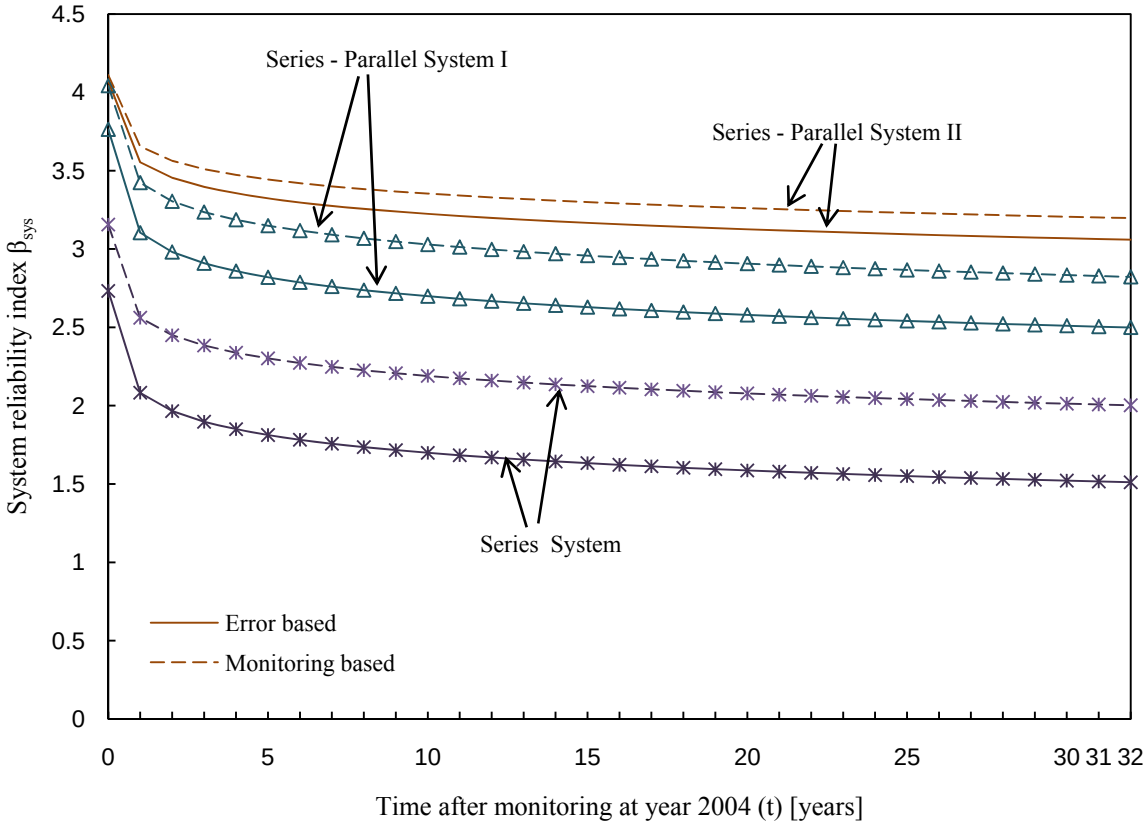

Figure 6.22 Comparison between two approaches on system level

Table 6.1 Statistical information of daily maximum live load stress for the four estimated strain gages

Descriptor	CH_17	CH_18	CH_19	CH_20
Number of days monitored	82	82	82	82
Average daily maximum stress, μ_{Yn} (Mpa)	56.03	35.23	31.47	26.82
Std. dev. of the daily maximum stress, σ_{Yn} (Mpa)	9.24	5.20	6.83	11.90
Maximum recorded daily maximum stress (Mpa)	76.39	48.09	54.43	56.81

Table 6.2 Parameters for selected timeframes of EVDs for sensor CH_18

	Average daily maximum stress, μ_{Yn} (Mpa)	Std. dev. of the daily maximum stress, σ_{Yn} (Mpa)	Coefficient of variation	Location factor	Shape factor
1 Day EVD	35.23	5.20	0.15	32.89	4.06
2 Day EVD	38.10	4.44	0.12	36.10	3.46
3 Day EVD	39.34	4.32	0.11	37.40	3.37
6 Day EVD	41.93	3.36	0.08	40.41	2.62
9 Day EVD	43.82	2.96	0.07	42.49	2.30
12 Day EVD	43.96	3.29	0.07	42.47	2.57

Table 6.3 9 day and 75 year prediction parameters of the type I Gumbel distribution

	Sensor	CH_17	CH_18	CH_19	CH_20
Daily EVD	Mean of mean (Mpa)	56.026	35.230	31.471	26.818
	Mean of standard deviation (Mpa)	9.237	5.201	6.833	11.897
9-day EVD	Mean of mean (Mpa)	71.047	43.817	42.516	46.397
	Mean of standard deviation (Mpa)	5.654	2.955	4.753	6.135
32-year EVD	Mean of mean (Mpa)	102.589	60.303	69.029	80.622
	Mean of standard deviation (Mpa)	5.654	2.955	4.753	6.135

Table 6.4 Random variables used in the error based approach

Random variable	Notation	Distribution type	Parameters (Mpa)	Source
Steel yield strength	R	Normal	(380, 26.6)	Frangopol, et.al (2008)
Dead load of steel	L_{DS}	Normal	(116.3, 4.65)	Frangopol, et.al (2008)
Dead load of concrete	L_{DC}	Normal	(108.8, 4.35)	Frangopol, et.al (2008)
Available data error	ε_{obs}	Normal	$(0, 0.22\mu_{Yn})$	Estimated
Observation timeframe error	$\varepsilon_{timeframe}$	Normal	$(0, 0.03\mu_{Yn})$	Estimated

CHAPTER 7

CONCLUSIONS

7.1. Conclusions

The following conclusions can be drawn from this study:

1. The time-variant reliability of structural members may decrease, remain the same or even increase, depending on member forces, material properties, cross section areas, deterioration rates, component ductility and structural configuration.
2. Member forces may experience sudden changes due to force redistribution after failure of one or more components.
3. The component with the lowest reliability index in a weakest-link system should receive monitoring priority. Conversely, in parallel fail-safe systems, the most reliable component should receive monitoring priority.
4. The monitoring data can be used to develop prediction models for fatigue sensitive structures by changing the effective stress range and the number of cycles per year.
5. The application of statistics of extremes combined with the monitoring data is useful in process of handling a large amount of data in bridge reliability analysis.
6. The selection of most appropriate observation timeframe for the PDF of EVDs depends not only on the numbers of available maximum value observations, but also on standard deviation of EVD.

7.2. Notations

CHAPTER 2

$g_{comp,i}$: Component performance function under limit state *i*

$R_{comp,i}$: Resistance of component with limit state *i*

$S_{comp,i}$: Load effect associated with limit state *i*

P_f: Probability of failure

ϕ: Cumulative Gaussian probability distribution function

β: Reliability index

μ_R: Mean value of resistance

μ_s: Mean value of load effect

σ_R: Standard deviation of resistance

σ_S: Standard deviation of load effect

V_R: Coefficient of variation (COV) of component resistance

V_S: Coefficient of variation (COV) of component load effect

$P_{f(sys)}$: Probability of failure of the system

$P_{s(sys)}$: Survival probability of a system

g_i: The *i*th failure mode

E_i: Event associated with the occurrence of *i*th failure mode

CHAPTER 3

$g_i(t)$: Performance function of failure mode *i* at time *t*

$R_s(t))_i$: Component resistance of failure mode *i* at time *t*

$(Q(t))_i$: Load effects of failure mode *i* at time *t*

CHAPTER 4

DR: Deterioration rate

LIR: Load increase rate

E: Modulus of elasticity

P: Vertical load

$\mu_p(t)$: Mean value of vertical load P at time *t*

$\mu_p(t-1)$: Mean value of vertical load P at time *t*-1

$\mu_p(0)$: Mean value of vertical load P at time 0

$\sigma_p(t)$: Standard deviation of vertical load P at time *t*

$\sigma_p(t-1)$: Standard deviation of vertical load P at time *t*-1

$\sigma_p(0)$: Standard deviation of vertical load P at time 0

COV_p: Coefficient of variation (COV) of vertical load P

H: Horizontal load

$\mu_H(t)$: Mean value of horizontal load H at time *t*

$\mu_H(t-1)$: Mean value of horizontal load H at time *t*-1

$\mu_H(0)$: Mean value of horizontal load H at time 0

$\sigma_H(t)$: Standard deviation of horizontal load H at time *t*

$\sigma_H(t-1)$: Standard deviation of horizontal load H at time *t*-1

$\sigma_H(0)$: Standard deviation of horizontal load H at time 0

COV_H: The coefficient of variation (COV) of horizontal load H

$A_i(t)$: Cross section area of the component i at time t

$A_i(t-1)$: Cross section area of the component i at time t-1

$A_i(0)$: Cross section area of the component i at time 0

$\mu_{R_i}(t)$: Mean of the resistance of component at time t

$(\mu_{F_y})_i$: Mean of the random yield stress Fy of component i

$\sigma_{R_i}(t)$: Standard deviation of the resistance of component i at time t

$\sigma_{R_i}(t-1)$: Standard deviation of the resistance of component i at time t - 1

$\sigma_{R_i}(0)$: Standard deviation of the resistance of component i at time *0*

CHAPTER 5

A: Fatigue detail coefficient

S_{re}: Equivalent stress range

n_i: Number of cycles accumulated at stress S_i

D: Fraction of life consumed by exposure to the cycles at the different stress levels

W_i: Critical damage accumulation index

$g(X)$: Performance function

$X = \{X_1, X_2, \dots, X_n\}^T$: Vector of random variables

μ_Q: Mean value of load effect

σ_Q: Standard deviation of load effect

M: Monitored load effect

μ_M: Mean value of monitored load effect

σ_M: Standard deviation of monitored load effect

μ_{M_i}: Mean value of monitored load associated with sensor *i*

σ_{M_i}: Standard deviation of monitored load associated with sensor *i*

N_s: Number of cycles

e_s: Sensor error

$\beta^o_{i,e,f}$: Component *i* fatigue reliability integrated with monitoring sensor reading

μ_f: Allowed effective stress range regarding AASHTO guidelines

σ_f: Standard deviation of the allowed effective stress range

v: COV of the allowed effective stress range

$\mu^o_{M_i}$: Mean value of effective stress range associated with sensor *i*

$\sigma^o_{M_i}$: Standard deviation of the effective stress range associated with sensor *i*

f_s: Factor assigned to sensor errors

m: Material constant

$\Delta\ F$: Nominal fatigue resistance

N_t: Fatigue life in terms of cycles to failure

Δ: Miner's critical damage accumulation index

s_c: Cut-off threshold

λ: Location parameter of lognormal's PDF

ζ: Scale parameter of lognormal's PDF

$E(S)$: Mean of the stress range

$Var(S)$: Standard deviation of the stress range

α: Scale parameter of Weibull distribution

β: Shape parameter of Weibull distribution

λ: Rate parameter of Gamma distribution

k: Shape parameter of Gamma distribution

n_i: Number of observations in the predefined stress-range bin

N_{total}: Total number of observations during the monitoring period

S_{ri}: Number of cycles for each stress range

$ADTT$: Average Daily Truck Traffic

$N(y)$: Cumulated stress number of cycles

y: Number of years

α: Traffic increase rate per year

$\Phi^{-1}(\cdot)$: Inverse standard normal cumulative distribution function

e: Error factor of loading considered as a random variable

$N_{S_{re}}$: Number of cycles to failure

N_{avg}: Average daily number of stress cycles

t: Component fatigue life

$CAFL$: Constant amplitude fatigue limit

N_{CAFL}: Number of cycles corresponding to the CAFL

β_L: Lower bound for reliability index

β_u: Upper bound for reliability index

CHAPTER 6

n: Sample size

X: Initial random variable

$F_X(x)$: Initial distribution function

Y: Extreme value

Y_n: Maximum values of random variables (X_1, X_2,…, X_n)

α_n: Shape factor of type I Gumbel distribution

u_n: Characteristic value of type I Gumbel distribution

μ_{Y_n}: Mean value of maximum values Y_n

σ_{Y_n}: Standard deviation of maximum values Y_n

γ: Euler's number

$\sigma_{\mu_{Y_n}}$: Standard deviation of mean value of maximum values Y_n

$\sigma_{\sigma_{Y_n}}$: Standard deviation of standard deviation of maximum values Y_n

m: Number of observations of the maximum value

$\mu_{\mu_{Y_n}}$: Mean of mean value of maximum values Y_n

$\mu_{\sigma_{Y_n}}$: Mean of standard deviation of maximum values Y_n

L_{DS}: Dead load caused by steel

L_{DC}: Dead load caused by concrete

L_L: Monitoring-based EVD live load

ε_{obs}: Error term associated with the available data

$\varepsilon_{timeframe}$: Error term associated with timeframe of EVD

μ_{DS}: Mean value for dead load stress caused by steel

μ_{DC}: Mean value for dead load stress caused by concrete

σ_{DS}: Standard deviation for dead load stress caused by steel

σ_{DC}: Standard deviation for dead load stress caused by concrete

REFERENCES

American Association of State Highway and Transportation Officials (AASHTO). (2007). LRFD Bridge Design Specifications. 4th Edition, Washington, D.C.

Ang, A. H-S and Tang, W.H., (1984). Probability Concepts in Engineering Planning and Design: Decision, Risk and Reliability. Volume II, *John Wiley and Sons*, NY.

Ang, A. H-S and Tang, W.H., (2007). Probability Concepts in Engineering: Emphasis on Applications to Civil and Environmental Engineering. 2nd Edition, *John Wiley and Sons*, NY

Balageas, D. , Fritzen, C., and Güemes, A. (2006). Structural health monitoring, London; Newport Beach, CA: ISTE, 2006

Catbas, F.N., Susoy, M., Frangopol, D.M., Structural health monitoring and reliability estimation: Long span truss bridge application with environmental monitoring data, *Engineering Structures*, Elsevier, 2008.

Chung, H.Y., Fatigue reliability and optimal inspection strategies for steel bridges. Dissertation, Civil and Environmental Engineering Department, The University of Texas at Austin, Austin, TX; 2004

Cornell, C.A. (1967). Bounds on the reliability of structural systems. *Journal of Structural Division*, ASCE, 93(ST1).

Ditlevsen, O. (1979). Narrow reliability bounds for structural systems. *Journal of Structural Mechanics,* 7(4), 453-472.

Estes, A.C. and Frangopol, D.M., (1998). RELSYS: a computer program for structural system reliability. *Structural Engineering and Mechanics*, 6(8), 901-919.

Estes, A.C. and Frangopol, D.M., (2005). Life-cycle evaluation and condition assessment of structures. Chapter 36. In: W.-F. Chen and E.M. Lui, eds. Structural engineering handbook, second edition. CRC Press, 36-1-36-51.

Enevoldsen,I., (2008). Practical implementation of probability based assessment methods for bridges. In: H.-M. Koh and D.M. Frangopol, eds. *Bridge maintenance, safety, management, health monitoring and informatics*. London: Taylor & Francis Group/CRC Press.

Frangopol, D.M. and Curley, J.P., (1987). Effects of damage and redundancy on structural reliability. *Journal of Structural Engineering*, ASCE, Vol.113, No.7, New York

Frangopol, D.M. and Messervey, T.B., Chapter 89 Maintenance Principles for Civil Structures., John Wiley & Sons, Ltd, 2009.

Frangopol, D.M., Strauss, A. and Kim, S. (2008a). Bridge reliability assessment based on monitoring. *Journal of Bridge Engineering*, ASCE, 13(3), 258-270.

Frangopol, D.M., Strauss, A. and Kim, S. (2008b). Use of Monitoring Extreme Data for the Performance Prediction of Structures: General Approach. *Engineering Structures*, Elseview, 30(12), 3644-3653.

Ghosn, M., Moses, F., and Wang, J., (2003). Design of highway bridges for extreme events. NCHRP TRB Report 489, Washington, DC.

Ghosn, M. and Moses, F., (1986). Reliability calibration of a bridge design code. *Journal of Structural Engineering*, 112(4), 745-763.

Ghosn, M., Moses, F. and Frangopol, D.M. (2010). Redundancy and robustness of highway bridge superstructures and substructures. Structure and Infrastructure Engineering, Taylor and Francis, 6(1-2), 257-278.

Hodgson, I.C., Yen, B.T., and Bowman, C., Field testing and evaluation of electroslag welds on the Commodore Barry Bridge. ATLSS Report 08-04. Lehigh University, Bethlehem, PA, USA.

Hodgson, I.C., Yen, B.T., Stanley, R.B., and Prior, R.C., Field testing and evaluation of electroslag welds on the Commodore Barry Bridge.

Fisher, J.W., Kulak, G.L., and Smith, I., A fatigue primer for structural engineers, *National Steel Bridge Alliance*, 1998.

Fisher, J.W., Nussbaumer, A., Keating, P.B., and Yen, B.T., Resistance of welded details under variable amplitude long-life fatigue loading. National Cooperative Highway Research Program (NCHRP). Report 354. Transportation Research Board, National Research Council, Washington (DC); 1993.

Kwon, K. and Frangopol, D.M., Bridge fatigue reliability assessment using probability density functions of equivalent stress range based on field monitoring data, *International Journal of Fatigue*, 32(2010)1221-1232

Keating, P.B. and Fisher, J.W., Evaluation of fatigue tests and design criteria on welded details. National Cooperative Highway Research Program (NCHRP). Report 286. Transportation Research Board, National Research Council, Washington (DC); 1986.

Liu, M., Frangopol, D.M., and Kim, S. (2009a). Bridge safety evaluation based on monitored live load effects. *Journal of Bridge Engineering*, ASCE, 14(4), 257-269.

Liu, M., Frangopol, D.M. and Kim, S. (2009b). Bridge system performance assessment from structural health monitoring: A case study. *Journal of Bridge Engineering*, ASCE, 135(6), 733-744.

Mahmoud, H.N., Connor, R.J. and Bowman, C.A. (2005). Results of the fatigue evaluation and field monitoring of the I-39 Northbound Bridge over the Wisconsin River. ATLSS Report 05-04. Lehigh University, Bethlehem, PA, USA.

Messervey, T.B., (2009). Integration of structural health monitoring into the design, assessment, and management of civil infrastructure. Thesis (PhD). University of Pavia, Pavia, Italy.

Messervey, T.B. and Frangopol, D.M., (2007). Bridge live load effects based on statistics of extremes using on-site load monitoring. In: Frangopol, Kawatani, and Kim, eds. *Reliability and optimization of structural systems: Assessment, design, and life-cycle performance.* London: Taylor & Francis Group, 173-180.

Messervey, T.B. and Frangopol, D.M., Application of the statistics of extremes to the reliability assessment and performance of monitored highway bridges, *Structure and Infrastructure Engineering*, Vol.7, Nos. 1-2, Jan-Feb 2011, 87-99.

Federal Highway Administration, National Bridge Inventory, available online at http://www.fhwa.dot.gov/bridge/britab.cfm (dated accessed August 2010)

Okasha, N.M. and Frangopol, D.M., (2010i). Time-variant redundancy of structural systems. Structure and Infrastructure Engineering, Taylor & Francis, 6(1-2), 279-301.

Strauss, A., Kala, Z., Bergmeister, K., Hoffmann, S. and Novak, D., Technologische Eigenschaften von St*ä*hlen im europ*ä*ischen Vergleich. Stahlbau, Ernst & Sohn 2006; 75(1):55-60.

Weidlinger Associates (1988), "Commodore Barry Bridge, Electroslag Welds Investigation." Final Report prepared for the Delaware River Port Authority.

Wikipedia, http://en.wikipedia.org/wiki/Commodore_Barry_Bridge

Wirsching, Fatigue reliability for offshore structures. *Journal of Structural Engineering*, ASCE, New York, 1984; 110(10):2340-56.

Wisconsin department of transportation. Wisconsin vehicle classification data. Report, Division of Transportation Investment Management, Bureau of Highway Programs; 2002

VITA

Yingjun Zou was born on Sep. 8th, 1984 in Zhuzhou, Hunan Province, China. She is the daughter of Tong Zou and Cheng Liang, who are residents in Zhuzhou.

Yingjun Zou earned her Bachelor of Engineering Degree in Civil Engineering from Beijing Jiaotong University, Beijing, China in June 2009. In her fourth year of education, she went to Germany for internship in Deutsche Post in 2007. Then she moved to UK to work in a bridge team in Mouchel until Feburary, 2009. After two years of working in Europe, she went back to University to finish her study in June 2009. After graduation, she came to Lehigh University to pursue her Master of Science Degree in Structural Engineering. Yingjun Zou will receive her degree in May 2011.